#### POLITECNICO DI TORINO

## MASTER'S DEGREE IN ENERGY AND NUCLEAR ENGINEERING



Master's Thesis in Renewable Energy Systems

### Integrated Cogeneration and Heat Recovery System for Industrial Process Optimization

Supervisor Candidate

Prof. Luciano ROLANDO Léopoldine CRISTIANI

315208

October 2025 Academic year 2024-2025

#### Abstract

This thesis presents the design and analysis of a *cogeneration system integrated* with heat recovery for an industrial plant. The study focuses on optimizing the production of hot water, steam, and electricity by exploiting the energy content of natural gas and waste heat streams from existing processes.

The main objectives were to enhance energy efficiency, reduce fuel consumption, and lower operational costs. To achieve this, a steam generator with flue gas heat recovery was modeled and dimensioned, coupled with a cogeneration unit supplying heat for preheating, process steam, and electrical power to the plant. The design process accounted for thermodynamic performance, operational constraints, and integration with existing infrastructure.

An economic analysis was conducted to evaluate the feasibility of the intervention. This included calculation of fuel savings, return on investment, and payback period, demonstrating the potential benefits of the proposed system in terms of energy efficiency and cost reduction.

The results show that the integrated heat recovery and cogeneration system can significantly *improve overall energy performance*, providing both *environmental and economic advantages*. This study highlights the practical application of cogeneration and waste heat recovery in the industrial sector and serves as a reference for future energy efficiency projects.

## Table of Contents

Li	st of	Table	s	VI			
Li	st of	Figur	es	IX			
A	Acronyms						
0	Inti	roducti	ion	1			
1	Cog	generat	tion and Heat Recovery Overview	6			
	1.1	Comb	ined Heat and Power (CHP)	6			
		1.1.1	Classification of Cogeneration Technologies	7			
		1.1.2	High-Efficiency Cogeneration	9			
		1.1.3	Global CHP Market Dynamics and Operational Characteristics	9			
	1.2	Heat 1	Recovery Systems (HR)	13			
		1.2.1	Classification of Waste Heat	14			
		1.2.2	Framework for Waste Heat Recovery Potential Assessment .	15			
		1.2.3	Waste Heat Recovery in Energy-Intensive Industries	19			
2	Hea	at Reco	overy System Test Case	21			
	2.1	Pre-in	tervention Thermal Power Plant	22			
	2.2						
		2.2.1	Analytical Approach to Steam Generator Simulation	26			
		2.2.2	Economizer Design and Sizing	35			
	2.3	Heat 1	Recovery System	43			
		2.3.1	Sizing of Heat-Recovery Exchangers	44			
		2.3.2	Flue Gas Flow Management	46			
		2.3.3	Ventilator Sizing	49			
		2.3.4	Pump Sizing	55			
3	Nui	merica	l Model Development	59			
	3.1	Aspen	Plus Overview	59			

		3.1.1	Steam Generator Simulation in Aspen Plus	60
		3.1.2	Results	64
4	$\mathbf{Cog}$		ion System Test Case	69
	4.1		ss Scheme of the CHP Unit and HR Integration	
	4.2		n of the Cogeneration System and Heat Recovery Integration .	
		4.2.1	Preliminary Data and Input Parameters	
		4.2.2	Electric Load Analysis and CHP Unit Selection	
		4.2.3	CHP Thermal Energy Management	
		4.2.4	Sizing of Heat Recovery and Auxiliary Systems	80
5	Eco	nomic	Results	82
	5.1	Therm	nal Power Plant Retrofit and HR System Results	82
		5.1.1	Performance Improvements: Energy Efficiency and Fuel Savings	
		5.1.2	Economic Assessment	
	5.2		System Performance and Economic Assessment	
		5.2.1	CHP System Fuel Consumption and Energy Outputs	
		5.2.2	Economic Assessment	102
6	Con	clusio	ns	109
$\mathbf{A}$	ECO	) Data	asheet	112
В	RC2	2 and 1	RC3 Manufacturer Datasheet	114
$\mathbf{C}$	P&1	ID of t	che Heat Recovery System	118
D	P&1	ID of t	the CHP system	124
Bi	bliog	raphy		128

### List of Tables

1.1	Classification of waste heat sources by temperature level, typical dis- tribution of recoverable industrial losses, and corresponding sources	
	and applications	14
2.1	Preliminary data	24
2.2	Mass flow rates results entering and exiting the feedwater tank	25
2.3	Air Composition	27
2.4	Water Specifications	29
2.5	Flue Gas Specifications	34
2.6	Input parameters and output results for the SG operating at full load.	35
2.7	Design and Operating Parameters of the Economizer under Full-Load	
	Steam Generator Conditions	39
2.8	Comparison of full-load and part-load performance of the steam	
	generator with economizer	40
2.9	ECO hoppers dimensions	43
2.10	RC2 and RC3: Design and Operating Conditions at Full and Medium	
	Load	45
2.11	RC2 and RC3 Hopper Dimensions	46
2.12	Sizing of Manifold $SG_1$ and $SG_2$ at nominal capacity of both steam	
	generators	48
2.13	Sizing of Manifolds 1, Manifold 2 and Manifold 3 at maximum load	
	operating condition	49
	Distributed and localized pressure losses along the critical path	52
2.15	Summary of total pressure drops for each duct segment and HX,	
	evaluated under both maximum and medium load conditions	52
	Summary of input parameters and results for fan sizing	54
	Hydraulic Concentrated and Distributed Pressure Drops	56
2.18	Pump Sizing Parameters, NPSH Evaluation, and Selected Pump	58
3.1	Russian Gas Composition	63
3.2	Aspen Plus Results and Relative Variation	65

<b>პ</b> .პ	for the SG with ECO	68
4.1 4.2	Annual electrical energy consumption of Substations A, B, and C Comparison of Simulated CHP Configurations Based on Electrical	73
4.2	Load Profile	75
4.3	Technical Specifications of Heat Recovery Units	77
4.4	Thermal performance of heat recovery systems in the CHP unit	
	simulation	78
4.5	CHP Unit Specifications at Full Load.	79
4.6	Natural gas savings from heat recovery systems and CHP unit	
4.7		79 81
5.1	Operating data and natural gas consumption before and after retrofitting	8
5.2	Annual reduction in fuel consumption due to RC3	84
5.3	Annual reduction in fuel consumption	85
5.4	Annual fuel savings and related economic benefits from the retrofit	
	v	85
5.5	Detailed investment cost breakdown with total and enterprise markup	
		87
5.6		89
5.7	Summary of parameters used to calculate the WACC for both the	വാ
5.8	1 0	93
5.0	NPV and PBT for the company and the investment enterprise under the three-year contract model	94
5.9	NPV and PBT for the company and the investment enterprise under	JI
0.5	- *	95
5.10	NPV and PBT for the company and the investment enterprise under	
	1 V	95
5.11	Annual Natural Gas Consumption, Savings, and outputs of the CHP	
	Unit	98
5.12	Correction Factors for Avoided Grid Losses in Separate Electricity	
		.00
5.13	Harmonised Efficiency Reference Values for Separate Electricity	
		.00
5.14	Summary of CHP Unit Efficiencies and Primary Energy Savings	0.7
	Including Heat Recovery from Flue Gases $(HR_{FG})$	.01
5.15	Summary of CHP Unit Efficiencies and Primary Energy Savings	01
ር 1 <i>ር</i>	Excluding Heat Recovery from Flue Gases $(HR_{FG})$	
0.10	- i rices or paecifichy and inalinal Gas Considered in line 5thdy I	UZ

5.17	Operational costs sustained by the plant before the implementation
	of the CHP system
5.18	Estimated operational costs of the plant after integrating the CHP
	and heat recovery systems
5.19	Initial Investment (CAPEX) for the CHP Unit and Auxiliary Systems 104
5.20	Results of the PES, RISP, and White Certificates (TEE) associated
	with the CHP unit
5.21	Summary of the key parameters used to calculate the WACC 107
5.22	Net Present Value (NPV) and payback time (PBT) for the cogener-
	ation project

# List of Figures

1	Global Final Energy Consumption by Sector with Industrial Share	
0	Breakdown by Country [3]	1
2	GHG emissions by country at the global level	2
3	GHG emissions by country in the European Union	3
4	Climate Clock, September 2025	4
1.1	Energy performance of cogeneration compared to separate produc-	
	tion of electricity and heat [13]	7
1.2	Energy flow schematics for topping and bottoming cycle cogeneration	
	systems	8
1.3	Fuel Mix Breakdown for Global and European CHP systems [17]	10
1.4	Global trends in CHP production from 2011 to 2021, illustrating	
	both electric and thermal output [17]	11
1.5	European trends in CHP production from 2011 to 2021, illustrating	
	both electric and thermal output [17]	11
1.6	CHP Gross Electricity Production (EU-27) [18]	12
1.7	Estimated global waste heat distribution of 2012 in PJ, according to	
	a theoretical approach, showing energy flows from primary energy	
	sources through sectors and losses [22]	15
1.8	Classification framework of WHP categories as proposed by Forman	
	et al. [23]	16
1.9	Waste Heat and Carnot's potential by sector [22]	17
1.10	Global and EU industrial shares of WHP and CWHP distributions	
	[22, 23]	18
2.1	Pre-intervention thermal power plant scheme	22
2.2	Input and output feedwater tank	23
2.3	Simplified Scheme of the Retrofitted Thermal Power Plant Under	
	Medium Load Conditions	26
2.4	Indirect method for evaluating boiler efficiency	32
2.5	Technical Layout of the ECO Heat Exchanger	38
2.6	ECO and Hoppers Exploded view	41

2.7 2.8 2.9 2.10 2.11	Labeled hoppers references.  Heat Recovery Thermal Power Plant Scheme.  Technical drawing – Front and plan view with manifold identification.	42 43 44 46 56
3.1	Aspen Plus process flow diagram of the steam generator based on NG combustion	61
3.2	Aspen Plus process flow diagram of the steam generator with economizer under full-load conditions	66
4.1 4.2	Hourly electricity consumption profile of Primary Substation A from	70 74
4.3	Hourly electricity demand profile and coverage by CHP units of 500,	76
5.1 5.2	Main Third-Party Financing (TPF) models showing debt allocation	88
5.3	Cumulative Cash Flow for the Investment Enterprise under the	90 96
5.4	Cumulative Cash Flow for the Company under the Three EPC	97
5.5	Discounted cumulative cash flows of the cogeneration unit over its	.08
A.1 A.2	Economizer Datasheet provided by the manufacturer, Full Load 1 Economizer Datasheet provided by the manufacturer, Medium Load. 1	
B.1 B.2 B.3 B.4	RC2 Datasheet provided by the manufacturer, Full Load 1 RC2 Datasheet provided by the manufacturer, Medium Load 1 RC3 Datasheet provided by the manufacturer, Full Load 1 RC3 Datasheet provided by the manufacturer, Medium Load	15 16
C.1 C.2 C.3 C.4 C.5	Top view of the aeraulic system, P&ID	20 21 22
D.1 D.2	Hydraulic P&ID of the GVR unit	
	X	

### Acronyms

CAPEX Capital Expenditures

CAPM Capital Asset Pricing Model

CAR Cogenarazione ad Alto Rendimento
CB Certificati Bianchi or White Certificates

CF Cash Flow

CHP Combined Heat and Power CWHP Carnot Waste Heat Potential

DCF Discounted Cash Flow DPBT Discounted Payback Time

ESCo Energy Service Company

EPC Engineering, Procurement, and Construction

GHG Greenhouse Gas

GSE Gestore dei Servizi Energetici

GVR Gas Vapour Recovery

HEC High Efficiency Cogeneration HRSG Heat Recovery Steam Generator

HX Heat Exchanger

IEA International Energy Agency

NPSH Net Positive Suction Head

NPV Net Present Value

OPEX Operational Expenditures

PBT Payback Time

PES Primary Energy Saving [%]

RISP — Risparmio di energia primaria [MWh]

SG Steam Generator

TEE — Titoli di Efficienza Energetica

toe tonnes of oil equivalent

WACC Weighted Average Cost of Capital

WHR Waste Heat Recovery

### Introduction

In 2023, the industrial sector consumed over 170 exajoules (EJ) of final energy, roughly 39% of total global energy demand. Between 2010 and 2023, industrial energy consumption increased by more than 5% per year in India and by about 2% in China, while it decreased on average by 1% annually in the European Union. Currently, China accounts for the largest share of global industrial energy use, exceeding the combined consumption of several major regions including the European Union, the United States, Southeast Asia, India, and Japan. This situation is illustrated in Figure 1, which presents a pie chart showing the global shares of energy consumption by sector and, specifically, the breakdown of industrial energy use by country [1, 2].

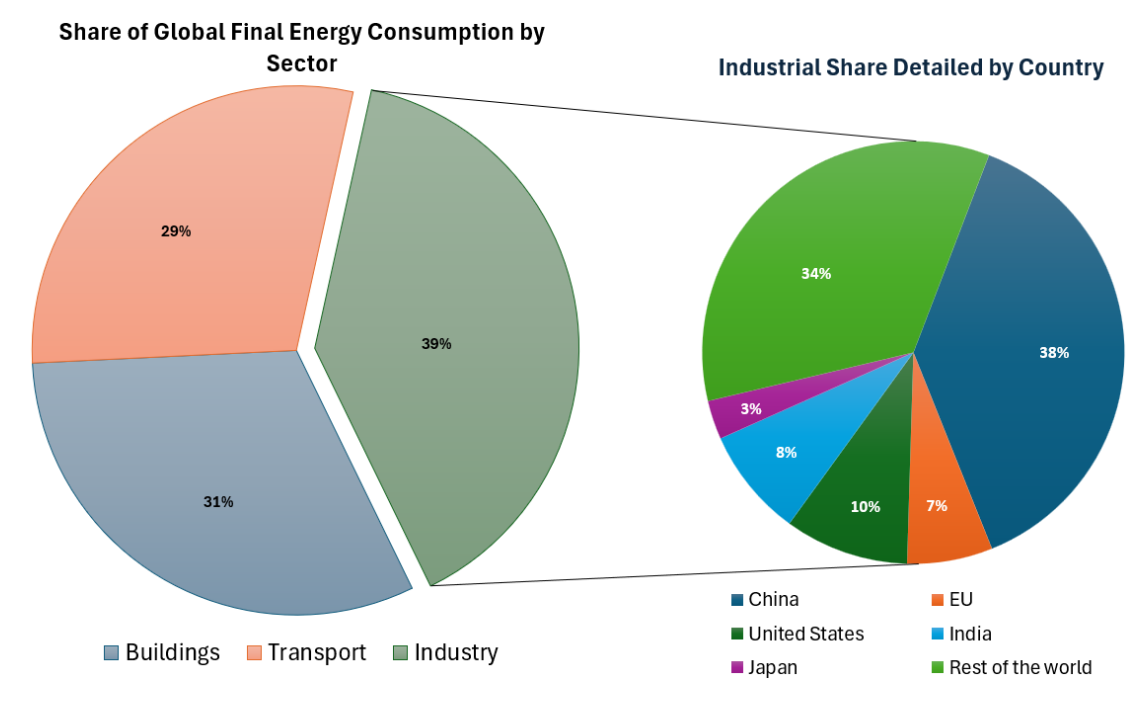


**Figure 1:** Global Final Energy Consumption by Sector with Industrial Share Breakdown by Country [3].

Within the EU, industry accounts for about 24.1% of final energy consumption and contributes approximately 34.1% of final  $CO_2$  emissions associated with energy use [4]. The European Union also contributes substantially to global greenhouse gas (GHG) emissions, ranking as the fourth-largest emitter in the world with a 7.1% share of global  $CO_2$  emissions. Figure 2 shows GHG emissions by country on a global scale [5].

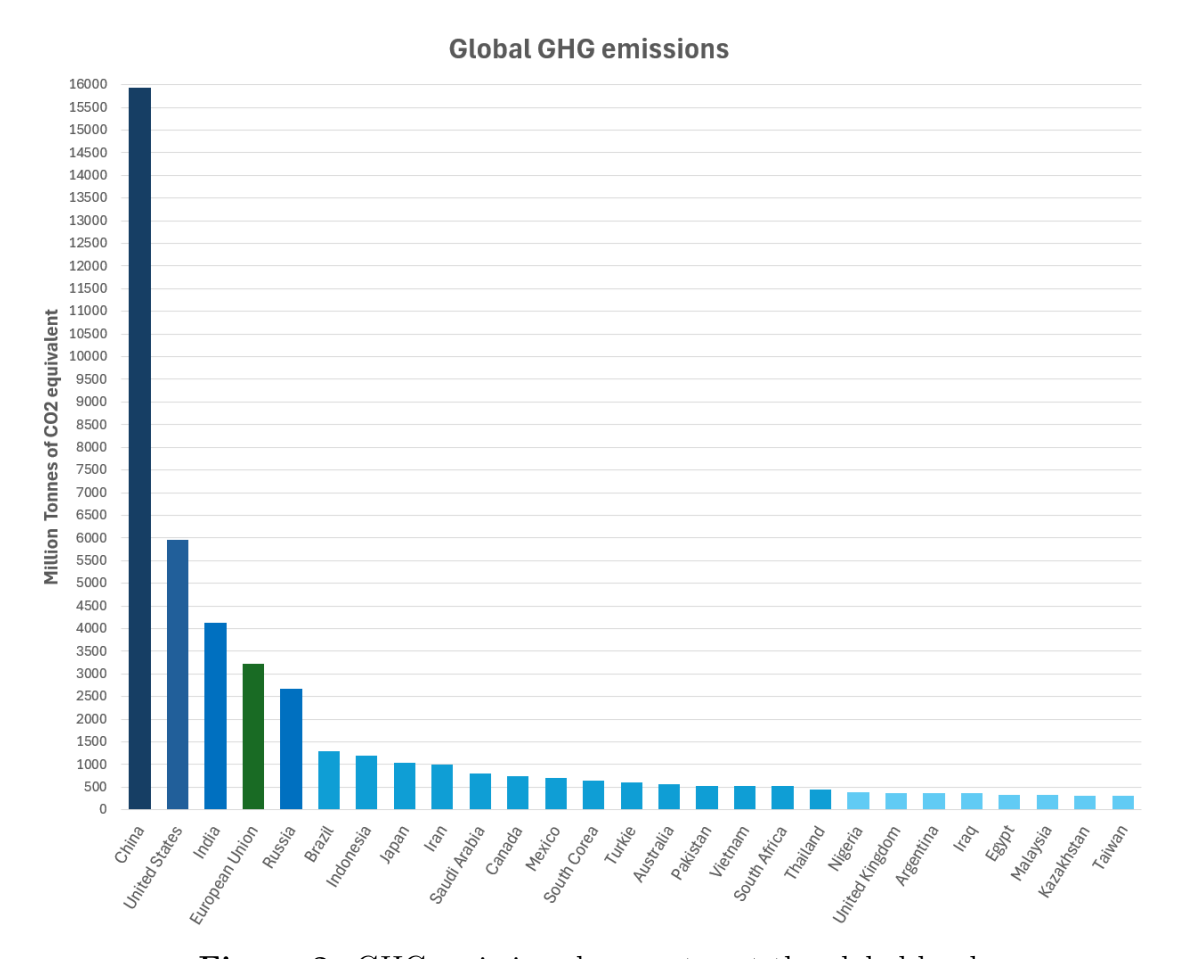


Figure 2: GHG emissions by country at the global level.

Within Europe, Italy is the third-largest emitter, responsible for approximately 12% of the EU's total  $CO_2$  emissions. Figure 4 shows GHG emissions by country within Europe.

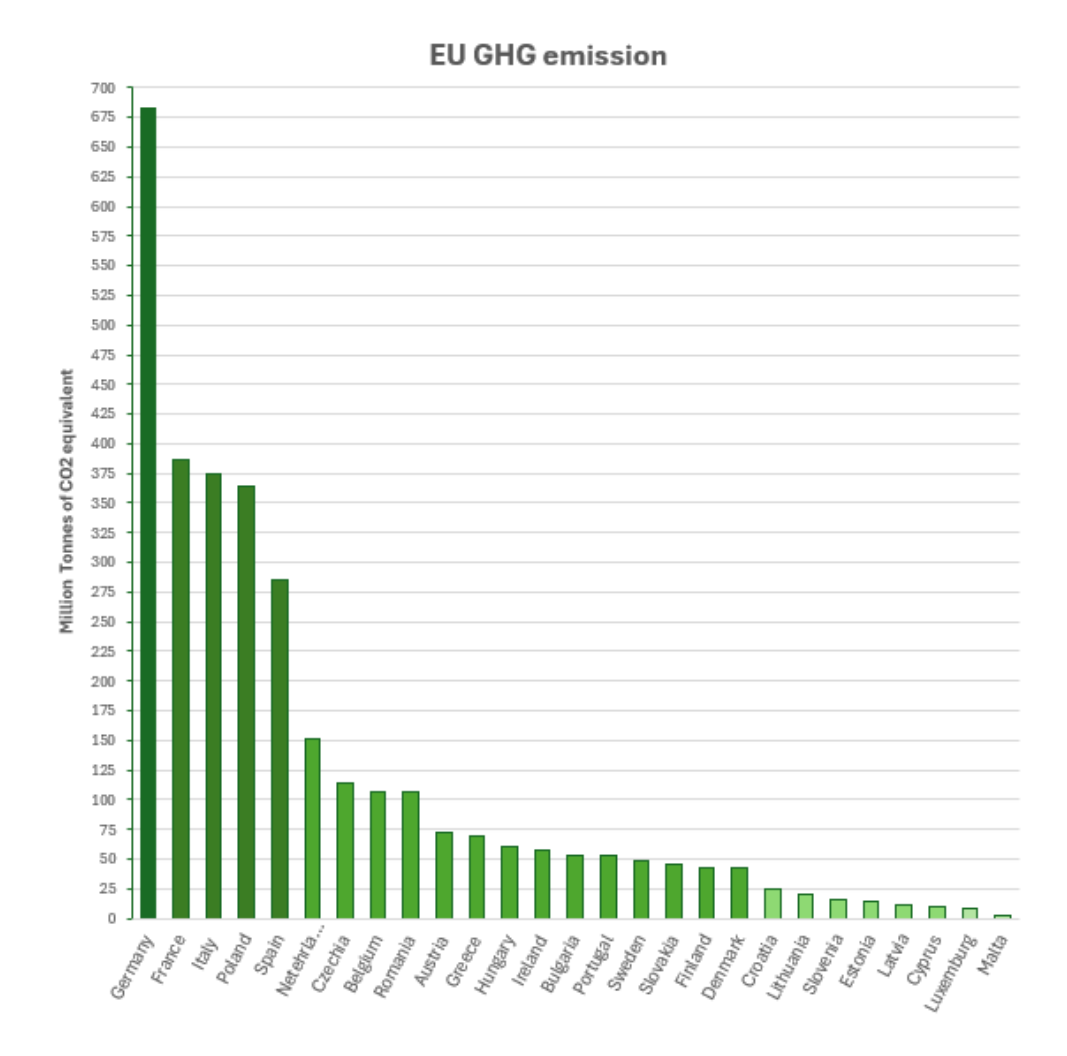


Figure 3: GHG emissions by country in the European Union.

In a context of rising energy consumption and the progressive depletion of fossil fuel reserves, the global energy landscape is becoming increasingly unstable and unsustainable. This scenario demands urgent action to transition toward cleaner and more resilient energy systems. The industrial sector, in particular, plays a critical role: it must drastically reduce its dependence on fossil fuels and minimize the environmental impact of its operations, especially in terms of greenhouse gas (GHG) emissions.

At the international level, the Paris Agreement [6] has become the cornerstone of global climate action. Its primary objective is to constrain the rise in global mean temperature to well below 2 °C above pre-industrial levels, while actively striving to limit the increase to 1.5 °C, in order to reduce the risks and impacts associated with global warming. To meet this goal, the European Union and many

other countries have adopted binding climate targets. The EU, for instance, has committed to:

- a net reduction of at least 55% in GHG emissions by 2030, compared to 1990 levels (European Commission. European Climate Law: Regulation (EU) 2021/1119) [7];
- achieving climate neutrality (net-zero emissions) by 2050, making this goal legally binding across all member states.

According to the International Energy Agency (IEA), meeting these and other key milestones is essential to keep the so-called "climate clock" from advancing unchecked [8]. The IEA's roadmap highlights the measures required to reduce greenhouse gas emissions, accelerate renewable energy adoption, and improve energy efficiency. Achieving these targets is crucial for slowing the pace of climate change and avoiding the most severe impacts of global warming. Without adhering to and succeeding in these critical milestones, the climate clock will continue ticking, pushing the world closer to irreversible environmental consequences. Therefore, committed and effective action is vital for mitigating climate change and safeguarding the future of our planet.



Figure 4: Climate Clock, September 2025.

Given that industry accounts for roughly 20–25% of global  $CO_2$  emissions [9], energy-intensive sectors such as chemicals, cement, steel, and food processing face mounting pressure to pursue rapid decarbonisation. This includes adopting circular economy practices, improving energy efficiency, and investing in low- or zero-carbon technologies. These legislative and policy frameworks provide a strong incentive for industrial transformation. They not only define environmental responsibility but also offer a strategic opportunity for industries to increase competitiveness, resilience, and alignment with future market and regulatory expectations.

Against this backdrop of ambitious policy targets and growing industrial energy demand, this thesis investigates how concrete interventions at plant level can contribute to both decarbonisation and cost savings. To address this challenge, industries typically pursue two main strategies:

- integrating renewable energy sources;
- reducing overall energy consumption.

However, in industrial settings, decision-making is often guided more by economic efficiency than by energy considerations. While improving energy efficiency doesn't always guarantee immediate financial returns, since some upgrades may require substantial investment, there are many interventions that can make a facility more energy efficient and also reduce costs over time. Although both strategic approaches hold value, they are not universally applicable.

The adoption of renewable energy is attractive due to its long-term sustainability and potential cost benefits, yet in many industrial contexts, renewables alone cannot meet total energy needs, and their initial installation remains costly. The second strategy, reducing energy demand, can be more widely applied and is typically achieved through better energy management and the recovery of waste energy already present within the system.

This master thesis investigates strategies to enhance energy efficiency in the industrial sector, integrating both technical and economic perspectives on energy optimisation. The analysis is conducted through a case study of a textile company, which, like many industrial facilities, relies heavily on both thermal energy and electricity to sustain its operations. The primary aim is to explore practical strategies for reducing energy consumption, improving operational efficiency, and lowering greenhouse gas emissions, thereby supporting the broader transition toward more sustainable industrial practices.

The first project focused on retrofitting the existing thermal power plant by replacing one of the old steam generator (SG) with a new unit equipped with an economizer, alongside the installation of a heat recovery system. In this configuration, a substantial share of the flue gas thermal energy was recovered and reused within the plant, significantly improving overall efficiency. The project encompassed the detailed design of the heat exchangers, evaluation of the system's thermal performance, and a comprehensive economic analysis to estimate cost savings and the expected payback period.

In a second phase, a CHP unit was implemented, also integrated with a heat recovery system. This system enabled the simultaneous generation of electricity and recovery of thermal energy from industrial processes, further improving the efficiency of the plant.

The outcomes of both projects were evaluated comprehensively in terms of energy performance, potential fuel savings, economic feasibility, and environmental benefits, including the reduction of greenhouse gas emissions. By combining these interventions, the thesis demonstrates a systematic approach to industrial energy optimization, providing insights into retrofit strategies while contributing to the academic discussion on sustainable energy management in industry.

### Chapter 1

## Cogeneration and Heat Recovery Overview

# 1.1 Combined Heat and Power (CHP): Principles, Policy, and Global Market Context

Cogeneration, also known as combined heat and power (CHP), is the simultaneous generation of electricity and useful heat within a single installation using one primary energy source. This integrated approach achieves much higher overall efficiency than the separate production of heat and power, because the heat from combustion, normally wasted in conventional plants, is recovered and utilized [10].

CHP systems are applied both in the industrial and civil sectors. In industry, they are often used for self-production, supplying steam or other heat-transfer fluids (such as hot or superheated water, diathermic oil or hot air) for manufacturing processes, while the generated electricity is either self-consumed or fed into the grid. In the civil sector, CHP provides heat at relatively low temperatures for space heating or district heating networks, and it can also support cooling through absorption systems.

Facilities with a steady demand for both thermal and electrical energy, such as hospitals, nursing homes, swimming pools, sports centers, shopping malls, food industries, paper mills, refineries, and chemical plants, are particularly well suited for cogeneration. In mixed-use cases, high-temperature heat is typically allocated to industrial processes, while lower-temperature heat is used for building heating within the same site [11].

As illustrated in Fig. 1.1, conventional power generation typically discards a large share of the fuel's energy content, with about 60% lost as waste heat and resulting net efficiencies close to 30% once transmission losses are included. In

comparison, cogeneration plants capture and repurpose this thermal energy, such as by supplying hot water or steam to nearby industries or buildings, so that a much larger fraction of the input fuel is put to productive use. This integrated approach can raise overall useful-energy utilization to roughly 65–90%, leaving only about 10–35% of the input energy as losses [12].

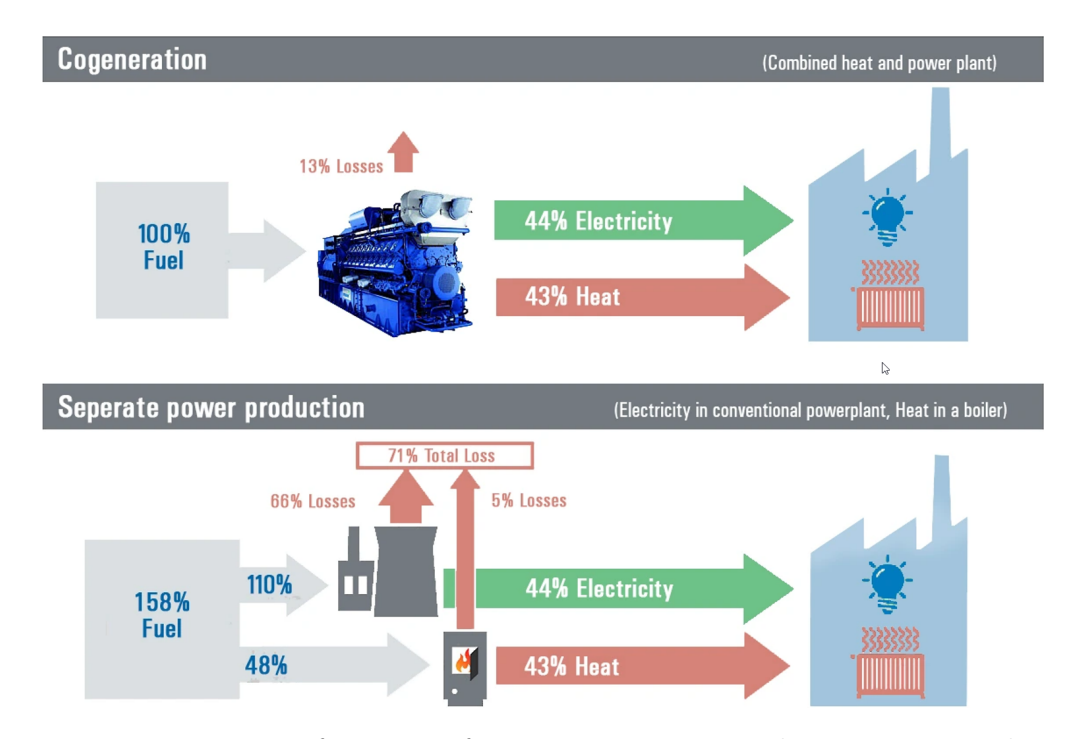


**Figure 1.1:** Energy performance of cogeneration compared to separate production of electricity and heat [13].

#### 1.1.1 Classification of Cogeneration Technologies

Cogeneration plants can be classified according to the sequence of energy use and the operating configuration adopted, as illustrated in the scheme shown in Fig. 1.2. Two main categories exist: *topping cycles* and *bottoming cycles* [14].

- ❖ Topping-cycle cogeneration: the fuel is first used to generate electrical or mechanical power. The waste heat from the prime mover is then recovered to supply process heat, steam, or hot water for industrial or district heating needs. This is the most common form of cogeneration.
  - Gas-turbine topping system: a gas turbine drives a generator; the hot exhaust gases pass through a heat recovery steam generator (HRSG) to produce process steam or heat.

- Combined-cycle topping system: a gas turbine generates power; its exhaust produces steam in a heat recovery boiler, which then drives a secondary steam turbine.
- Diesel or gas engine with heat recovery: engine exhaust and jacket-cooling heat are recovered in a heat recovery boiler to produce process steam or hot water for further use.
- Steam-turbine topping system: high-pressure steam produced by a boiler is expanded in a steam turbine to generate power; the exhaust low-pressure steam is used for process heating.
- ❖ Bottoming-cycle cogeneration: the primary fuel first produces hightemperature thermal energy for the industrial process. The waste heat from the process is then recovered, typically in a heat recovery boiler, to produce steam, which drives a turbine-generator to produce power.
  - Typical applications Cement production, steel plants, glass and ceramics manufacturing, petrochemical processes.
  - Typical configuration High-temperature process waste heat is recovered
    in a boiler that feeds a secondary power cycle, which can be implemented
    as:
    - Steam Rankine Cycle (SRC) uses water as working fluid; requires waste heat temperatures above 260 °C.
    - Organic Rankine Cycle (ORC) employs organic fluids with lower boiling points; suitable for sources down to ∼150 °C; provides higher turbine efficiency than SRC under these conditions.

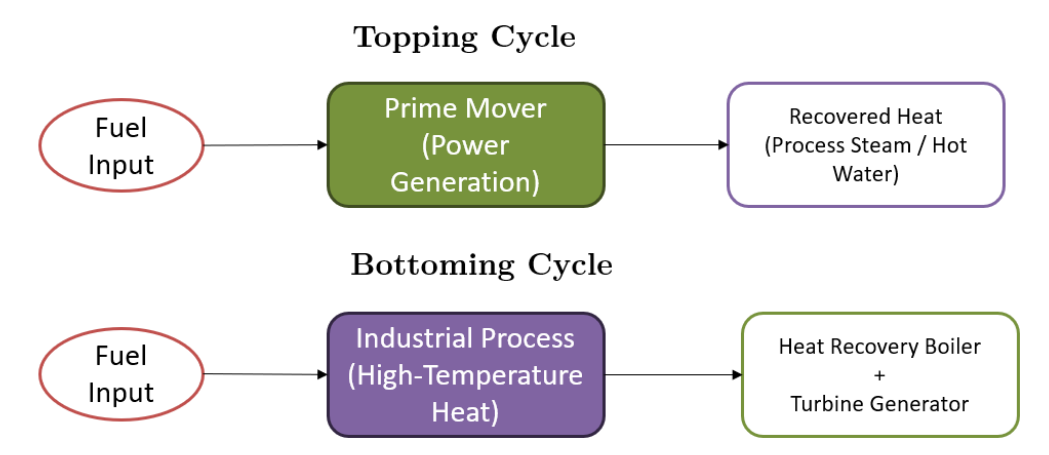


**Figure 1.2:** Energy flow schematics for topping and bottoming cycle cogeneration systems.

Some cogeneration plants also utilise biomass sourced from industrial residues or municipal solid waste. These are generally referred to as *biomass cogeneration systems*.

#### 1.1.2 High-Efficiency Cogeneration

At the European level, the Energy Efficiency Directive (Directive 2012/27/EU) [10] establishes the criteria for *High-Efficiency Cogeneration (HEC)*. According to this framework, a cogeneration plant qualifies as high-efficiency if it achieves primary energy savings, calculated in accordance with Annex II of the Directive, compared to the separate production of electricity and heat using reference values specified in Commission Delegated Regulation (EU) 2015/2402 — Annex I for separate electricity production and Annex II for separate heat production [15]. In practical terms:

- the output from cogeneration units must achieve at least 10% primary energy savings compared with the reference values for separate production of heat and electricity.
- small-scale and micro-cogeneration units that deliver measurable primary energy savings may also be classified as high-efficiency cogeneration systems.

In Italy, these European provisions have been transposed into national legislation (for instance, Legislative Decree 20/2007 implementing Directive 2004/8/EC) and operationalised through incentive schemes such as White Certificates for plants officially recognised as *Cogenerazione ad Alto Rendimento (CAR)* [16].

Globally, heat generation represents a major share of final energy consumption, exceeding 50% of the total. Unlike overall energy use per person, which differs widely across regions, per capita heat demand is relatively uniform, emphasizing the universal significance of this sector. Nevertheless, the heating sector often receives comparatively little attention in energy policy and research, especially when compared to electricity and transport.

## 1.1.3 Global CHP Market Dynamics and Operational Characteristics

Combined heat and power (CHP) systems are widely deployed across the world, with varying degrees of maturity and growth depending on the region. The following overview highlights current market characteristics and projected trends, focusing on key aspects such as geography, technology, fuel, unit size, and end-user sectors [17].

Market trends: Asia-Pacific leads global CHP deployment and continues to expand rapidly, while Europe and North America are mature markets with limited growth. Future expansion is expected in Asia and South America, whereas Western markets may stagnate or contract due to high fuel costs and tighter emission regulations.

**Technology Landscape:** Gas and steam turbines are the established and dominant CHP technologies, widely deployed as large units across the industrial sector. Looking ahead, fuel cells are expected to see significant growth. Their adoption will initially focus on micro-CHP systems for the residential and commercial sectors, with larger-scale installations also emerging, particularly in countries like the US, Japan, and South Korea.

Fuel Sources and Regional Variation: Globally, the CHP sector primarily relies on coal and natural gas, with biofuels and waste contributing only marginally. The long-term trend involves a gradual shift to cleaner sources: natural gas is expected to remain central, renewables will see moderate expansion, and hydrogen use is anticipated to increase, particularly with the growth of fuel cell technology. A key regional distinction is illustrated in Figure 1.3. While coal still dominates the global CHP fuel mix, European data shows an inverse trend: strict environmental policies have prioritized natural gas, giving it a higher share than coal. Europe also demonstrates a proportionally higher share of biofuels.

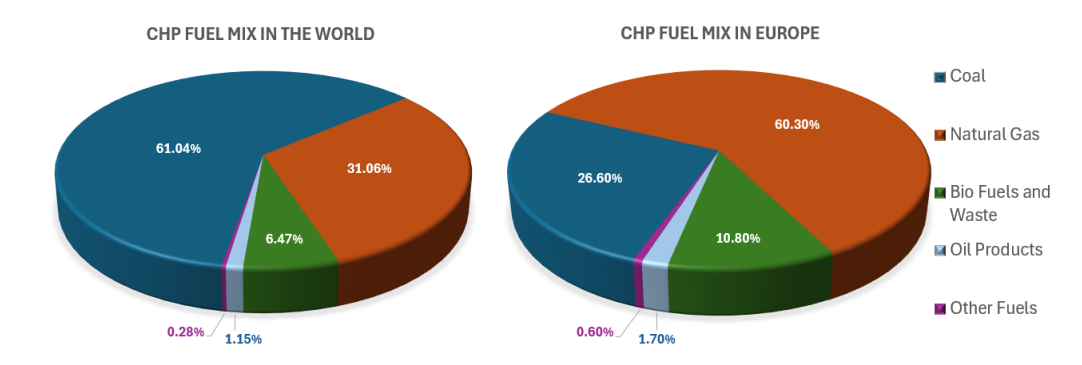


Figure 1.3: Fuel Mix Breakdown for Global and European CHP systems [17].

Size and End Users: Large-capacity CHP units dominate industrial sectors such as refineries, chemical plants, pulp and paper, and food and beverage industries. Smaller units (up to 10 MW), including micro-CHP, are increasingly used in commercial and residential applications like hospitals, universities, district heating, and data centers, providing on-site power, local distribution, or grid/district heating integration.

Drawing upon statistics provided by the International Energy Agency (IEA) and Eurostat, an analysis of Combined Heat and Power (CHP) systems reveals substantial global and regional contributions.

Globally, CHP plants generated an estimated 4,398 TWh of electricity and nearly 12,642 TWh of thermal energy in 2021. This generation represents approximately 16% of the total world electricity output, as detailed in Figure 1.4.

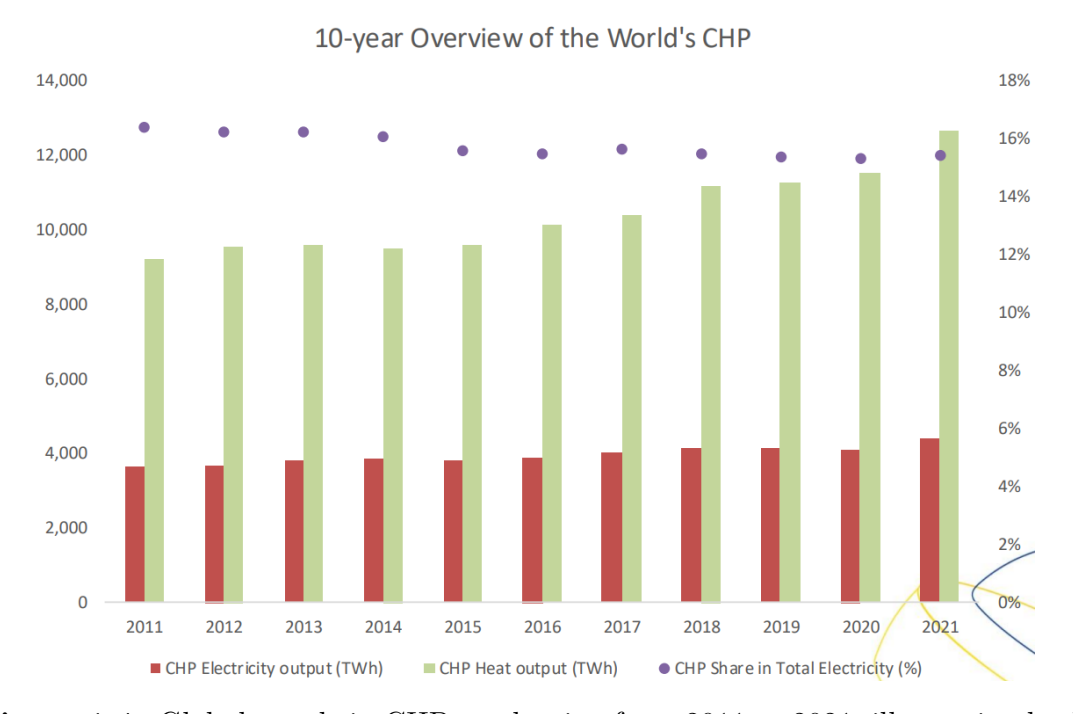


Figure 1.4: Global trends in CHP production from 2011 to 2021, illustrating both electric and thermal output [17].

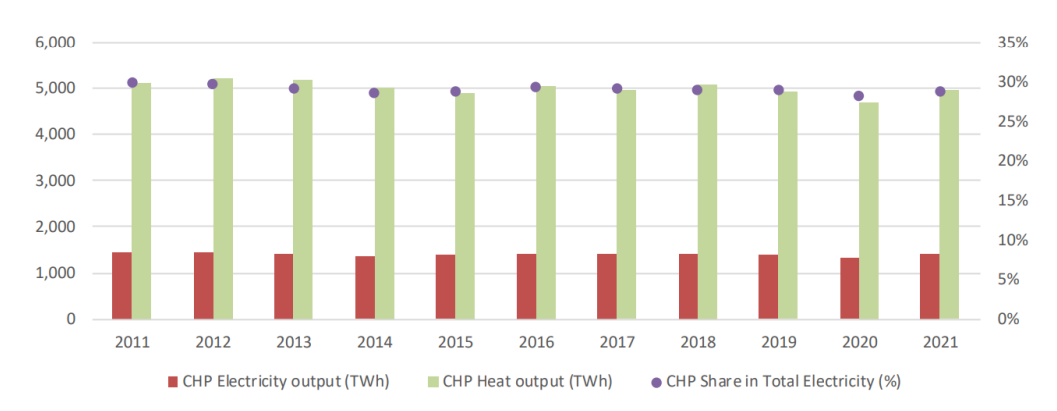


Figure 1.5: European trends in CHP production from 2011 to 2021, illustrating both electric and thermal output [17].

The contribution of CHP to Europe's energy system is dramatically higher than the global average. The share of CHP in Europe's total electricity generation reaches up to 29%, almost double the worldwide figure. This significant differential highlights Europe's vital role in leveraging high-efficiency cogeneration for enhanced energy efficiency and the mitigation of environmental impacts, a trend further illustrated in Figure 1.5.

A detailed examination of regional output, as illustrated in Figure 1.6, based on Eurostat data [18], highlights the varied adoption of Combined Heat and Power (CHP) technologies across the EU-27.

Italy stands out as a significant contributor, securing the third-highest rank in gross CHP electricity production, following only Germany and Poland. Italy's substantial output, typically contributing around 14% to the total European CHP electricity generation, firmly establishes the country as a major proponent of cogeneration technologies on the continent. This position is further solidified by the country's proactive policies supporting biogenic fuels: Italy is the European Union's second-largest producer of biogases after Germany and has shown rapid growth owing to effective incentives. The country supports biogas-based electricity production in CHP plants through a feed-in-tariff system, primarily utilizing agricultural residues as feedstock [19].

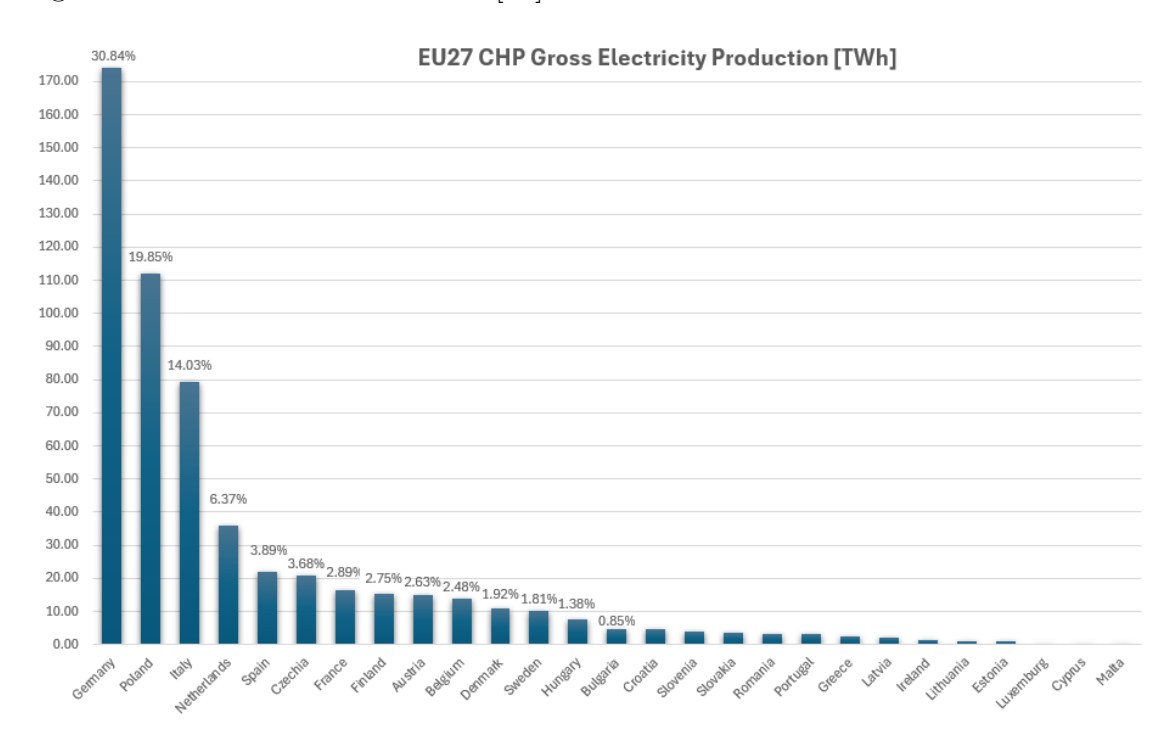


Figure 1.6: CHP Gross Electricity Production (EU-27) [18].

In conclusion, the strong performance of key member states like Italy underscores

that CHP systems are instrumental in the transition towards a more sustainable and efficient energy landscape, confirming their critical importance in both global and European contexts.

# 1.2 Heat Recovery Systems: Concepts, Framework, and Sectoral Distribution

Industrial waste heat refers to thermal energy produced as a byproduct during manufacturing and processing activities that is not harnessed for productive purpose.

This heat can originate from various sources, including:

- high-temperature exhaust gases from combustion processes;
- heat dissipated from the surfaces of equipment and machinery;
- hot materials discharged directly from production lines.

The sheer scale of this energy loss is significant. Estimates suggest that between 20% and 50% of total industrial energy input is ultimately lost as waste heat [20]. Crucially, studies indicate that an estimated 18% to 30% of this wasted thermal energy is technically recoverable, presenting a major opportunity to boost industrial energy efficiency [21].

These losses, though partly unavoidable, can be significantly reduced through improved equipment efficiency and the implementation of waste heat recovery (WHR) technologies. WHR captures unused thermal energy and redirects it for beneficial use within the facility. Common applications for this recovered heat include:

- generating electricity;
- preheating combustion air or process fluids;
- driving absorption chillers for cooling;
- providing facility or space heating.

By deploying WHR systems, industries can significantly lower their fuel consumption, reduce their overall energy demand, cut emissions, and make a vital move toward greater energy security and sustainability.

#### 1.2.1 Classification of Waste Heat

In industrial energy conversion, a significant portion of the input energy is not converted into useful services but is instead discharged as exhaust gases, effluents, or other forms of thermal loss. Much of this waste heat retains valuable energy potential that can be recovered, thereby increasing overall process efficiency. Losses due to irreversibilities, friction, radiation, or chemical inefficiencies, however, are generally non-recoverable [22].

Conceptually, the wasted energy can be recovered through two main strategies:

- process-integrated recovery: the energy is reused directly within the same process (e.g. preheating incoming fluids with outgoing hot gases);
- facility-wide energy recovery: waste energy is captured within a facility and redistributed for use elsewhere within the site or to external networks, such as district heating or electricity grids.

In the industrial sector, according to studies reported in [22], only 49% of the total energy input is effectively converted into energy services, while the remaining 51% is lost. Of these losses, approximately 30% are attributed to exhaust and effluents, and 21% to other losses. Since the exhaust and effluent losses are the losses that can be partially recovered, these represent the primary focus of Waste Heat Recovery (WHR) strategies.

To accurately quantify the amount of waste heat available, it is essential to complement the analysis with a qualitative assessment, as not all heat holds the same thermodynamic potential. For this purpose, Table 1.1 summarizes the classification of waste heat sources according to their temperature level, the typical distribution of recoverable exhaust and effluent losses in industrial processes, as well as the main sources and possible recovery applications [22, 23].

Temperature Class	Typical Share	Typical Sources	Recovery Potential & Application
High-Temperature $T > 300^{\circ}C$	38%	Furnaces, kilns, incinerators, and flares	High potential for recovery and reuse in other processes or for power generation
Medium-Temperature $100^{\circ}\text{C} < \text{T} < 300^{\circ}\text{C}$	20%	Exhaust gases from engines, dryers, and similar equipment	Heating, preheating, or low-grade power generation
Low-Temperature $T < 100$ °C	42%	Heat from cooling water or low-grade exhaust	Preheating or low-temperature drying

**Table 1.1:** Classification of waste heat sources by temperature level, typical distribution of recoverable industrial losses, and corresponding sources and applications.

To provide a broader perspective, Figure 1.7 illustrates the estimated global waste heat distribution, starting from primary energy carriers and tracing the flows through electricity generation and the main end-use sectors: transportation, industrial, residential, and commercial. For each sector, the diagram further distinguishes the fraction of energy effectively used for energy services, the share of exhaust and effluent losses (subdivided into the three temperature classes defined above), and other losses, thereby highlighting both the magnitude and quality of the recoverable waste heat.

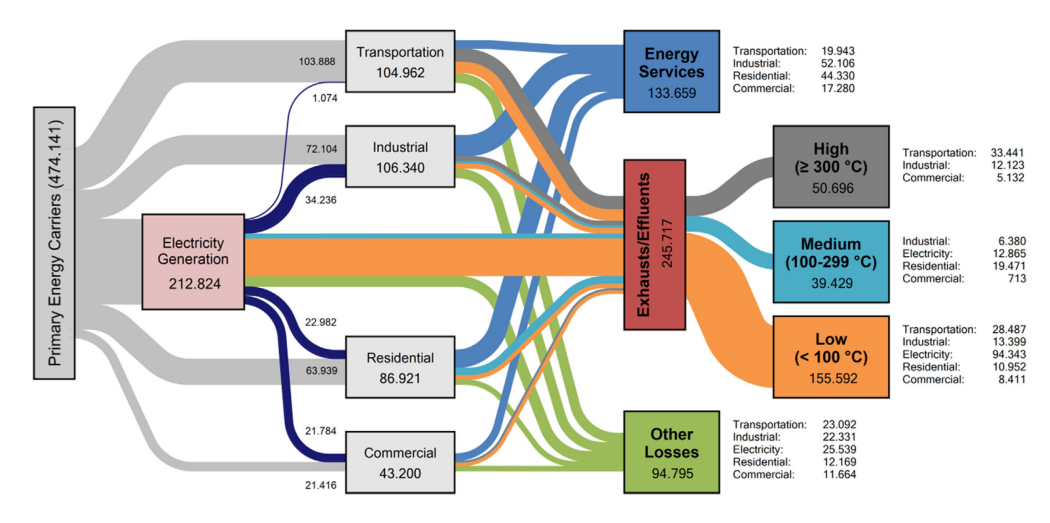


**Figure 1.7:** Estimated global waste heat distribution of 2012 in PJ, according to a theoretical approach, showing energy flows from primary energy sources through sectors and losses [22].

## 1.2.2 Framework for Waste Heat Recovery Potential Assessment

In the context of industrial energy systems, the principle of energy conservation must be complemented by an assessment of energy quality, typically expressed through exergy. Exergy is defined as the maximum useful work that can be obtained as a system comes into equilibrium with its environment, and it is always degraded in real processes due to irreversibilities. From a thermodynamic standpoint, any energy quantity can be expressed as the sum of exergy and anergy [23]:

- exergy represents the fraction that can be fully converted into mechanical work;
- anergy corresponds to the portion suitable only for providing internal heat.

Low-temperature waste heat, which is widespread in industrial processes, generally has a low exergy content. Converting such low-grade heat into mechanical work

or electricity involves significant irreversibilities and yields very low efficiencies, as dictated by the Carnot limit. This thermodynamic inefficiency often makes such recovery economically and energetically unjustifiable.

Estimating the Waste Heat Recovery Potential (WHRP) across industrial sectors requires a structured approach that moves from theoretical maximums to practical, economic realities. The methodology outlined here provides a robust framework for assessing this potential, primarily across EU industrial sectors.

Several studies have investigated the quantification of waste heat recovery potential (WHRP) and its environmental benefits.

For instance, one notable global assessment applies the Carnot efficiency to emissions from the power generation, transportation, and construction sectors [22]. This thermodynamic benchmark allows researchers to evaluate the maximum potential emission reductions achievable if the theoretical recovery of waste heat were fully realized.

However, the WHRP analysis must move beyond this fundamental theoretical physical potential. To provide a practical estimate, the assessment must address technical and economic constraints.

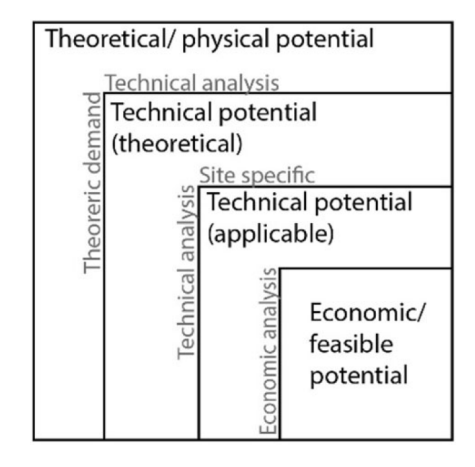


Figure 1.8: Classification framework of WHP categories as proposed by Forman et al. [23].

The evaluation of WHRP is therefore typically broken down into progressively constrained categories, as represented schematically in Figure 1.8, following the model developed by Forman and Brückner et al. [23, 24]. The figure outlines the hierarchical structure across four levels, which are further explained in the following section.

Theoretical Physical Potential It considers only physical constraints and represents the maximum recoverable heat if all waste heat could be perfectly converted into useful work without losses, without considering whether heat can be extracted from the carrier or reused.

**Technical Work Potential** It assesses the recoverable work by incorporating real-world constraints, which is further divided into two subcategories.

I. Theoretical Technical Potential: estimates the maximum recoverable work from industrial waste heat streams by applying the Carnot efficiency, which

fundamentally dictates the quality, or exergy content, of the heat. The Carnot factor links the recoverable work to the temperature difference between the heat source  $(T_{high})$  and the receiving sink  $(T_{low})$  (often the environment) [25, 26].

$$\eta_{\text{Carnot}} = 1 - \frac{T_{\text{low}}}{T_{\text{high}}}$$
(1.1)

Then, the Carnot potential is applied to the theoretical waste heat amount (WHRP), providing a more realistic estimate of the maximum useful work extractable from the waste heat, and thus represents the Theoretical Technical Potential:

$$CWHRP = WHRP \cdot \eta_C \tag{1.2}$$

Applying this factor significantly reduces the estimated recovery potential across all sectors (Fig. 1.9), primarily because low-grade waste heat represents the largest share and therefore lowers the overall quality of the available heat [22].

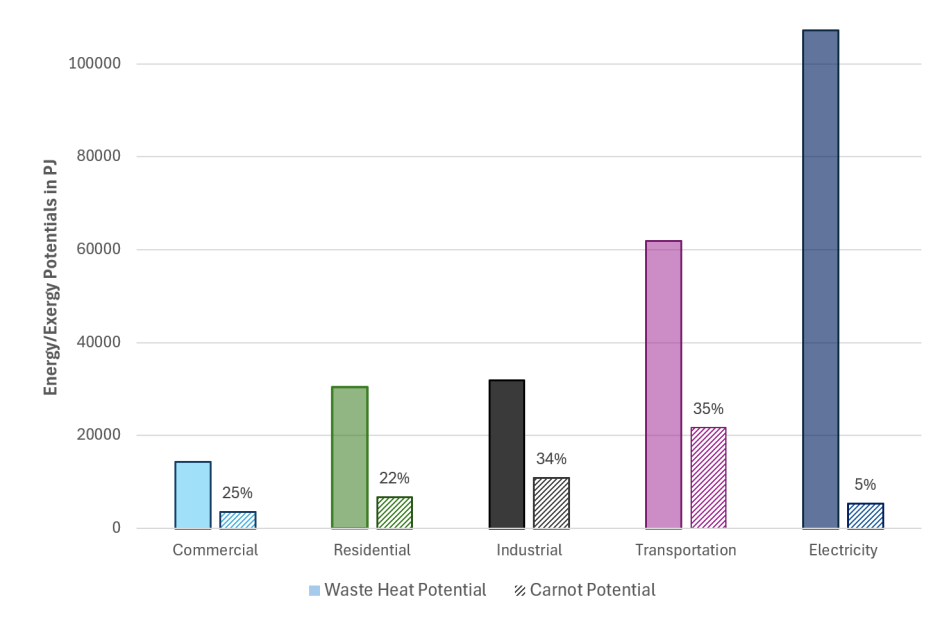


Figure 1.9: Waste Heat and Carnot's potential by sector [22].

In industrial settings, the available potential is reduced to approximately 34% of the initial theoretical physical potential. A detailed breakdown by temperature confirms this quality shift:

• low-grade waste heat drops from 42% of the theoretical physical potential to only 17% of the CWHP;

• high-grade waste heat dramatically increases its relative importance, rising from 38% of the theoretical physical potential to 63% of the exergy potential (CWHP), reflecting its superior thermodynamic quality.

Figure 1.10 illustrates how the share of waste heat shifts between temperature levels when transitioning from the physical to the technical potential.

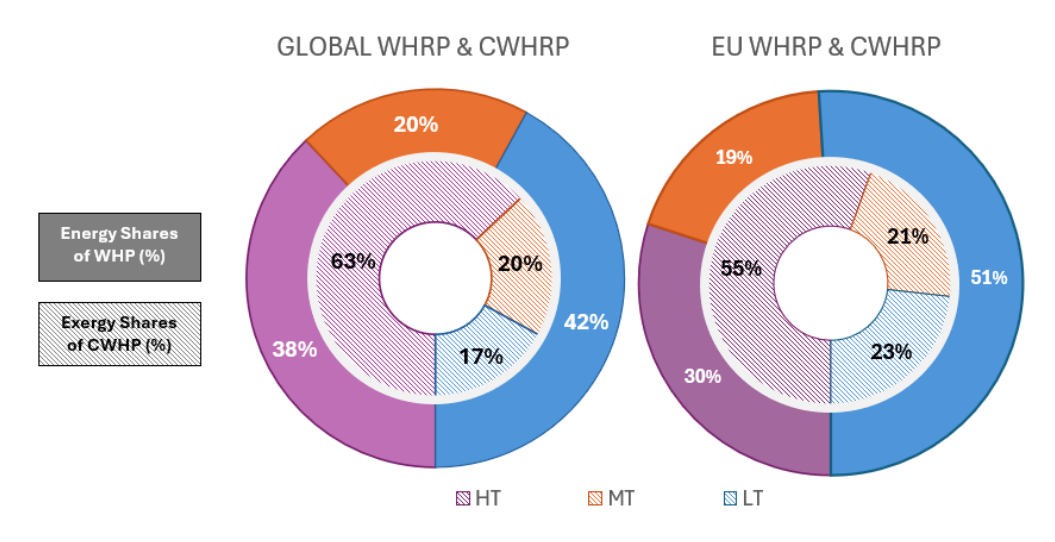


**Figure 1.10:** Global and EU industrial shares of WHP and CWHP distributions [22, 23].

The EU industrial sector's Waste Heat Recovery Potential (WHRP) largely follows the global pattern. As illustrated in Figure 1.10, the EU's theoretical potential is similarly dominated by Low-Temperature (LT) sources, which shift dramatically in importance once the Carnot efficiency is applied. While the overall trend is consistent, the EU exhibits a slightly greater proportion of LT waste heat, leading to a marginally lower share for High-Temperature (HT) sources in the final CWHRP estimate [23].

II. Applicable Technical Potential: further narrows the recovery fraction by accounting for technology-specific boundary conditions. This step is critical because it introduces the limitations imposed by the real performance, efficiency, and operational constraints of the specific Waste Heat Recovery (WHR) technology chosen for implementation.

**Economic Potential** This final and most restrictive level represents the fraction of waste heat that is technically applicable and financially viable. Assessing the Economic Potential requires a comprehensive financial analysis, taking into account:

- Capital and Operational Costs: the required investment for the recovery technology;
- Payback Time: the period required to recover the initial investment through energy savings and available incentives;
- Market Conditions concerning prevailing energy prices and available financial mechanisms (e.g., subsidies, tax breaks, or White Certificates).

In practice, waste heat recovery faces several technical and financial challenges. Temperature mismatches, temporal and spatial differences between supply and demand, and process-specific factors, such as corrosive flue gases, often limit recoverable potential. Financial barriers, including high capital costs, long payback periods, and market uncertainties, further restrict implementation.

Exergoeconomic analysis provides a valuable framework to evaluate potential recovery strategies, combining thermodynamic efficiency with economic feasibility to identify cost-effective solutions. From a thermodynamic perspective, the most effective use of low-grade waste heat is in applications that match its temperature, such as process heating or district heating, rather than converting it to electricity. This approach reduces energy losses, maximizes efficiency, and makes the most of the available thermal resource [23, 24].

#### 1.2.3 Waste Heat Recovery in Energy-Intensive Industries: Opportunities, Limitations, and Key Considerations

In industrial sectors such as food and tobacco processing, as well as the production of paper, chemicals, and polymers, the nature of the processes allows for the recovery of low-grade heat. These industries often involve high-temperature operations, such as combustion, calcination, or chemical reactions, followed by stages that require medium- or low-temperature heat, including drying, preheating, or washing. This simultaneous presence of heat sources and demands at different temperature levels within the same facility creates favourable conditions for internal heat integration. As a result, implementing energy recovery systems becomes both technically feasible and economically advantageous.

Conversely, industries like glass, iron, and steel manufacturing predominantly operate at very high process temperatures and generate waste heat primarily in the form of high-temperature flue gases. These sectors often lack internal processes that require low- or medium-grade heat, thus limiting the potential for direct internal heat recovery at lower temperature levels. However, part of the high-grade waste heat can still be recovered and reused internally, for instance, for preheating combustion air or raw materials. Moreover, excess high-temperature heat can be exploited externally through technologies such as the Organic Rankine Cycle

(ORC), which converts thermal energy into electricity using working fluids with low boiling points [27].

Alternatively, with suitable heat exchange systems, this thermal energy can be downgraded and supplied to district heating networks, contributing to broader decarbonization and energy efficiency goals.

Despite these opportunities, several technical and economic challenges hinder widespread WHR in the glass and steel industries. A key issue is the high contamination of exhaust gases, particularly those originating from blast furnaces, coke ovens, basic oxygen furnaces (BOFs), and electric arc furnaces (EAFs), which often contain corrosive compounds and particulates. Effective heat recovery from such streams necessitates corrosion-resistant equipment alongside sophisticated gas cleaning systems, resulting in high capital costs. Furthermore, production rates in these sectors typically fluctuate between 70% and 100% of the nominal plant capacity, introducing intermittency in waste heat availability. These fluctuations can lead to operational instability, thermal cycling, and increased corrosion risks, particularly under off-design conditions. As a result, system efficiency may be compromised, and the variability in energy output can lead to longer payback periods, thereby undermining the economic viability of heat recovery investments in these industries.

In conclusion, the feasibility and effectiveness of heat recovery systems depend on a wide range of parameters that must be carefully evaluated for each specific industrial context. Key factors include the type of industry, the grade of thermal energy available for recovery, and the extent to which this energy can be internally exploited. Additionally, the quality of the waste heat, particularly the presence of contaminants in flue gases, plays a critical role in determining the complexity and cost of recovery technologies. Economic considerations, such as capital investment, system efficiency under variable operating conditions, and expected payback periods, further influence the practicality of implementation. Therefore, a case-by-case assessment is essential to identify the most suitable heat recovery strategies and to ensure their technical and economic viability.

## Chapter 2

# Heat Recovery System Test Case

The case study concerns a textile company located in the Como district, known for its long tradition in high-quality fabric production. In line with its sustainability goals, the company recently upgraded its thermal power plant, replacing one of the two steam generators and installing an innovative heat recovery system. This system captures flue gas waste heat and reuses it for heating replenishment tanks and washing water, thereby reducing natural gas consumption.

As part of the same optimization strategy, a cogeneration system was later integrated into the facility. It generates electricity, significantly reducing dependence on the grid, and recovers heat from multiple sources. The engine jacket cooling supplies low-temperature heat for washing water, while the flue gases are exploited through a Gas Vapour Recovery (GVR) unit to produce 10-bar steam. This reduces the steam demand from the thermal power station, lowering fuel consumption and enhancing overall efficiency. Downstream of the GVR, a second recovery stage is implemented to preheat the feed water tank, further improving the plant's efficiency.

This chapter explores the technical aspects of the intervention, focusing on both the retrofitting of the factory's thermal power station and the integration of the cogeneration unit with the heat recovery systems. Particular attention is given to the processes by which thermal energy is captured and reused, ranging from flue gas heat exchangers to steam generation and water preheating. The overall upgrade, which combines the replacement of the steam generator, the installation of advanced heat recovery solutions, and the implementation of a cogeneration system, delivers substantial energy savings, improved operational performance, and a marked reduction in environmental impact, reinforcing M.'s strong commitment to sustainability.

## 2.1 Pre-intervention Thermal Power Plant

The following analysis presents a simplified overview of the original thermal power plant layout, highlighting both the water-steam and flue gas circuits. Figure 2.1 illustrates the overall configuration of the system before the retrofit.

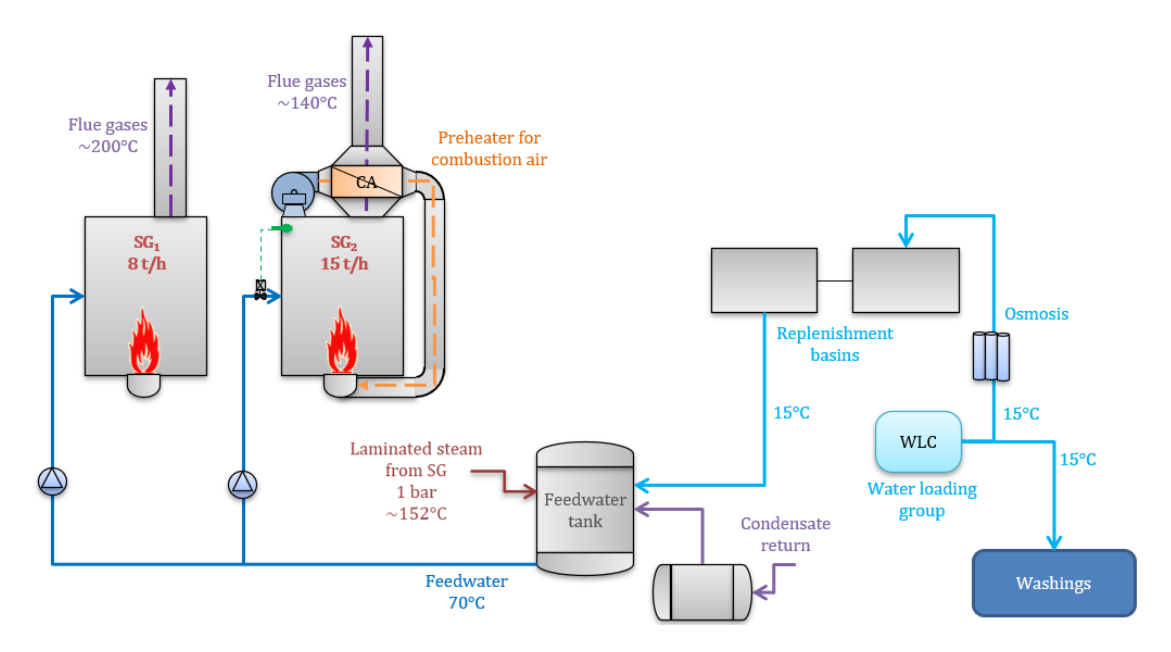


Figure 2.1: Pre-intervention thermal power plant scheme.

The thermal power plant comprehend two steam generators:

- **SG**<sub>1</sub> with a nominal capacity of 8 t/h for steam production. This generator is non-priority and serves as a back-up;
- **SG**<sub>2</sub> with a nominal capacity of 15 t/h for steam production. This steam generator is provided of a preheater for combustion air that exploits flue gas to preheat the combustion air before it enters the combustion chamber in order to enhance thermal efficiency, this generator is the priority one.

Both steam generators are supplied with feed water at 70 °C, which is drawn from the feed water tank. The feed water tank is replenished by two sources:

- water from the condensate return tank, typically at 90 °C, which collects condensate from steam distribution system;
- makeup water from the atmospheric replenishment basins, which is supplied at 15 °C. Before entering the basins, this water undergoes a rigorous osmosis

process to ensure it meets the strict purity standards required for boiler feed water.

According to the data provided by the company, it is estimated that the condensate return accounts for approximately 20% of the total feed water exiting the tank, while the remaining 80% consists of makeup water and steam injected from the steam generator. Thus, part of the generated steam is recirculated into the feed water tank to raise its temperature to 70 °C. This steam injection process ensures efficient preheating of the feed water before it is pumped to the steam generators.

An average steam demand of 7 t/h for end-use applications is assumed as the basis for the preliminary data analysis. To meet this demand, the plant must generate around 7.5 t/h of steam, as part of the steam is recirculated. In this scenario, the priority steam generator  $(SG_2)$  is expected to operate at approximately 50% of its nominal capacity, corresponding to a steam production rate of 7.5 t/h.

The amount of steam required to achieve the desired temperature (70 °C) in the feed water tank can be calculated, taking into account both its inflows and outflows (Fig. 2.2):

- condensate return entering at around 90 °C;
- water from replenishment basins entering at Steam from SG 15 °C;
- steam produced by SG at 11 bar, laminated to atmospheric pressure and injected in the feed water tank;

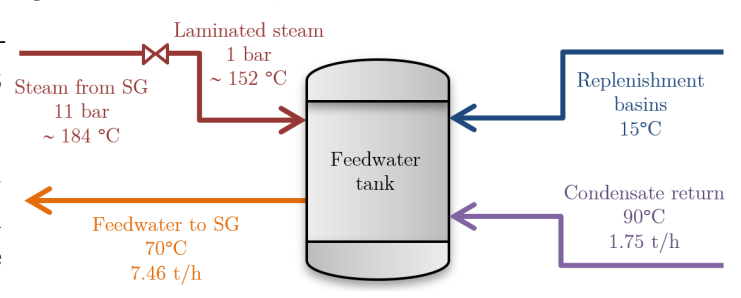


Figure 2.2: Input and output feedwater tank.

• feed water exiting the feed water tank at 70 °C and pumped up to the steam generator.

By applying the principles of energy and mass balance and solving the corresponding system of equations (2.1), considering the specifications outlined in Table 2.1 and the definitions below, it will be possible to estimate the steam recirculated.

$$\begin{cases}
G_1 = 0.2 \cdot (G_1 + G_2 + G_s) \\
G_1 + G_2 = G_u \\
Q_1 = G_s \cdot [(h_{ss} - h_s) + r + c_p \cdot (T_s - T_o)] \\
Q_2 = G_1 \cdot c_p \cdot (T_1 - T_o) \\
Q_3 = G_2 \cdot c_p \cdot (T_2 - T_o) \\
Q_1 + Q_2 = |Q_3|
\end{cases}$$
(2.1)

Condensate return							
	$G_1$	$20\%~\mathrm{G}_\mathrm{O}$					
$ m p_{atm}$	$\mathrm{T}_1$	90 °C					
Water from re	Water from replenishment basins						
	$G_2$	unknown					
$ m p_{atm}$	$T_2$	15 °C					
Stean	n fron	n SG					
	Gs	unknown					
p = 11  bar	Т	184 °C					
	$h_{\rm s}$	2780.50  kJ/kg					
	$T_{\mathrm{ss}}$	152 °C					
	$h_{ss}$	$2780.50~\mathrm{kJ/kg}$					
$ m p_{atm}$	$h_{\rm s}$	$2675.53~\mathrm{kJ/kg}$					
	$h_l$	418.99  kJ/kg					
	r	$2256.54~\mathrm{kJ/kg}$					
Feedwater to SG							
	$G_{O}$	2.43  kg/s					
$ m p_{atm}$	$T_{\mathrm{O}}$	70 °C					

Table 2.1: Preliminary data.

- $Q_1$  heat released by superheated steam as it undergoes three phases:
  - desuperheating: cooling down to the saturation temperature  $T_s$ ;
  - condensation: transitioning from saturated steam to saturated liquid;
  - subcooling: further cooling until the final temperature  $T_o$  is reached.
- $T_{ss}, h_{ss}$  temperature and enthalpy of superheated steam at  $p_{atm}$ .
- $T_s, h_s$  temperature and enthalpy of saturated dry steam at  $p_{atm}$ .
- $h_l$  enthalpy of saturated liquid at  $p_{atm}$ .
- r latent heat of vaporization at  $p_{atm}$ .

• the amount of steam produced and recirculated;

- the amount of water from the replenishment basins and the condensate return;
- the natural gas consumption;
- the flue gas flow rate.

This analysis will yield:

These results provide a comprehensive understanding of the plant's performance under the given operating conditions and are summarized in Table 2.2.

Conden	Condensate return				
$G_1$	$\sim 1.49 \; \mathrm{t/h}$				
Water from rep	Water from replenishment basins				
$G_2$	$\sim 5.51 \text{ t/h}$				
Steam injected i	n the feedwater tank				
$ G_{\rm s}$	$\sim 0.46~\mathrm{t/h}$				
Feedwater to SG					
$G_{o}$	$\sim 7.46~\mathrm{t/h}$				

**Table 2.2:** Mass flow rates results entering and exiting the feedwater tank.

It can be observed that the amount of steam injected into the feed water tank to reach the desired temperature represents approximately the 6% of the total steam produced in the steam generator.

## 2.2 Thermal Power Station Retrofitting

As part of the thermal power station modernization, the existing 8 t/h Bono boiler has been replaced with a more efficient 12 t/h Mingazzini unit equipped with an economizer (datasheet available on the manufacturer's website [28]). This upgrade improves energy efficiency and optimizes fuel utilization by integrating waste heat recovery.

The economizer plays a crucial role in this process, capturing residual heat from the flue gas to preheat the feed-water before it enters the boiler. This approach significantly reduces the flue gas exit temperature, minimizing thermal losses and enhancing the boiler's efficiency. The increase in efficiency translates into lower fuel consumption, reduced operating costs, and a decrease in environmental impact due to lower emissions.

In the new system configuration, assuming a medium steam demand of 7 t/h, the high-efficiency 12 t/h boiler will become the primary steam generator, operating under standard conditions to meet the plant's requirements. Meanwhile, the 15 t/h boiler will serve as a backup unit, stepping in during peak demand periods or maintenance operations on the primary boiler. This redundancy ensures operational reliability, preventing disruptions in steam supply and allowing for continuous and efficient plant operation.

By integrating a more advanced steam generator and optimizing heat recovery, this upgrade represents a significant step toward greater energy efficiency, cost-effectiveness, and sustainability in the thermal power station.

In Fig. 2.3, the scheme of the upgraded thermal power plant is shown. In this configuration,  $SG_1$  has a higher nominal capacity and improved efficiency, thanks

to the addition of an economizer that exploits flue gas at around 220 °C to heat the water. Under medium load conditions,  $SG_2$  is switched off, and the amount of steam injected into the feed-water tank is reduced, if not entirely eliminated according to the operating conditions, as the water is preheated by the ECO of  $SG_1$  before entering the steam generator.

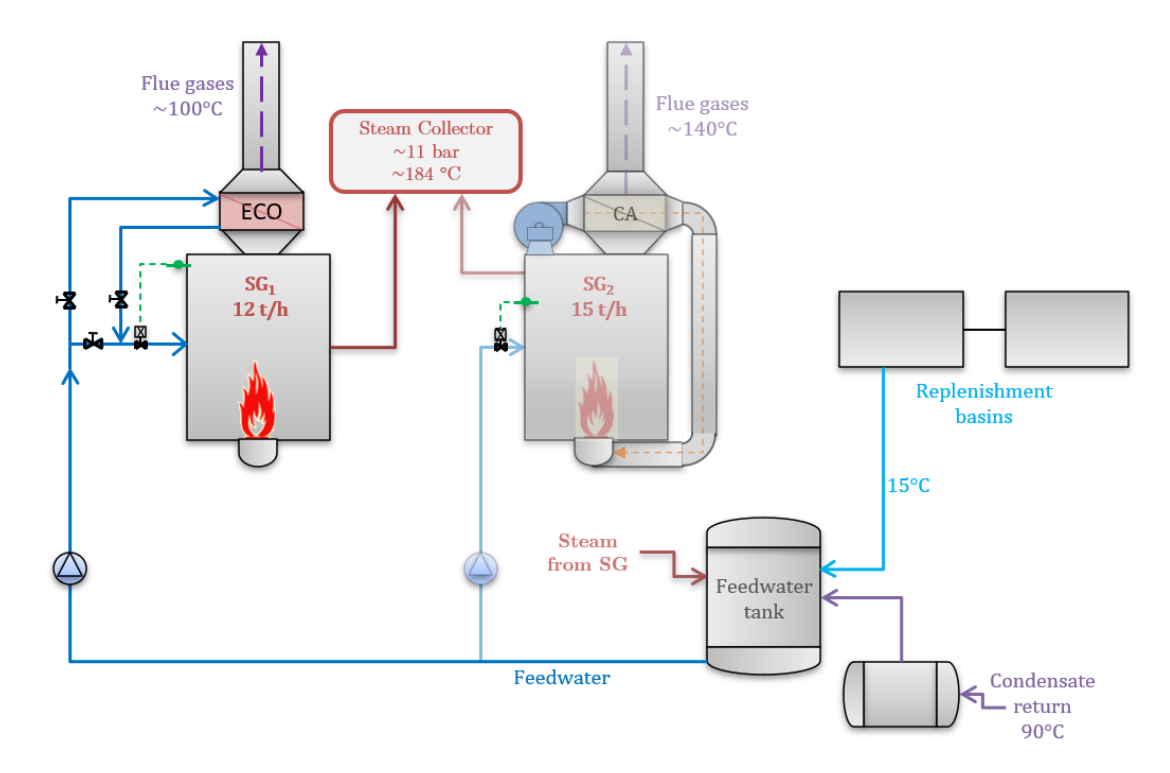


**Figure 2.3:** Simplified Scheme of the Retrofitted Thermal Power Plant Under Medium Load Conditions.

## 2.2.1 Analytical Approach to Steam Generator Simulation

After the steam generator has been selected, its technical specifications are thoroughly assessed on the basis of the nameplate information provided in the manufacturer's datasheet, which can be requested to the supplier [28]. This involves examining key parameters such as steam production capacity, operating temperatures, efficiencies and fuel type, using both preliminary data and information from its datasheet. These specifications are crucial in determining the generator's suitability for the plant's operational needs and ensure it can deliver the required steam output efficiently and reliably. Subsequently, energy and mass balances are performed to verify the steam output, the fuel consumption, and overall efficiency.

Finally, the steam generator is modelled in Aspen Plus (see *Chapter 3*). The

simulation reproduces the boiler's behaviour under full-load conditions, first without the economizer and then with it, enabling a direct comparison between the analytical results and those obtained with Aspen Plus. This step is essential to validate the model's accuracy and demonstrate its reliability in predicting real-world performance.

#### Combustion Process: Air Supply, Excess Air, and Fuel Injection

The **combustion air** is approximated as a mixture of 21% oxygen  $(O_2)$  and 79% nitrogen  $(N_2)$ , with a relative humidity of 70% and a reference temperature of 20°C [29]. The relative humidity allows calculation of the water vapour content, which in turn enables a precise determination of both the composition of the air reacting with methane (Table 2.3) and the resulting flue gases (Table 2.5).

	Air Specifications				
	T 20 °C				
	Р	1.01325	bar		
	$\varphi$	70	%		
	$P_{sat\_H2O}$ (20°C)	0.02339	bar		
	ω	$\omega$ 0.0102 kg/kg <sub>dry</sub>			
	Element	Molar fraction $(y_i)$	M [g/mol]		
Dry Air	$N_2$	0.79	28		
Diy Air	$O_2$	0.21	32		
	$N_2$	0.777	28		
Humid Air	$\mathrm{O}_2$	0.207	32		
	$\mathrm{H_{2}O}$	0.016	18		

**Table 2.3:** Air Composition.

To ensure complete combustion and prevent the formation of harmful pollutants, industrial steam generators operate with an excess air supply beyond the theoretical amount required for stoichiometric combustion. Typically, this value ranges between 10% to 20% [30].

This parameter must be properly managed, since it affects both the efficiency and safety of combustion [29].

 $Advantages\ of\ excess\ air:$  adequate excess air ensures complete combustion, preventing fuel residues and deposits on heat exchanger surfaces.

- ✓ Improves combustion stability by maintaining a uniform flame and reducing fluctuations in boiler operation; also lowers the risk of localized oxygen deficiency, which could cause incomplete combustion and hotspots.
- ✓ Reduces harmful emissions from incomplete combustion, such as:
  - carbon monoxide (CO);
  - unburned hydrocarbons;
  - particulate matter and soot, which increase maintenance and corrosion risks

Drawbacks of Excess air: it increases energy losses in the flue gas and reduces the overall efficiency of the steam generator. Specifically, it:

- × introduces additional N<sub>2</sub> into the combustion process, which absorbs heat without contributing to combustion, thus reducing the amount of heat transferred to the working fluid and increasing thermal losses in the exhaust gases;
- × increases combustion gas volume, leading to greater stack losses, as more heat escapes through the chimney instead of being used for steam generation.

Additionally, while a moderate excess air supply helps reduce CO emissions, a too lean mixture raises the flame temperature, promoting the formation of nitrogen oxides  $(NO_x)$ , which contribute to air pollution.

The oxygen content in the flue gas indicates the level of excess air. For high-efficiency methane-fired boilers, an optimal value is typically 2–3%  $O_2$  [31]. In this study, excess air is set to achieve 3%  $O_2$  in the exhaust, balancing efficiency and emission control.

The required excess air ratio ( $\lambda$ ) is determined from the condition that the dry flue gas contains 3% O<sub>2</sub> by volume (i.e., by molar fraction), resulting in:

$$\lambda \approx 1.15 \tag{2.2}$$

This approach guarantees that the combustion process avoids unburned fuel, reduces pollutant emissions, and supports optimal thermal efficiency.

Turning to the **fuel** injected into the steam generator, for the purpose of analytical calculations it is modelled as pure CH<sub>4</sub>. Within the company's internal gas distribution network, methane is supplied at 450 mbarg and must be reduced to 350 mbarg before injection into the burner to meet operational requirements. This pressure adjustment ensures proper combustion conditions while aligning with system constraints. The fuel is injected at a pressure slightly higher than the combustion air to ensure stable and efficient mixing. This pressure differential is essential because:

- promotes proper mixing of methane and air, facilitating complete combustion and minimizing pollutant formation;
- prevents backflow of air into the fuel line, avoiding potential safety risks;
- ensures flame stability, reducing fluctuations that could lead to inefficiencies or incomplete combustion.

The system uses a monobloc modulating natural gas burner with spark ignition, where high-voltage electrodes ignite the combustion process. Key features include:

- port fuel injection (PFI) so that methane is injected into the intake airflow before reaching the combustion zone;
- electronic flow control, where independent servo motors regulate gas and air flow with high precision;
- digital cam system which ensures accurate modulation of the fuel-air ratio;
- inverter-controlled fan that adjusts speed to optimize airflow and improve efficiency.

These features guarantee efficient combustion, compliance with emission limits ( $NO_x \le 120 \text{ mg/Nm}^3$ ,  $CO \le 50 \text{ mg/Nm}^3$  at 3%  $O_2$ ) according to BS EN 676:2003+A2:2008 standard [32], and safe operation through a fully automated control system. The inverter further enhances combustion stability and reduces electricity consumption, improving overall energy efficiency. Maintaining an optimal pressure difference between fuel and air is crucial for achieving high combustion efficiency while ensuring safe and reliable operation.

To calculate the required methane flow, the feed water and steam conditions are considered as summarized in Table 2.4.

Water				
m	$12000 \mathrm{\ kg/h}$			
$c_{\mathrm{p}}$	$4.186~\mathrm{kJ/kgK}$			
$T_{in}$	70 °C			
$T_{ m out}$	184.07 °C			
р	11 bar			
$h_{\rm v}$	1999.9  kJ/kgK			

Table 2.4: Water Specifications.

Unlike the preexisting configuration, in this analysis the feed water from the storage tank is assumed to enter at 70 °C, without accounting for the injection of recirculated steam. This assumption reflects the future integration of a dedicated heat recovery system, implemented within the same project, which will preheat the feed water using waste heat from flue gas. For the purpose of this steadystate calculation, it is assumed that the entire steam production is available for downstream users, and no steam is diverted for feed water preheating. It is important to highlight, however, that during transient conditions, particularly during system start-up, the flue gas flow rate and temperature may initially be insufficient to achieve the required preheating. During these transient phases, rather than diverting a portion of the produced steam for feed water preheating, it is more practical to gradually increase the feed water flow. This allows the steam generator to convert the injected water into steam while the flue gases gradually reach the required flow rate and temperature, enabling them to preheat the feed water to the desired temperature. Despite this dynamic behaviour, the impact is considered negligible in the context of the steady-state energy balance evaluated in this study.

## Steam Generator Performance: Efficiency Assessment, Influencing Factors, and Loss Mechanisms

The thermal power absorbed by the water to reach evaporation is given by:

$$\dot{Q}_{\text{steam}} = \dot{m}_{\text{H}_2\text{O}} \cdot \left[ c_p \cdot (T_{\text{out}} - T_{\text{in}}) + h_v \right]$$
 (2.3)

Determining the amount of fuel required by the steam generator requires knowledge of its efficiency, which quantifies the fraction of the fuel's energy effectively transferred from the combustion process to the water, after accounting for all losses. There are two common methods to determine the SG efficiency [33].

- Direct method, also known as the *input-output method*. This approach requires only the measurement of the useful energy output and the fuel energy input. Based on the principle of energy conservation, it calculates efficiency as the ratio of output energy to input energy.
- Indirect method, also called heat loss method. Instead of directly measuring energy input and output, this method assesses boiler efficiency by identifying and quantifying the various types of energy losses. Figure 2.4 illustrates the concept, showing how each loss component originates at a specific stage of the combustion process.

The main parameters that affect the efficiency of a natural gas-fired conventional steam boiler are:

- SG Load Steam generators tend to perform most efficiently when running at moderate loads, typically between 65% and 75% of their rated capacity. At lower loads, especially below 50%, maintaining complete combustion requires supplying more excess air, which leads to greater energy loss through flue gas. As a result, operating under 50% load is generally associated with reduced efficiency [34].
- Dry flue gas temperature Dry flue gas temperature directly is related to dry flue gas losses (L<sub>1</sub>) represented by the heat carried away by hot combustion gas exiting the boiler through the stack. Since not all the energy from fuel combustion can be transferred to the waterside, a portion escapes with the flue gas. These losses depend mainly on the flue gas temperature and composition, which are influenced by fuel properties and excess air levels. Although unavoidable, they can be reduced by lowering the stack temperature, typically using an economizer to preheat feed water, thereby improving overall boiler efficiency. These losses typically account for 8% to 15% of the fuel's energy input.
- Moisture present in the air and fuel Heat losses due to moisture (L<sub>2</sub>) arise from both the moisture content in the combustion air and in the fuel itself. During combustion, this moisture absorbs energy to evaporate and eventually becomes superheated steam, carrying away heat that could otherwise be used for steam generation. These losses are particularly relevant when burning solid fuels such as coal, wood, or biomass, which often contain high levels of moisture. However, in the case study considered, the steam generator is fuelled by natural gas, which contains no inherent moisture. Therefore, losses due to moisture in the fuel are negligible. The only minor contribution comes from the humidity in the combustion air, which has a minimal impact on the overall boiler efficiency and can also be considered negligible [35].
- Excess combustion air Combustion air plays a crucial role in the efficiency of a steam generator. Insufficient air supply can lead to incomplete combustion losses (L<sub>3</sub>), fuel is not fully oxidized into CO<sub>2</sub> and H<sub>2</sub>O, resulting in the formation of carbon monoxide (CO) and unburned hydrocarbons. These byproducts represent energy that was not effectively utilized, thus reducing overall efficiency. Proper air-fuel mixing is essential to ensure that each fuel molecule has access to adequate oxygen. Monitoring and controlling combustion air is therefore key to minimizing losses and improving boiler performance.
- Radiation and convection losses  $(L_4)$  In a boiler, radiation, and convection losses occur as heat is transferred from the hot surfaces to the cooler surroundings. These losses are influenced by the temperature differences and

surface area of the boiler. Proper insulation and optimized operation can help minimize them. According to the American Boiler Manufacturers Association (ABMA), radiant loss remains constant in terms of absolute energy loss (kJ), regardless of the boiler load [36]. As a result, at lower loads, the percentage of radiant loss increases. While these losses are typically low, ranging from 0.1% to 5%. In the considered case study, according to the boiler capacity steam flow, they account for approximately 1% at full load [37].

• Other energy losses  $(L_5)$  - Boiler energy losses can arise from time-related factors that aren't immediately detectable and usually emerge during annual efficiency assessments. One example is blowdown, which involves releasing hot water or steam to remove sludge or other impurities left behind during evaporation. This sludge reduces heat transfer efficiency, and may contaminate steam. To maintain standard levels of suspended and total dissolved solids (TDS), water is drained periodically from the steam drum. This discharge carries thermal energy, resulting in energy losses, and requires additional fuel to maintain temperature and pressure. Blowdown losses can range from 0.5% to 10%, depending on factors like boiler type, operating pressure, water treatment, and makeup water quality. Another energy loss occurs when the boiler operates in minimum firing or sleep mode, where it runs at low load to maintain pressure and temperature, even without immediate heat demand. In this mode, fuel is still consumed but not fully utilized, leading to wasted energy [38].

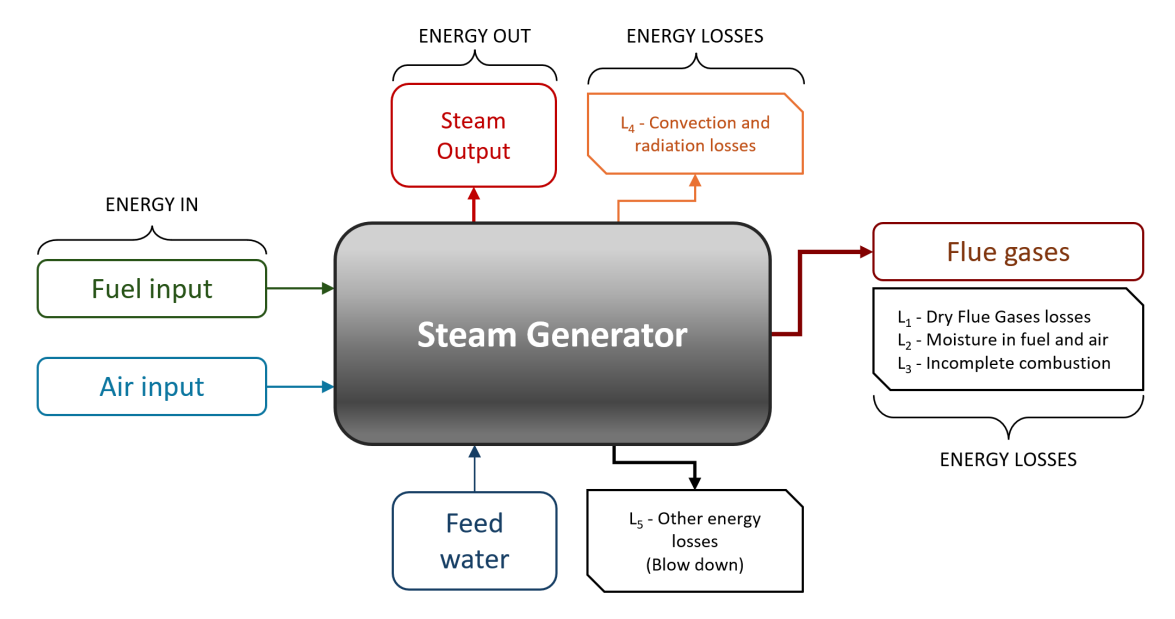


Figure 2.4: Indirect method for evaluating boiler efficiency.

According to the steam generator specifications, the maximum thermal efficiency is stated to be 90%, meaning that 90% of the chemical energy contained in the fuel is released by the combustion gas and made available for heat transfer to the system. Generally, maximum efficiency is achieved when the boiler operates at 65-85% of its full load capacity [39, 40]. At full load, boiler efficiency tends to decrease slightly due to increased flue gas stack losses. This is primarily caused by the higher volume and velocity of the flue gas, which reduce the residence time in the heat recovery sections. As a result, the flue gas has insufficient time to transfer their thermal energy effectively, leading to elevated exhaust temperatures and reduced heat recovery [41]. So, including only dry flue gas losses (L<sub>1</sub>) and convection and radiation losses (L<sub>5</sub>), we can define the different contribution as follows:

• the useful heat absorbed by the water:

$$\dot{Q}_{\text{steam}} = \eta_{\text{SG}} \cdot \dot{Q}_{\text{fuel}} \tag{2.4}$$

• the heat losses due to convection and radiation from the heat exchanger surfaces (L<sub>5</sub>):

$$\dot{Q}_{\text{conv,rad}} = 1\% \ \dot{Q}_{\text{fuel}} \tag{2.5}$$

• the thermal losses associated with the flue gas  $(Q_{\rm f.g.})$  can be estimated through the overall energy balance of the boiler system:

$$\dot{Q}_{\text{steam}} + \dot{Q}_{\text{conv,rad}} + \dot{Q}_{\text{f.g.}} = \dot{Q}_{\text{fuel}}$$
 (2.6)

Given the amount of thermal power needed (Eq. 2.3), the required methane volumetric flow rate is:

$$\dot{V}_{\rm CH_4} = \frac{\dot{Q}_{\rm steam}}{\eta_{\rm SG} \cdot \text{LHV}} \tag{2.7}$$

In addition, knowing the molar composition of the air (Table 2.3) and the excess air  $\lambda$ , it is possible to determine the total volume of air introduced into the combustion process:

$$\dot{V}_{\text{air}} = \dot{V}_{\text{CH}_4} \cdot 2\lambda \cdot (n_{\text{O}_2} + n_{\text{N}_2} + n_{\text{H}_2\text{O}})$$
(2.8)

Furthermore, based on the combustion reaction, the flue gas composition (Table 2.5) and the volumetric flow rate of methane (Eq. 2.7) are known, thereby enabling the volumetric flow rate of the wet flue gas to be evaluated as follows:

$$\dot{V}_{\text{f.g.}} = \dot{V}_{\text{CH}_4} \cdot [2\lambda(n_{\text{O}_2} + n_{\text{N}_2} + n_{\text{H}_2\text{O}}) + n_{\text{CH}_4}]$$
 (2.9)

Flue Gas					
$T_{ref}$	25°C	,			
$c_{\mathrm{p}}$	1.12 kJ/	kgK			
Element	Molar fraction $(y_i)$	$M~[\mathrm{g/mol}]$			
$N_2$	0.713	28			
$O_2$	0.025	32			
$\mathrm{H_{2}O}$	0.180	18			
$CO_2$	0.082	44			
$M_{f.g.}$	27.62 g/mol				
ρ	$1.232~\mathrm{kg/Nm}^3$				

**Table 2.5:** Flue Gas Specifications.

Finally, the relationship between the flue gas outlet temperature and the residual thermal power it carries, is given by:

$$T_{\text{out f.g.}} = T_{ref} + \frac{\dot{Q}_{\text{f.g.}}}{c_{p,f.g.} \cdot \dot{m}_{f.g.}}$$
 (2.10)

where  $T_{ref}$  and  $c_{p,f.g.}$  denote, respectively, the reference temperature and the flue gas specific heat capacity [42] whose values are reported in Table 2.5. The mass flow rate of the flue gas is calculated as:

$$\dot{m}_{f.g.} = \dot{V}_{f.g.} \cdot \rho_{f.g.} = \dot{V}_{f.g.} \cdot \frac{M_{f.g.}}{V_M}$$
 (2.11)

and the molar mass of the flue gas is given by the weighted sum of the molar masses of the main components:

$$M_{f.g.} = y_{\text{CO}_2} \cdot M_{\text{CO}_2} + y_{\text{O}_2} \cdot M_{\text{O}_2} + y_{\text{N}_2} \cdot M_{\text{N}_2} + y_{\text{H}_2\text{O}} \cdot M_{\text{H}_2\text{O}}$$
 (2.12)

To ensure simplicity and flexibility in adjusting the initial conditions, particularly to account for variations in operating load, all the above equations and interdependencies between the relevant parameters were implemented in an Excel spreadsheet. This enables the calculation of volumetric flow rates of air, fuel, and flue gases, as well as the thermal power released by the combustion gases and the associated losses. The corresponding results, based on the steam generator operating at full load, are summarized in the table below (Table 2.6).

	Input data			Results		
	ṁ	$12000 \mathrm{\ kg/h}$	Fuel	$\dot{ m V}_{ m CH4}$	$941.8~\mathrm{Nm}^3/\mathrm{h}$	
Water	${ m T_{in}}$	70 °C		$\lambda_{\rm air}$	1.15 [-]	
	${ m T_{out}}$	184.07 °C	Air	$\dot{ m V}_{ m humid~air}$	$10476.7~{ m Nm}^3/{ m h}$	
	Load [%]	100 %		$ m \dot{V}_{dry~air}$	$10307.4 \text{ Nm}^3/\text{h}$	
	$\mathrm{LHV}_{\mathrm{fuel}}$	$8550 \text{ kcal/Nm}^3$		$\dot{V}_{\mathrm{wet\ f.g.}}$	$11418.4 \; \mathrm{Nm}^3/\mathrm{h}$	
	$\%O_2$ (f.g.)	3 %	Flue Gas	$\dot{V}_{dry~f.g.}$	$9365.6~\mathrm{Nm}^3/\mathrm{h}$	
Steam	SG Efficien	cy and Losses		$T_{out, f.g.}$	230 °C	
Generator	$\eta_{SG\_max}$	90% (datasheet)		${ m \dot{Q}_{fuel}}$	$9358.4~\mathrm{kW}$	
	$\eta$ $_{\scriptscriptstyle SG}$	88.24% (100% load)	Thermal	$\dot{Q}_{steam}$	8258.0 kW	
	$L_{\ conv,rad}$	1%	Power	$\dot{Q}_{conv, \; rad}$	93.6 kW	
	$L_{\it f.g.}$	10.76%		$\dot{Q}_{\mathrm{f.g.}}$	1006.8 kW	

Table 2.6: Input parameters and output results for the SG operating at full load.

### 2.2.2 Economizer Design and Sizing

The new steam generator incorporates a finned-tube economizer to recover residual heat from the high-temperature flue gas and use it to preheat the water coming from the feed water tank, entering the steam generator. By lowering the flue-gas outlet temperature, an economizer increases the overall boiler efficiency by roughly 3-7% compared to a standard unprovided boiler [43]. Preheating the feed water reduces the enthalpy lift required in the steam generator, thereby cutting fuel consumption for a given steam output. A preliminary sizing of the economizer is performed using 3STC a software developed by 3S Saldature Speciali Segrate, a company specialized in finned-pack heat exchangers, finned-tube heat exchangers, and bare-tube heat exchangers [44]. Inputs include:

#### Flue-gas conditions:

- dry-bulb temperature,
- absolute humidity,
- mass flow rate.

#### Feed water conditions:

- inlet temperature,
- mass flow rate,
- desired outlet temperature.

This minimum temperature difference ( $\Delta T_{\min}$ ) is a key parameter in heat exchanger network (HEN) synthesis, as it directly influences both energy recovery potential and capital expenditure. A lower  $\Delta T_{\min}$  enhances process heat integration by allowing more energy to be recovered internally; however, it also requires a larger

heat exchanger surface area, leading to increased capital costs. Conventionally, a single  $\Delta T_{\rm min}$  value is applied across the entire process, determined through a capital—energy trade-off analysis that aims to balance operational energy savings with investment costs. In practice,  $\Delta T_{\rm min}$  is typically selected in the range of 5-15 °C and must not be violated throughout the network to ensure the feasibility of heat transfer and the reliability of the economic evaluation [45, 46].

For this type of application, specifically, for a SG economizer, a cross-flow finned tube heat exchanger with continuous fins is typically employed. This configuration is well-suited for recovering heat from hot flue gas to preheat water. Water flows inside the tubes, while the flue gas passes perpendicularly across the shell side. The tubes are embedded in a continuous fin pack, which significantly increases the external heat transfer surface area and enhances thermal exchange in the cross-flow arrangement.

Finned tube materials are selected according to the thermal and environmental conditions of operation:

- Fins: aluminium or galvanized steel are commonly used for their high thermal conductivity and low weight.
- ⋆ Tubes:
  - carbon steel is typically employed for standard applications;
  - stainless steel is preferred in corrosive environments, especially when flue gases contain acidic components, due to its superior long-term corrosion resistance despite higher cost.

This configuration offers notable advantages:

- ✓ High thermal efficiency.
- ✓ Compact design.

However, several limitations should be considered:

- × susceptibility to fouling, particularly when flue gases contain dust or particulate matter, which may clog the finned surfaces and reduce performance.
- × cleaning is generally more complex than in bare-tube exchangers.
- $\times$  fins may deteriorate over time in corrosive environments unless protective materials or coatings are used.
- $\times$  dense fin configurations can lead to relatively high pressure drops on the gas side.

Once the design parameters, such as fluid flow rates, inlet temperatures, and fluid properties, are defined, the preliminary sizing of the heat exchanger is carried out based on these inputs along with an initial estimate of the heat transfer area. The total water flow is then distributed across an appropriate number of circuits and ranks, in order to meet the required thermal performance while maintaining fluid velocities and pressure drops within acceptable limits.

These configuration parameters are carefully adjusted to obtain the optimal trade-off between enhanced convective heat transfer, acceptable pressure losses, and controlled flow velocities. On the *waterside*, flow velocities typically range from 0.9 to 2.4 m/s, high enough to enhance heat transfer but low enough to keep pumping power reasonable. For the *flue gas side*, velocities usually fall between 0.6 and 1.5 m/s: lower velocities help reduce fouling, while upper limits are set to avoid erosion-corrosion inside the tubes and prevent impingement or flow-induced vibrations on the shell side [38].

In the heat exchanger sizing process, two key parameters are tuned: the circuit number and the rank. These affect internal flow distribution and, through more detailed analysis, determine the number of tube passes, influencing thermal performance, pressure drops, and mechanical design.

- A low number of circuits results in a larger flow area, which reduces fluid velocity and consequently minimizes pressure drop. However, this configuration limits the number of tubes involved in heat exchange, potentially reducing the available surface area and thus lowering thermal effectiveness. Conversely, increasing the number of circuits enhances the available heat transfer surface and improves thermal performance, but at the cost of higher flow velocities and pressure losses.
- The rank of the heat exchanger, i.e., the number of tube rows crossed by the gas, is a key design parameter. It is initially estimated using dedicated software and then finalized by the technical team, which defines the number of passes per rank based on performance and operational requirements. A low rank yields lower fluid velocities, leading to reduced pressure drops, simpler construction, and easier maintenance. However, the associated reduction in heat transfer coefficients means that a larger overall heat transfer surface may be required to meet the same thermal duty. On the other hand, a high rank leads to higher fluid velocities in each pass, promoting greater turbulence and resulting in a higher Reynolds number, which increases the heat transfer coefficient. This configuration is favourable for thermal performance, but it comes with higher pressure drops, increased pumping power requirements, more complex construction, and greater difficulty in mechanical cleaning.

Thus, the choice of circuit and rank configuration is a matter of careful balance

between thermal efficiency, hydraulic performance, mechanical feasibility, and maintenance needs.

After completing the preliminary sizing, the supplier's technical team refines and finalizes the design. Figure 2.5 presents the technical layout of the economizer, including detailed dimensions from the manufacturer's datasheet (full datasheet provided in Appendix A).

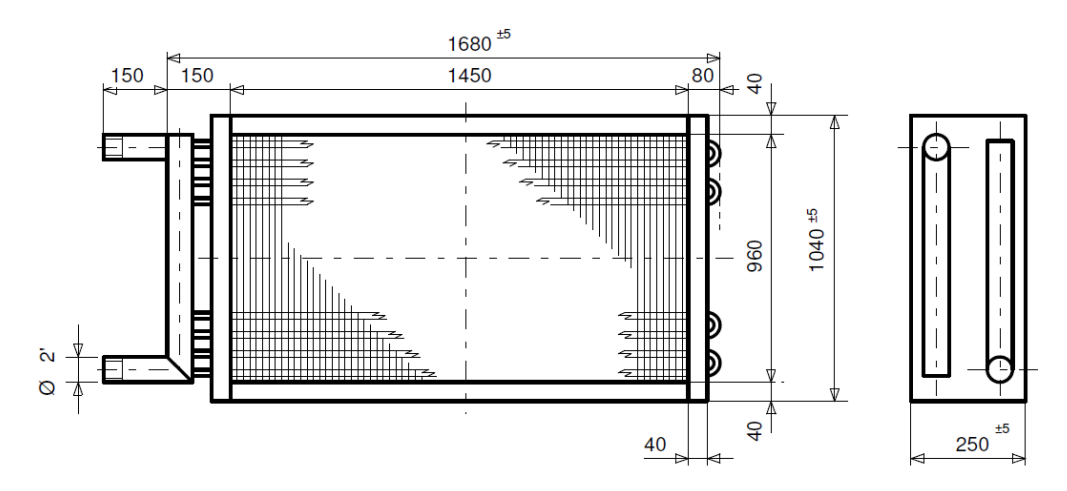


Figure 2.5: Technical Layout of the ECO Heat Exchanger.

The SG economizer is dimensioned under steady-state, full-load conditions through an iterative calculation process supported by the 3STC software, using the flue gas temperature and flow rate obtained from the previous analysis (Table 2.6).

- 1. *Initial conditions:* start with the flue gas temperature and flow rate from the baseline configuration.
- 2. First sizing: dimension the economizer by increasing the number of ranks and circuits to enhance heat recovery and reduce water velocity to acceptable levels.
- 3. Trade-off evaluation: check the resulting pressure drop and pumping power. Increase the number of ranks and circuits only if the additional thermal gains justify the added complexity and cost.
- 4. Software output: obtain from 3STC the predicted flue gas outlet temperature, recovered thermal power, and feed water outlet temperature.
- 5. Steam generator re-simulation: update the SG model with the new preheated feed water temperature (100 °C). This reduces the burner's thermal load, lowering fuel consumption and consequently the flue gas flow rate.

- 6. *Iteration:* re-dimension the economizer based on the new flue gas flow rate and repeat the procedure.
- 7. Convergence: Continue the cycle until the flue gas flow rate and the outlet temperatures of both flue gas and feed water converge and stabilize.

Table 2.7 summarizes the input and output parameters used for the simulation. It is also worth noting that, for simplicity, flue gas density is approximated to that of air.

	Economizer Technical Specifications					
	$ m \dot{V}_{dry~f.g.}$		8818.32	$\mathrm{Nm}^3/\mathrm{h}$		
		ρ	1.293	$\mathrm{kg/m}^3$		
		$\dot{M}_{dry~f.g.}$	11402.1	kg/h		
	Fa	ce velocity	1.7	m/sec		
Flue Gas	Pre	essure Drop	100	Pa		
riue Gas	In	put Data	0	utput Data		
	$T_{ m dry\ bulb}$	230 °C	$T_{\rm dry\ bulb}$	105.9 °C		
	ω	$133~{\rm g/kg_{dry~air}}$	ω	$124.2~\mathrm{g/kg_{dry~air}}$		
	$\varphi$	0.6~%	$\varphi$	13.5~%		
	$h_{\rm f.g.\ in}$	618.9  kJ/kg	$h_{\rm f.g.~out}$	440.1  kJ/kg		
		m		$12000   \mathrm{kg/h}$		
		Velocity	1.55  m/sec			
Water	Pre	essure Drop	40.9 kPa			
		$T_{\mathrm{in}}$	70 °C			
		${ m T}_{ m out}$	104.97	$^{\circ}\mathrm{C}$		
	Finned Length		487.97	kW		
HX Coil			144.9	$m^2$		
Features			1450	mm		
reatures	Fin	ned Height	960	mm		
	n° c	eircuits = 15		rank = 5		

**Table 2.7:** Design and Operating Parameters of the Economizer under Full-Load Steam Generator Conditions.

The performance of the steam generator (SG) with economizer is summarized in Table 2.8, which combines results at both full-load and part-load conditions for ease of comparison and highlights the key parameters relevant for the subsequent economic evaluation, namely fuel consumption and recoverable thermal power.

		Full Load		Part Load			
		$\dot{\mathrm{m}}$	12000	kg/h	7000 kg/h		
	Water	${ m T_{in}}$	70	$^{\circ}\mathrm{C}$	70	$^{\circ}\mathrm{C}$	
ECO		${ m T_{out}}$	104.97	$^{\circ}\mathrm{C}$	105.7	$^{\circ}\mathrm{C}$	
ECO		$\dot{V}_{dry\;f.g.}$	8818.3	$\mathrm{Nm}^3/\mathrm{h}$	5153.9	$\mathrm{Nm}3/\mathrm{h}$	
	Flue Gas	$T_{\rm in,f.g.}$	230	$^{\circ}\mathrm{C}$	220	$^{\circ}\mathrm{C}$	
		$T_{out,\;f.g.}$	105.90	$^{\circ}\mathrm{C}$	93.00	$^{\circ}\mathrm{C}$	
	TT7 /		104.97 °C <sup>□</sup>		105.70 °C		
Steam	Water	$T_{\mathrm{out}}$	184.07 °C		184.07 °C		
Generator	Fuel	$\dot{V}_{CH4}$	886.7	$\mathrm{Nm}^3/\mathrm{h}$	518.3 Nm3/h		
	Air	$\dot{V}_{dry\;air}$	$9705.1 \text{ Nm}^3/\text{h}$		5672.2  Nm3/h		
	$\dot{Q}_{ m fuel}$	8811.6	kW	100%	5150.0 kW	100%	
Thermal	$\dot{Q}_{steam\_SG}$	7770.0	kW	88.18%	$4526.4~\mathrm{kW}$	87.89%	
Power	$\dot{Q}_{ECO}$	487.97 kW		5.54%	$290.77~\mathrm{kW}$	5.65%	
rower	$\dot{Q}_{conv, \; rad}$	93.6 kW		1.06%	93.6 kW	1.82%	
	$\dot{Q}_{ extit{f.g.}}$	459.97 kW		5.22%	239.21 kW	4.64%	
η <sub>GV_ECO</sub>			93.72%	)	93.5	93.54%	

**Table 2.8:** Comparison of full-load and part-load performance of the steam generator with economizer.

In both full-load and part-load operation, the addition of the economizer results in an efficiency gain of approximately 6 percentage points, corresponding to a reduction in fuel consumption.

At full load, this gain translates to a reduction in fuel consumption of about 50 Nm<sup>3</sup>/h, with the steam generator reaching an efficiency of 93.72%.

Under medium-load conditions, corresponding to a feed water flow rate of 7 t/h (roughly 60% of full capacity), the SG maintains high efficiency (93.54%). Since the SG typically reaches its maximum efficiency at loads between 65% and 85% [39, 40], the lower operating point explains the slight reduction in the overall SG efficiency. The flue gas outlet temperature decreases from 230 °C at full load to 220 °C at part load, while the fraction of fuel energy recovered by the economizer slightly increases. Convection and radiation losses remain approximately constant [36], so

their relative impact grows at reduced loads, slightly diminishing the portion of heat effectively transferred to the working fluid.

Regardless of the operating load, the integration of the economizer consistently delivers a significant performance improvement, with an observed efficiency gain of almost 6 percentage points. This enhancement is maintained even when the flue gases enter the economizer at reduced temperatures, demonstrating the system's robustness across varying thermal conditions. The results are in good agreement with typical values reported in the literature for non-condensing economizers operating under comparable conditions [43, 47].

#### ECO hoppers sizing

To optimize heat recovery and ensure uniform distribution of the flue gas across the entire heat exchange surface, two flue gas conveyors (hoppers) are flanged to the inlet and outlet of the economizer, as illustrated in Fig. 2.6.

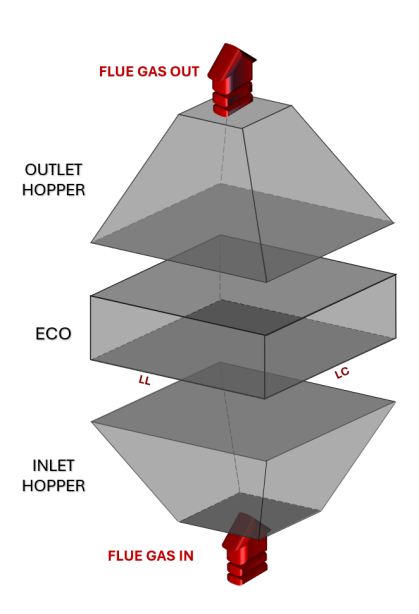


Figure 2.6: ECO and Hoppers Exploded view.

The hoppers direct the flue gas towards and outwards the heat exchanger with maximum efficiency, minimizing pressure drops and reducing flow disturbances. They are typically shaped as frustums of rectangular pyramids. This geometry is not arbitrary: the walls are inclined at an angle greater than 45° with respect to the plane perpendicular to the direction of flue gas flow at the economizer inlet. Such an inclination is chosen to promote smooth gas deflection and avoid recirculation zones that could reduce heat transfer efficiency. The height of the hoppers is determined through trigonometric calculations based on this inclination

angle, as illustrated in Fig.2.7.

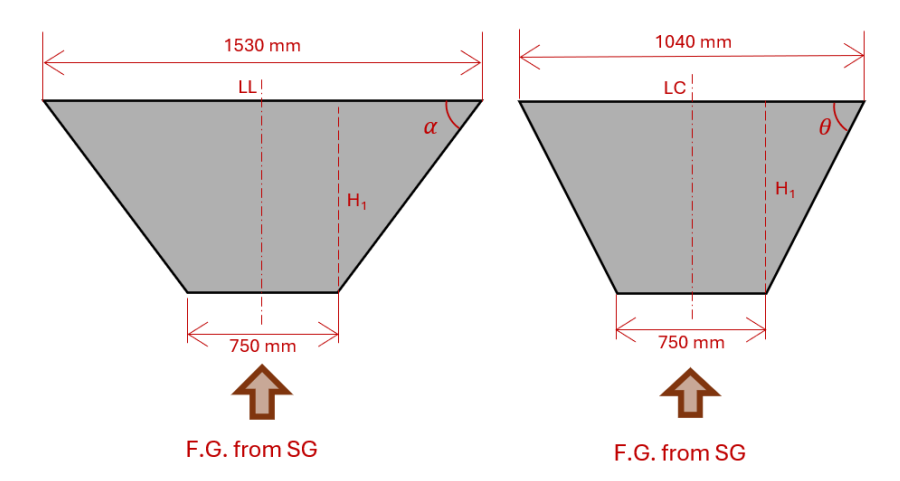


Figure 2.7: ECO hoppers sizing.

The geometric parameters shown in Figure 1.7 are defined below to clarify the nomenclature used in the hopper sizing calculations.

LL refers to the side length of the hopper's rectangular flange that mates with the economizer's longer side.

LC refers to the side length of the hopper's rectangular flange that mates with the economizer's shorter side.

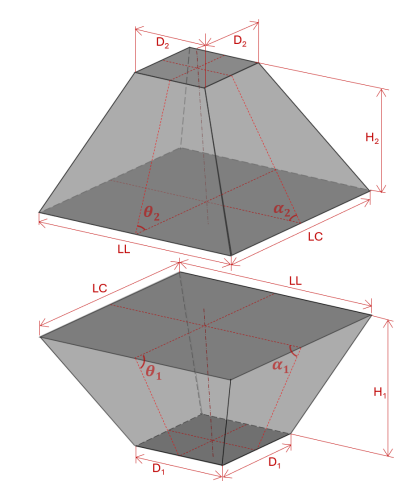
D represents the side length of the square cross-section of the hopper flange that connects to the steam generator.

By imposing  $\alpha \ge 45^{\circ}$ , it follows from trigonometric reasoning that  $\theta > 45^{\circ}$ . The minimum hopper height can therefore be calculated by assuming  $\alpha = 45^{\circ}$ :

$$H_{min} = \tan \alpha \cdot \left(\frac{LL - D}{2}\right) = 390 \ mm \tag{2.13}$$

 $H_1$  is set to 400 mm, resulting in a slightly larger angle:  $\alpha \simeq 45.7^{\circ}$ . The corresponding  $\theta$  is verified to be approximately 70.1°.

The same sizing procedure is applied to the outlet hopper. The dimensions of the hoppers at the economizer's inlet and outlet are summarized in the following table.



INLE	INLET HOPPER		OUTLET HOPPER		
$D_1$	$750~\mathrm{mm}$	$D_2$	$700 \; \mathrm{mm}$		
LL	$1530 \; \mathrm{mm}$	LL	$1530~\mathrm{mm}$		
LC	$1040~\mathrm{mm}$	LC	$1040~\mathrm{mm}$		
$H_1$	$400 \; \mathrm{mm}$	$H_2$	$450 \mathrm{\ mm}$		
$\alpha_1$	45.7 °	$\alpha_2$	47.3 °		
$\Theta_1$	70.1 °	$\Theta_2$	69.3 °		

Figure 2.8: Labeled hoppers references.

Table 2.9: ECO hoppers dimensions.

## 2.3 Heat Recovery System

As part of the factory's upgrade toward greater energy efficiency and sustainability, a heat-recovery system has been installed to recover useful thermal energy from the flue gases produced by the thermal power station. As illustrated in the simplified scheme (Fig. 2.9), the exhaust streams from the two steam generators are combined into a single manifold (see also  $Appendix\ C$  for the full aeraulic P&ID) and directed through a purpose-designed hopper into two series-connected cross-flow finned-tube heat exchangers with continuous fins, linked by a plenum.

The first heat exchanger (RC2) maximizes heat transfer from high-temperature flue gas. Water from the first replenishment tank, supplied from the cooling tower at 15 °C and treated via osmosis, passes through RC2, where it is raised to an intermediate temperature, before entering the second replenishment tank and then proceeding to the feed water tank. Here, it mixes with condensate return, before being pumped back into the thermal power station. By recovering as much heat as possible at this stage, the boiler's firing requirements are significantly reduced.

The plenum between RC2 and RC3 ensures uniform pressure distribution and flue-gas flow into the second exchanger, preventing hot-spotting or bypassing and providing space for flow stabilization and maintenance access.

The second exchanger (RC3), located immediately downstream of RC2, extracts the remaining low-grade thermal energy from the flue gas to heat the water stored in the accumulation tank, which supplies the textile washing machines. As these machines operate with water temperatures not exceeding 40 °C, RC3 enables efficient utilization of low-grade heat, further reducing the thermal duty of the steam generator and contributing to overall fuel savings.

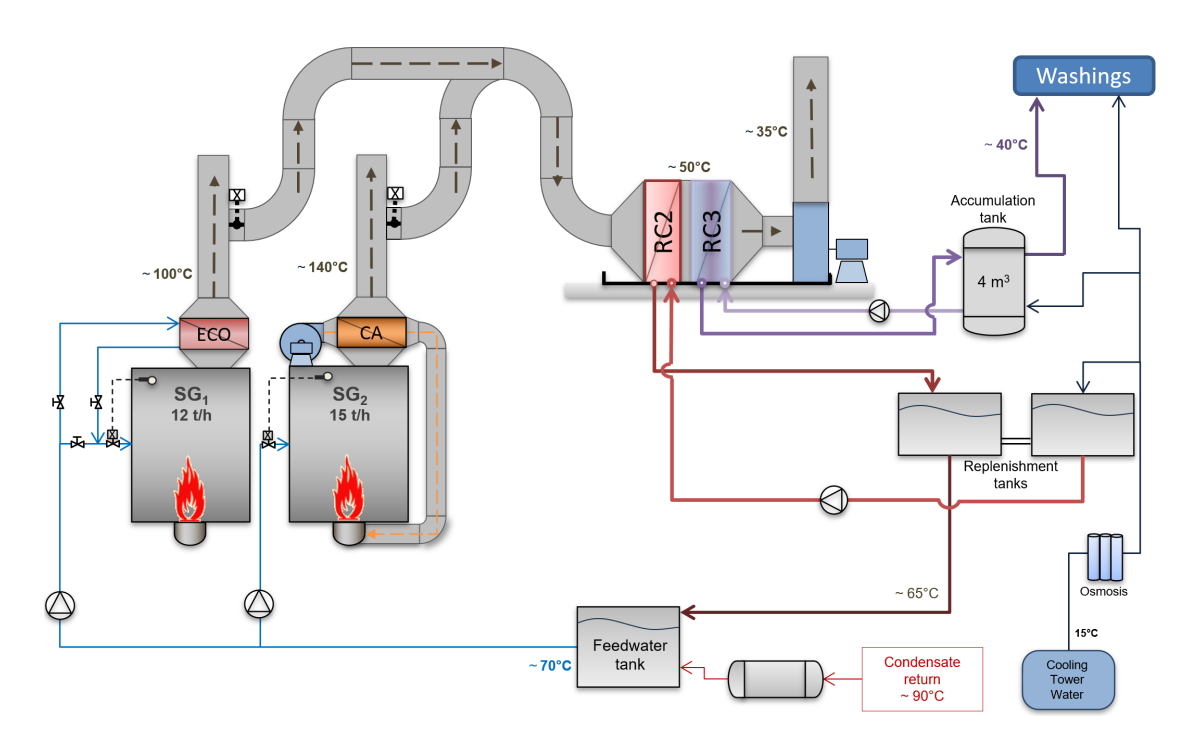


Figure 2.9: Heat Recovery Thermal Power Plant Scheme.

The heat exchangers for heat recovery are sized, followed by an on-site inspection to assess space availability and support the design of the aeraulic and hydraulic systems. The extraction fan has been then dimensioned based on a detailed pressure-drop analysis. The aeraulic system has been designed to ensure adequate draft, safe dispersion of flue gases, and compliance with environmental regulations, taking into account thermal, fluid-dynamic, and environmental criteria to guarantee efficient and safe operation.

## 2.3.1 Sizing of Heat-Recovery Exchangers

The heat recovery system has been sized to maximize energy recovery from the flue gases under typical operating conditions. For this process, a representative scenario is assumed:  $SG_1$  at full capacity (12 t/h of steam) and  $SG_2$  at partial load (8 t/h of steam). The resulting total flue gas flow rate and weighted average temperature are detailed in Table 2.13.

The subsequent sizing of the heat exchangers is governed by a cost-effectiveness analysis, mirroring the approach used for the steam generator economizer. While minimizing the temperature approach boosts heat recovery, the required increase in surface area and capital investment is ultimately deemed unjustifiable when the marginal heat recovered is minimal.

As a result of this analysis, the two heat exchangers are sized as follows:

- $\diamond$  RC2 has a heat exchange surface area of nearly 500 m<sup>2</sup>, achieving a thermal duty of approximately 1.1 MW.
- $\diamond$  RC3 is designed with a minimum temperature approach of 15 °C between the flue gas and the water. It extracts the remaining low-grade heat, achieving a thermal duty of about 470 kW, which requires a heat exchange surface area of roughly 200 m<sup>2</sup>.

The operational data for the two heat exchangers (RC2 and RC3), including the flow rates and temperatures for their inlet and outlet streams, are summarized in Table 2.10, alongside the corresponding steam production from each generator, for both full-load and medium-load operating conditions.

		Max Load Operation			Medium Lo	ad Opera	ation
Steam Generators		Load	$\dot{\mathbf{V}}_{dry\ f.g.}$ [Nm <sup>3</sup> /h]	$egin{array}{ c c c c c c c c c c c c c c c c c c c$	Load	$\dot{\mathbf{V}}_{dry\ f.g.}$ [Nm <sup>3</sup> /h]	$T_{f.g.}$ $[^{\circ}C]$
	Outputs	$SG_1 (12 t/h)$	8818	106	$SG_1 (7 t/h)$	5154	93
		$\mathrm{SG}_2\left(8\ \mathrm{t/h}\right)$	6051	170	$\mathrm{SG}_2\left(\mathrm{off}\right)$	-	-
H:	X RESULTS	RC2	RC3		RC2	RC	3
	$\dot{m V}_{dry~f.g.}$ [Nm <sup>3</sup> /h]	14870	14870	)	5154	5154	1
Fin	$m{T}_{in}$ [°C]	132	51	51		48.5	
$_{ m side}$	$T_{out}$ [°C]	51	51 42.5		48.5	35.86	
side	<b>△P</b> [Pa] 304		130		56	20	
	$oldsymbol{v}$ [m/s]	2	2		0.7	0.7	
	$\dot{m V}_{water}$ [l/h]	20000	20000	)	5600	7400	)
Tube	$T_{in}$ [°C]	15	15		15	15	
side	$T_{out}$ [°C]	61.9	35.3	35.3		39.83	2
side	$\Delta P$ [kPa]	193.7	88.8		20.1	15.7	
	$oldsymbol{v}$ [m/s]	2.1	1.77		0.59	0.66	5
HX	Th. power [kW]	1090	471.3		324.8	213.5	53
IIA	HX surface [m <sup>2</sup> ]	494.8	206.1		494.8	206.	1

**Table 2.10:** RC2 and RC3: Design and Operating Conditions at Full and Medium Load.

Following the sizing of the heat exchangers, the inlet hopper (at RC2) and outlet hopper (at RC3) have also been dimensioned. These components follow the same criteria used for the steam generator economizer hoppers (Figure 2.8), with their final dimensions summarized in Table 2.11.

RC2	RC2 inlet hopper		RC3 outlet hopper		
$D_1$	$700 \; \mathrm{mm}$	$D_2$	805  mm		
LL	$1500\;\mathrm{mm}$	LL	$1500 \; \mathrm{mm}$		
LC	$1320~\mathrm{mm}$	LC	$1320\;\mathrm{mm}$		
$\mathrm{H}_1$	$500 \; \mathrm{mm}$	$\mathrm{H}_2$	$450 \; \mathrm{mm}$		
$\alpha_1$	51.3 °	$\alpha_2$	52.3 °		
$\Theta_1$	58.2 °	$\Theta_2$	60.2 °		

Table 2.11: RC2 and RC3 Hopper Dimensions

## 2.3.2 Flue Gas Flow Management: Design and Sizing

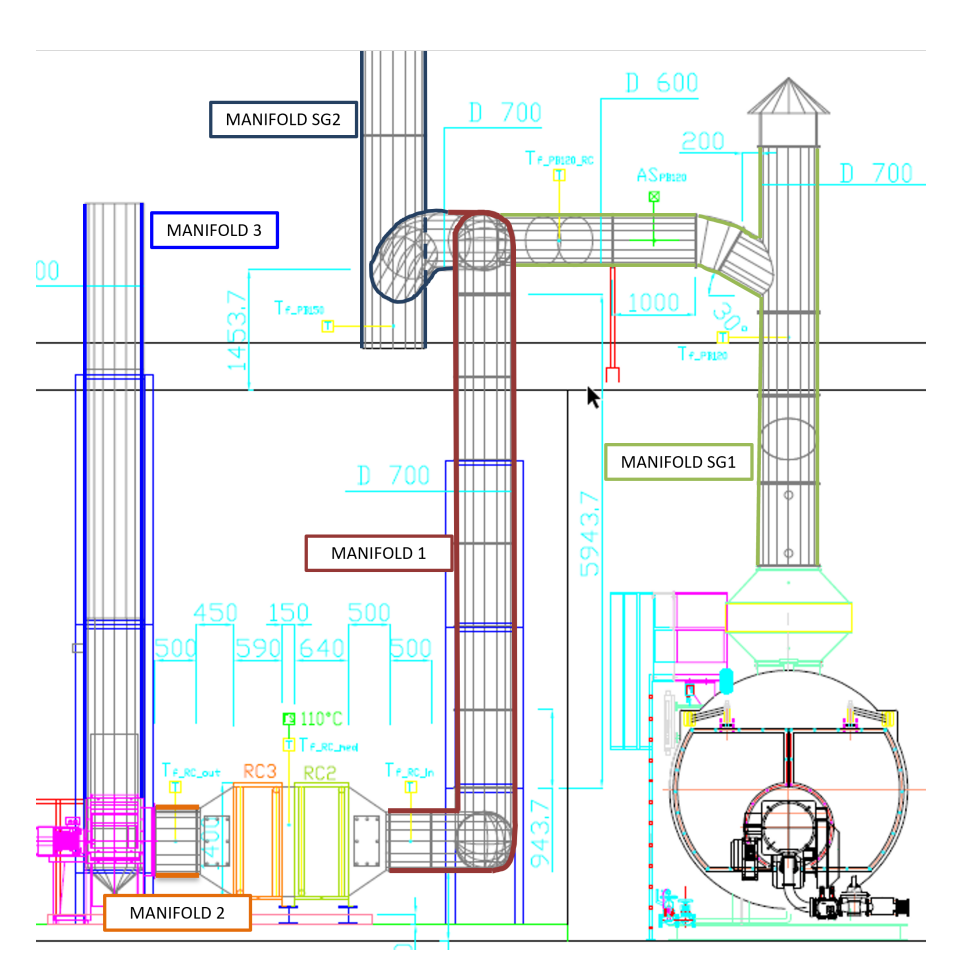


Figure 2.10: Technical drawing – Front and plan view with manifold identification.

The aeraulic system comprises all ductwork that conveys flue gases from the steam generators' chimneys to the heat recovery system and finally to the atmosphere. Figure 2.10, presents a front view of the system, highlighting its configuration and labelled ducts for quick reference. For a complete representation of the plant, including all detailed views, see the technical drawings in *Appendix C*.

The flue gases are captured directly from the chimneys of the steam generators through AISI 304 stainless steel aeraulic ducts, specifically selected for their high corrosion resistance and suitability for high-temperature exhaust gases typical of thermal power plants.

The aeraulic system has been designed to handle the peak flue-gas mass flow. In accordance with standard EN 13384-1 [48], all duct diameters are selected to maintain gas velocities within the 5–20 m/s range.

As a first step in the analysis, the theoretical internal diameter is determined for each section of the aeraulic system, based on the maximum volumetric flow rate it may be required to handle. The use of the maximum flow rate ensures the manifold is adequately sized under the worst-case condition, minimizing pressure losses and avoiding excessive gas velocities that could lead to erosion, noise, or back pressure on upstream components.

The flow rate is calculated starting from the volumetric flow rate of wet flue gas (under normal conditions) and the actual operating temperature (Table 2.8), then corrected to the operating temperature. In this preliminary sizing phase, a conservative maximum gas velocity of 18 m/s is assumed.

The theoretical internal diameter D is then computed by rearranging the continuity equation for incompressible flow:

$$\dot{V} = A \cdot v = \frac{\pi D^2}{4} \cdot v \quad \Rightarrow \quad D_{th} = \sqrt{\frac{4 \cdot \dot{V}_{\text{max}}}{\pi \cdot 3600 \cdot v_{max}}} \times 1000 \tag{2.14}$$

Where:

- $D_{th}$  is the duct theoretical internal diameter;
- $\dot{V}_{\rm max}$  is the maximum volumetric flow rate at operating temperature the duct may handle;
- $v_{max}$  is the assumed maximum velocity of the flue gas in the pipe.

Consequently, the manifolds connected to the chimneys of the two steam generators, prior to their confluence, have been sized based on the maximum flue gas flow rate each unit can generate, so by considering both steam generators at nominal capacity, as reported in Table 2.12.

Manifold $SG_1$ and Manifold $SG_2$				
	$oldsymbol{SG}_1$	$oldsymbol{SG}_2$		
Load	12 t/h	15 t/h		
Duct:	Manifold $SG_1$	Manifold ${ m SG}_2$		
$\dot{V}_{wet~f.g.}$	$10751~\mathrm{Nm}^3/\mathrm{h}$	$13833~\mathrm{Nm}^3/\mathrm{h}$		
$T$ $_{f.g.}$	105.9 °C	170 °C		
$\dot{\mathbf{V}}_{ extit{f.g.}}$ (effective)	$14919~\mathrm{m}^3/\mathrm{h}$	$22442~\mathrm{m}^3/\mathrm{h}$		
$D_{\it theoretical}$	$541~\mathrm{mm}$	664 mm		
$D_{ m  design}$	$600~\mathrm{mm}$	700 mm		
${f v}_{ m eff} (with \ D_{ m design})$	$14.7 \mathrm{\ m/s}$	$16.2 \mathrm{\ m/s}$		

**Table 2.12:** Sizing of Manifold  $SG_1$  and  $SG_2$  at nominal capacity of both steam generators.

The sizing procedure applied to all manifolds (collectors) handling the combined flue gases from both steam generators is based on the maximum expected load condition of the thermal power plant (Table 2.13). This conservative scenario assumes:

- SG<sub>1</sub> at full capacity (12 t/h of steam);
- SG<sub>2</sub> (rated at 15 t/h) at approximately 60% load (8 t/h of steam).

The overall goal of using this peak flow rate is to ensure adequate manifold dimensions, thereby minimizing pressure losses and preventing issues like erosion or back pressure. The flue gas temperature varies significantly between the collectors:

- Manifold 1: the temperature is calculated as a weighted average of the combined gases discharged at different temperatures from the two steam generators.
- Manifold 2: the temperature corresponds to the colder outlet conditions of the heat recovery exchangers. This value will be determined in the subsequent analysis focused on sizing the heat recovery system (Table 2.10).

Two specific design choices are made for efficiency and cost optimization:

• Manifold 1 diameter has been rounded down (resulting in a slightly undersized dimension) while remaining within the acceptable gas velocity range. This choice is justified because the system rarely operates at maximum load. Under the more frequent medium-load conditions, this slightly smaller diameter ensures efficient flow and an appropriate pressure drop. A larger diameter

would have led to unnecessarily low velocities, potentially causing inefficient flow distribution and incurring higher material costs.

• Manifold 2 diameter has been explicitly matched to the ventilator inlet. This design decision eliminates the need for an additional transition element, simplifying installation and reducing both material and fabrication costs while ensuring proper flow alignment into the ventilator.

Manifold 1, Manifold 2, Manifold 3					
	$oldsymbol{SG}_1$	$oldsymbol{SG}_2$			
Load	12 t/h		8 t/h		
$\dot{\mathbf{V}}_{ ext{wet f.g.}}$	$10751.2~\mathrm{Nm}^3/\mathrm{h}$		$7377.6~\mathrm{Nm}^3/\mathrm{h}$		
$T_{ m f.g.}$	105.9 °C		170 °C		
Duct:	Manifold 1	Mani	fold 2	Manifold 3	
$\dot{V}_{ m wet\ f.g.}$	$18129~\mathrm{Nm}^3/\mathrm{h}$	18129	$\mathrm{Nm}^3/\mathrm{h}$	$18129~\mathrm{Nm}^3/\mathrm{h}$	
$T$ $_{f.g.}$	$132.0~^{\circ}{\rm C}$	42.5	$^{\circ}\mathrm{C}$	42.5 °C	
$\dot{\mathbf{V}}_{ extbf{f.g.}}$ (effective)	$26890~\mathrm{m}^3/\mathrm{h}$	20950	$\mathrm{m}^3/\mathrm{h}$	$20950~\mathrm{m}^3/\mathrm{h}$	
$D_{\it theoretical}$	$727~\mathrm{mm}$	642	mm	642  mm	
$D_{ m  design}$	700 mm	805	mm	700 mm	
${f v}_{ m  eff} \ (with \ D_{ m  design})$	$19.4 \mathrm{\ m/s}$	11.4	m/s	$15.1 \mathrm{\ m/s}$	

**Table 2.13:** Sizing of *Manifolds 1, Manifold 2 and Manifold 3* at maximum load operating condition.

## 2.3.3 Ventilator Sizing and Aeraulic Pressure Drops

Once the heat exchangers and ducts have been sized (based on nominal conditions, defined lengths, and network singularities), the total pressure losses in the system can be computed. These losses include both distributed losses (due to wall friction) and concentrated losses (from elements like bends, tees, and cross-sectional changes).

The pressure drop analysis is crucial for selecting a suitable fan. The main objective is to identify the minimum pressure rise the fan must provide to ensure the required flow rate under the worst-case scenario, guaranteeing effective flue gas evacuation and reliable system performance.

This procedure involves the following steps:

I. Pressure Drop Analysis and Critical Path Identification: the pressure drop from each steam generator to the fan is determined separately. The

branch with the highest total pressure drop is considered the critical path, and it governs the fan's pressure requirement. For each branch, the total pressure drop  $\Delta P_{tot}$  consists of two main contributions:

• **Distributed losses** due to friction along the straight sections of ducts and can be calculated using the Darcy–Weisbach equation [49]:

$$\Delta P_{\text{distr}} = f \cdot \frac{L}{D} \cdot \rho \cdot \frac{v^2}{2} \tag{2.15}$$

where:

- f is the dimensionless friction factor (dependent on the Reynolds number and the relative roughness of the duct),
- $\cdot L$  is the duct length [m],
- D is the internal diameter of the duct [m],
- $\cdot \rho$  is the flue gas density [kg/m<sup>3</sup>],
- v is the gas velocity [m/s].

The friction factor f is:

- $\circ$  calculated analytically for  $laminar\,flow$  (Re < 2300) as  $f=\frac{64}{\mathrm{Re}},$
- $\circ$  obtained from the Moody diagram or the Colebrook equation for turbulent flow (Re > 4000) [50].
- Concentrated losses, also known as singularities, occur at specific elements in the duct network such as: bends, tees, contractions and expansions, dampers and valves. These losses are evaluated using the following equation:

$$\Delta P_{\rm conc} = \xi \cdot \rho \cdot \frac{v^2}{2} \tag{2.16}$$

where:

- $\xi$  is the dimensionless loss coefficient (depends on the type and geometry of the singularity);
- $\cdot \rho$  is the flue gas density [kg/m<sup>3</sup>];
- v is the local flow velocity [m/s].

The value of  $\xi$  is obtained from empirical tables that report standardized coefficients for the most common duct components [51, 52]. These values are determined through laboratory testing and are widely used in engineering practice for estimating localized pressure drops.

The analysis confirmed that the branch connected to SG<sub>1</sub> exhibits the highest overall pressure drop and thus defines the critical path and the operating point at the fan inlet.

II. Calculating Minimum Pressure Rise: the total resistance of the critical path is combined with the pressure drop across the final discharge section downstream of the fan (which conveys the flue gases to the atmosphere). This combined resistance dictates the minimum pressure rise the fan must provide to overcome system resistance.

The fan is then selected based on these pressure and flow requirements to handle the worst-case scenario.

Table 2.14 provides a comprehensive summary of all pressure losses along the most critical path, from SG1 to the fan and then to the environment. Both distributed losses and localized losses due to singularities are reported. Each singularity is listed with its corresponding pressure drop. The indices (i, j) refer respectively to the duct segment and the associated singularity.

	1 - Manifold SG1 - From SG1 to Manifold 1					
$\dot{f V}$ [	$m^3/h$	v [m/s]	D [mm]	L $[m]$	$\Delta P_{dist}/L~[Pa/m]$	$\Delta P_{distr}$ [Pa]
1	4922	14.66	600	4	2.94	11.77
(i, j)	(i, j) Fitting			ξ [-]	$\Delta P_{conc,j}[Pa]$	
(1, a)	Y, 60°, Di	verging j	unction b	ranch	0.90	106.35
(1, b)	But	terfly da	mper $(0^{\circ})$		0.20	23.63
(1, c)	Elbow	, 3 Gore,	30°, r/D	=1	0.10	11.82
(1, d)	Elbow	, 3 Gore,	45°, r/D	=1	0.20	23.63
(1, e)	Y, 60°, Co	nverging	junction	branch	0.84	98.67
$\Delta P_{\ conc}\ \ [Pa]$			264.09			
		$\Delta P_{tot,1}$	[Pa]		275.8	36
	2 -	· Manifo	ld 1 - Fr	om M	anifold SG1 to RC	$\mathbb{C}2$
$\dot{f V}$ [	$m^3/h$ ]	v [m/s]	D $[mm]$	L $[m]$	$\Delta P_{ m  dist}/L \ [{ m Pa/m}]$	$\Delta P_{distr}$ [Pa]
2	26897	19.41	700	14	4.41	61.78
(i, j)	(i, j) Fitting		ξ [-]	$\Delta P_{conc,j}[{ m Pa}]$		
(2, a)	(2, a) Elbow, 5 Gore, 90°, r/D=1			0.4	82.89	
(2, b) Elbow, 5 Gore, 90°, r/D=1			0.4	82.89		
(2, c) Elbow, 5 Gore, 90°, r/D=1			0.4	82.89		
(2, d) Hopper RC2			0.63	130.55		
	$oldsymbol{\Delta P}_{ ext{conc}}\left[ ext{Pa} ight]$			379.21		
$\Delta P_{tot,2}[ ext{Pa}]$			440.99			

	3 - Manifold 2 - From RC3 to Fan					
$\dot{oldsymbol{V}}$ [	$m^3/h$ ]	v [m/s]	D $[mm]$	L $[m]$	$\Delta P_{ m  dist}/L \ [{ m Pa/m}]$	$\Delta P_{distr}$ [Pa]
2	20952	11.43	805	0.5	0.18	0.64
(i, j)	(i, j) Fitting			ξ [-]	$\Delta p_{\; conc,j} \; [Pa]$	
(3, a)	(3, a) Hopper RC3			0.20	14.38	
		$oldsymbol{\Delta P}_{ ext{cone}}$	[Pa]		14.38	
	$\Delta P_{tot,3}[ ext{Pa}]$			15.02		
	4 - Manifold 3 - From Fan to Environment					
$\dot{oldsymbol{V}}$ [	$m^3/h$ ]	v [m/s]	D $[mm]$	L $[m]$	$\Delta P_{ m  dist}/L \ [{ m Pa/m}]$	$\Delta P_{distr}$ [Pa]
2	20952	15.12	700	9	1.27	11.47
(i, j) Fitting			ξ [-]	$\Delta P_{ conc,j}  [Pa]$		
(4, a) Y, 60°, Diverging junction - main			0.60	75.46		
	$oldsymbol{\Delta P}_{ ext{cone}}\left[ ext{Pa} ight]$			75.46		
$\Delta P_{tot,4}$ [Pa]			86.94	1		

Table 2.14: Distributed and localized pressure losses along the critical path.

Summing all pressure losses, including the drop across the heat exchangers, yields the total system resistance that the fan must overcome. The total resistance accounts for approximately 1.3 kPa, as shown in Table 2.15.

	Maximum Load	Medium Load	
	$(\dot{ ext{G}}_{ ext{steam}} = 20 \;  ext{t/h})$	$(\dot{G}_{steam} = 7 t/h)$	
Manifold SG1	275.9 Pa	83.4 Pa	
Manifold 1	441.0 Pa	42.0 Pa	
RC2 (datasheet)	304.0 Pa	56.0 Pa	
Plenum	20.0 Pa	20.0 Pa	
RC3 (datasheet)	130.0 Pa	20.0 Pa	
Manifold 2	15.0 Pa	1.7 Pa	
Manifold 3	86.9 Pa	13.3 Pa	
$\Sigma \Delta P$	1272.8 Pa	236.4 Pa	

**Table 2.15:** Summary of total pressure drops for each duct segment and HX, evaluated under both maximum and medium load conditions.

III. Fan sizing procedure: having determined the total pressure drop, the fan sizing process proceeds with the calculation of the mechanical power required under actual operating conditions, while referencing standard conditions (sea level, atmospheric pressure, and a temperature of 20 °C). Since the system is installed at an altitude of 320 m a.s.l., the actual operating pressure  $(p_{op})$  is slightly lower than the standard atmospheric pressure. This operating pressure can be estimated using the barometric formula, which describes the variation of atmospheric pressure with altitude:

$$p_{\rm op} = p_{\rm atm} \cdot \exp\left(-\frac{h}{7000}\right) \tag{2.17}$$

To ensure conservative sizing, the fan is dimensioned based on the worst-case thermal scenario in which the flue gas reaches the fan at a temperature of 80 °C, without transferring the expected thermal power to the heat exchangers. Under these conditions, the flue gas density,  $\rho$ , is estimated using the ideal gas law. Assuming the flue gas behaves similarly to air, the equation becomes:

$$\rho = \frac{p_{\rm op}}{R_{\rm air} \cdot T_{\rm op}} \tag{2.18}$$

where:

- $p_{op}$  [Pa] is the operating absolute pressure at the fan inlet (Eq. 2.17);
- .  $R_{air} = 287 \ [J \cdot (kg \cdot K)^{-1}]$  is the specific gas constant for dry air;
- .  $T_{\rm op}$  [K] is the operating absolute temperature of the flue gases at the fan inlet in the worst-case scenario.

Once the flue gas density under operating conditions has been determined, the power absorbed by the fan can be calculated using the following expression:

$$P_{\text{fan}} [kW] = \frac{\frac{\rho_0}{\rho} \cdot \dot{V}_n \cdot \Delta P_{tot}}{\eta_f \cdot \eta_m} \cdot \frac{1}{1000}$$
 (2.19)

where:

- .  $\rho_0$  [kg/m<sup>3</sup>] is the air density at reference conditions (20 °C, p<sub>atm</sub>);
- $\cdot \dot{V}_n$  [m<sup>3</sup>/s] is the nominal volumetric flow rate of the fan, expressed at reference condition (20 °C, p<sub>atm</sub>);
- $\Delta P_{tot}$  [Pa] is the total pressure drop the fan must overcome;
- $\eta_f$  is the fan efficiency (from manufacturer datasheet), and  $\eta_m$  is the efficiency of the electric motor (IE3 class, [53]).

Table 2.16 presents the input parameters and the results of the fan sizing process, including the estimated power absorbed by the fan under medium load conditions. To ensure reliability and account for system variability, a 25% design margin is added to the pressure drop.

		Reference Condition	Operating Condition	
h (a.s.l.)	[ m]	0	320	
$p_{\ atm}$	[Pa]	101'325	96'797	
T	$[^{\circ}C]$	20	80	
$\rho_{0}$	$[\mathrm{kg/m}^3]$	1.205	0.955	
$\eta_f$		$\eta_{m}$	$\eta_{i}$	
87%	, )	92.60%	97.50%	
	SG1	$12 \mathrm{~t/h}$	7 t/h	
Load	SG2	$8~\mathrm{t/h}$	off	
$\Delta P$	[Pa]	1'273	236.4	
$\Delta P + 25\%$	[Pa]	1'591	296	
$\dot{V}_{\scriptscriptstyle{0}}$	$[m^3/h]$	19'457.0	6'743.7	
$\dot{V}_{op}$	$[m^3/h]$	24'537.8	8'504.7	
$\eta_{t}$	[-]	80.49%	81.03%	
$P_{ m fan}$	[kW]	13.47	0.87	
$P_{\ tot}$	[kW]	13.82	0.89	

**Table 2.16:** Summary of input parameters and results for fan sizing.

At maximum load an overall efficiency of 80.5%, accounting for both the fan and electric motor efficiencies, has been derived from the performance curve of the selected 18.5 kW unit. Although the calculated power requirement would justify the use of a 15 kW fan (rounded up), an 18.5 kW model has been selected. This oversized choice provides operational flexibility, allowing for the handling of increased flue gas flow rates in the event of future plant upgrades, such as an expansion of the thermal power station or the integration of further heat recovery systems, which may require expelling a greater volume of flue gases. The final design solution consists of a suitably rated centrifugal fan, equipped with a three-phase, forced-ventilated motor and controlled via inverter, for the extraction and conveyance of combustion flue gases toward the heat recovery tower. The use of an inverter not only improves the overall system efficiency by minimizing energy waste under partial loads, but also provides precise control of the fan speed in response to the varying thermal and flow conditions of the plant. This configuration enables

the efficient extraction and conveyance of combustion flue gases toward the heat recovery tower. The selected inverter, with a rated efficiency of  $\eta_I = 97.5\%$  as specified in the manufacturer's datasheet and in Table 2.16, allows for the accurate determination of the electrical power drawn from the grid  $(P_{tot})$ .

### 2.3.4 Pump Sizing and Hydraulic Pressure Drops

The selection of the appropriate pump for the hydraulic system depends on the flow rate and head it must provide, which are, in turn, determined by the configuration of the system. The complete P&ID of the installation is reported in *Appendix C*. In this section, the hydraulic circuits are dimensioned, the pressure drops along the pipes are evaluated, and the circulation pumps are appropriately sized. The analysis focuses on two specific simple single-loop circuits:

- the first connects the heat exchanger RC2, which is responsible for preheating the water feeding the thermal power plant, to the replenishment tanks;
- the second connects the heat exchanger RC3, which preheats the water used for industrial washings, to the accumulation tank.

Both circuits are analysed to ensure proper flow distribution and reliable operation under the expected operating conditions. The sizing process proceeds as follows:

I. **Pipe Sizing** - The process begins by estimating the internal pipe diameter using the continuity equation (Eq. 2.14), based on the required maximum flow rate for each loop. A maximum recommended water velocity of 1.8–2 m/s is adopted for this estimation.

Based on the calculated diameter, a standard Nominal Diameter (DN) is selected by rounding up. With the actual diameter and flow rate established, the effective velocity is calculated, and the specific pressure drop per unit length is determined using standard pressure drop charts for water in steel pipes (Figure 2.11) [54]. Since both circuits are dimensioned for identical flow rates and pipe diameters, they share the same unit pressure loss.

- II. **Pressure Loss Calculation** Total pressure losses are calculated by summing both distributed and concentrated contributions:
  - Distributed Losses: Calculated by multiplying the unit pressure loss by the total pipe length. The length is estimated from on-site inspections and plant layout drawings.
  - Concentrated Losses: These occur due to singularities, such as bends, valves, filters, and inlets/outlets, and are assessed individually.

Table 2.17 summarizes all singularities and their corresponding concentrated pressure losses for both circuits. It also includes the distributed pressure losses along the piping and the pressure drops across the heat exchangers (Table 2.10).

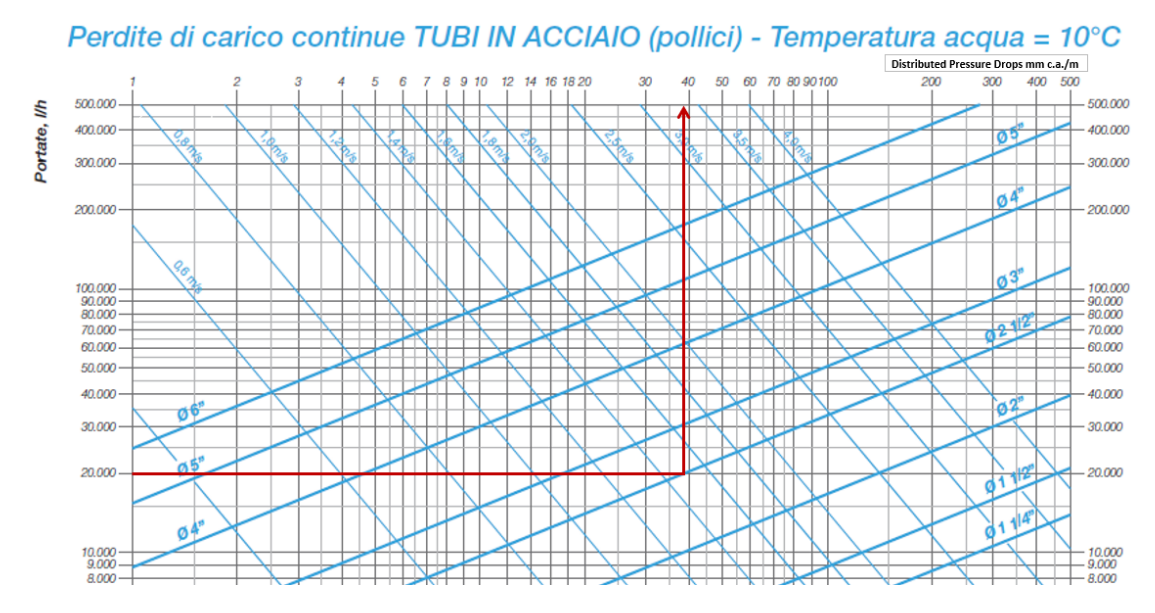


Figure 2.11: Distributed Pressure Drop Chart.

		Replenishment tank - RC2		Accumulation tank - RC3		
	Ů [l/h]	20'000			20'000	
	L [m]		40		30	
Pipe Features	DN ["]		2 1/2"		2 1/2"	
	V [m/s]		1.49		1.49	
	$\Delta P/L [Pa/m]$		377.6		377.6	
Singularities	ξ	#	$\Delta P$ $_{conc,\;i}$	#	$\Delta P_{ { m conc},  i}$	
Short 90° bend $(r/d = 1.5)$	0.8	26	23'226	30	26'799	
Gate valve	0.5	6	3'350	6	3'350	
Y-strainer	5	1 5'583		1	5'583	
Swing check valve	12	1	13'399	1	13'399	
Outlet	1.2	0	0	1	1'340	
Inlet	0.7	1 781.6		1	781.6	
$\Delta P_{ distr,tot}   ext{[Pa]}$		15'102.2		11'326.7		
$\Delta P_{\; conc,tot} \;\;\;  ext{[Pa]}$		46'339.6		51'252.7		
$\Delta P_{ m \it HX}$ [Pa]		193'700		88'800		
$\Delta \mathrm{P_{tot}}$ [Pa]		255'141.8		151'379.3		

Table 2.17: Hydraulic Concentrated and Distributed Pressure Drops.

The sum of all these contributions yields the total pressure drop for each circuit, based on which the circulation pumps can be properly sized. Based on the total head the pumps must overcome, a conservative approach is adopted by increasing the required head by 20%. This ensures proper sizing and reliable operation. The pump power can then be calculated using the following equation:

$$P = \frac{\rho \cdot g \cdot Q \cdot H}{\eta} \tag{2.20}$$

where:

- $\rho$  is the fluid density [kg/m<sup>3</sup>],
- g is the gravitational acceleration  $[m/s^2]$ ,
- Q is the volumetric flow rate [L/s],
- H is the total head [m], increased by 20%,
- $\eta$  is the overall pump efficiency, assumed equal to 80%.

Finally, the required pump power is calculated based on the total head and flow rate. Two pump models are then selected to ensure reliable operation under the given conditions, with particular attention to cavitation. The  $NPSH_{\rm required}$  (Net Positive Suction Head), which is provided by the manufacturer and depends on the pump's operating point, must be lower than the  $NPSH_{\rm available}$  of the system. The  $NPSH_{\rm available}$  is calculated using the following expression:

$$NPSH_{avail} = \frac{P_{atm} - P_{vap}}{\rho g} + \Delta z - Y$$
 (2.21)

where:

- $P_{\text{atm}}$ : atmospheric pressure [Pa],
- $P_{\text{vap}}$ : vapour pressure of water at the operating temperature [Pa],
- $\rho$ : water density [kg/m<sup>3</sup>],
- g: gravitational acceleration (9.81 m/s<sup>2</sup>),
- $\Delta z$ : height difference between the free surface of the suction tank and the pump axis [m],
- Y: head losses in the suction line [m].

The calculation takes into account the actual temperature of the water, the geometric elevation of the suction tank relative to the pump, and all pressure losses in the suction circuit. The comparison between  $NPSH_{\rm avail}$  and  $NPSH_{\rm req}$  confirms the absence of cavitation under operating conditions. All relevant data, including the computed pump power, selected pump models, and cavitation verification, are summarized in Table 2.18.

Pump Sizing					
	Pump 1	Pump 2			
ρ	1000	1000	$kg/m^3$		
$\Delta P$	315'141.8	176'379	Pa		
$\Delta P{+}25\%$	393'927.2	220'474	Pa		
H	40.2	22.47	m		
g	9.81	9.81	$m/s^2$		
Q	5.56	5.56	L/s		
η	80%	80%	_		
P	2.74	1.53	kW		
$P_n$	4.0	3.0	kW		
$NPSH_{ m req}$	2.61	3.22	m		
NPSH avail	11.2	7.0	m		
$NPSH_{ m req}~<~NPSH_{ m avail}$					

Table 2.18: Pump Sizing Parameters, NPSH Evaluation, and Selected Pump.

### Chapter 3

# Numerical Model Development

### 3.1 Aspen Plus Overview

Aspen Plus (Aspen Technology, Inc.[55]) is an advanced process simulation software developed by Aspen Tech, widely adopted in chemical, petrochemical, and energy industries for process design, optimization, and performance evaluation. The software is capable of modelling both steady-state and dynamic operations, enabling engineers to predict system behaviour under various operating conditions with high accuracy. Its strength lies in performing rigorous mass and energy balances, thermodynamic property calculations, and incorporating detailed equipment models within an integrated simulation environment.

#### Applications in Energy and Power Systems

Aspen Plus has become a standard tool in energy engineering due to its versatility and ability to simulate complex thermodynamic systems. Typical applications include:

- design and optimization of chemical processes;
- simulation of power plants, cogeneration units, and heat recovery systems;
- analysis of fuel combustion, heat exchangers, and steam cycles;
- environmental impact assessment through emissions modelling.

Its predictive capability for physical and chemical properties makes it suitable for systems where heat recovery, phase changes, and chemical reactions play a significant role.

In the context of this thesis, Aspen Plus was selected for modelling the steam generator because it offers:

- detailed thermodynamic modelling with accurate prediction of water, steam, and flue gases properties over a wide range of temperatures and pressures;
- integration with process optimization: enables scenario analysis and supports strategies for improving energy efficiency;
- validation capabilities: simulation results can be compared with experimental or manufacturer data for consistency.

The simulation allowed for:

- calculation of heat duty in each section of the steam generator;
- estimation of energy recovery potential through economizer integration;
- evaluation of efficiency under different operating scenarios.

#### 3.1.1 Steam Generator Simulation in Aspen Plus

The steam generator has been modelled and simulated using Aspen Plus. The simulation is performed under full-load conditions, using input data from the preceding thermodynamic analysis, further refined with additional specifications to more accurately represent real operating conditions. The results are compared with analytical calculations and manufacturer datasheet, confirming the model's accuracy and suitability for further analysis and optimization.

As shown in Fig. 3.1, the process flow diagram (PFD) of the steam generator modelled in Aspen Plus is presented.

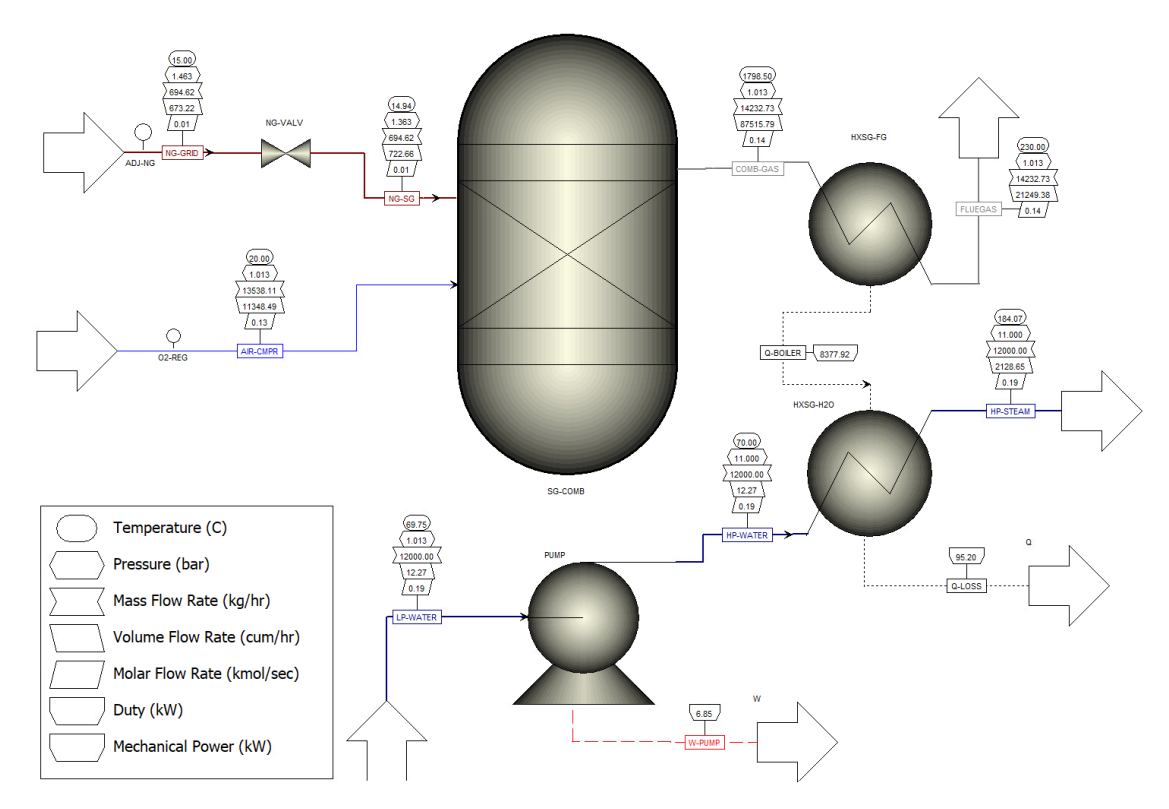


**Figure 3.1:** Aspen Plus process flow diagram of the steam generator based on NG combustion.

The system is structured around two tightly integrated subsystems.

- Combustion Chamber: where natural gas reacts with air, producing high-temperature flue gas. In the simulation model, natural gas, air, and combustion products are treated as pure components, with their thermodynamic behaviour described using the Peng–Robinson equation of state (EOS), suitable for high-temperature and high-pressure conditions.
- Water-Steam Circuit: where feed water is pressurized and converted into steam by absorbing thermal energy from the flue gas. Steam is modelled as pure water, with thermodynamic properties derived from correlations consistent with the ASME Steam Tables, ensuring accurate representation of phase change and enthalpy [56].

The steam generator (SG) is modelled as two thermally coupled subsystems via two heat exchanger blocks (HX-FG and HX-H<sub>2</sub>O). These blocks collectively represent the internal heat exchanger housed within the steam generator. According to the manufacturer's datasheet [28], this internal heat exchanger uses a three-pass configuration (the first pass in the combustion chamber, followed by the second

and third passes in the fire tubes) to enhance thermal efficiency. These two subsystems are thermally coupled through two heat exchangers blocks (HX-FG and HX-H<sub>2</sub>O), which represent the internal heat exchanger housed within the steam generator. From SG datasheet (available on the manufacturer's website [28]), the heat exchanger operates with a three-pass configuration (first pass in the combustion chamber, second and third in fire tubes) to enhance thermal efficiency.

The system was modelled in Aspen Plus following a structured three-step implementation procedure.

- 1. Process block configuration: definition and placement of the required unit operations to represent the main components of the steam generator;
- 2. Stream specification: assignment and connection of material and energy streams between the process blocks to accurately reflect the flow of mass and energy;
- 3. Control strategy implementation: integration of control elements to regulate operating conditions and ensure the system achieves the desired performance targets.

#### Process Blocks

- *Combustion Chamber:* modelled as an RGibbs reactor, where the equilibrium reaction between air and the fuel occurs.
- **Heat Exchangers:** represent the internal heat exchanger of the steam generator. The first heat exchanger (HX-FG) receives high-temperature combustion gases and transfers heat to the second exchanger (HX-H<sub>2</sub>O), where high-pressure water absorbs the heat and is converted into saturated steam. Although implemented as two separate blocks in Aspen Plus, they represent a single physical heat exchanger with multiple gas passes.
- *Pump:* A single-stage centrifugal pump, rated at 14 kW and compliant with IE2 efficiency standards [57], is specified to deliver water at 11 bar discharge pressure [58]. It is modelled using the following efficiency values:
  - Hydraulic efficiency:

$$\eta_h = \frac{\rho g Q H}{P_{\text{shaft}}} = 55\%$$
 (from characteristic curves, [58])

- Drive motor efficiency:

$$\eta_m = 90.3\%$$
 (IE2 efficiency level [57])

• Letdown valve: A pressure-reducing valve that lowers the natural gas supply pressure from 450 barg to approximately 350 barg, in accordance with the combustion chamber requirements.

#### Process Streams

• **Fuel:** is modelled as a refined hydrocarbon mixture using the molar composition of Russian natural gas delivered via the Tarvisio pipeline. The breakdown, shown in Table 3.1, includes methane  $(CH_4)$ , ethane  $(C_2H_6)$ , propane  $(C_3H_8)$  and butane  $(C_4H_{10})$ , accurately reflecting the blend encountered in real transmission pipelines.

Russian Gas (Tarvisio)	Molar Fraction (y <sub>i</sub> )
$\mathrm{CH}_4$	95.66
$\mathrm{C_2H_6}$	2.44
$\mathrm{C_{3}H_{8}}$	0.70
i-C <sub>4</sub> H <sub>10</sub>	0.11
$n-C_4H_{10}$	0.11
$\mathrm{N}_2$	0.68
-CO <sub>2</sub>	0.25

**Table 3.1:** Russian Gas Composition.

• Air: is supplied at atmospheric pressure as humid air (70% RH; see Table 2.3). The stoichiometric O<sub>2</sub> requirement is determined based on the combustion reactions of the hydrocarbons present in the fuel mixture:

$$CH_4 + 2O_2 \to CO_2 + 2H_2O$$
 (3.1)

$$C_2H_6 + 3.5O_2 \rightarrow 2CO_2 + 3H_2O$$
 (3.2)

$$C_3H_8 + 5O_2 \rightarrow 3CO_2 + 4H_2O$$
 (3.3)

$$C_4H_{10} + 6.5O_2 \rightarrow 4CO_2 + 5H_2O$$
 (3.4)

The software calculates the total stoichiometric  $O_2$  demand based on the reaction network and determines the corresponding baseline air flow. A Design Specification block is then used to iteratively adjust the air feed until the dry-basis  $O_2$  concentration in the flue gas reaches the target value — set at 3% in this case [31], thereby determining the required amount of excess air.

- Combustion Gases: off-gas composition is calculated by Aspen Plus using the Peng–Robinson EOS, which accurately handles the hydrocarbon–air mixture in process simulations.
- Water: feed water enters the cycle at 70 °C and atmospheric pressure. It is pressurized to 11 bar by the pump and directed through the heat exchanger

(HX-H<sub>2</sub>O), where it absorbs thermal energy from the combustion gas and is transformed into saturated steam.

#### Control Strategy

- Water Injection. This is the primary input variable. In the initial simulation, the system operates at full load with a water flow rate of 12 ton/h.
- Air Injection. Controlled by a manipulator that adjusts the air flow based on the fuel input, aiming to maintain the desired  $O_2$  concentration in the flue gas.
- **Fuel Injection.** Regulated by a feedforward control strategy that determines the necessary fuel flow as a function of:
  - the required thermal duty to heat and vaporize the water;
  - the steam generator efficiency, which is influenced by heat losses (stack gas, convection, and radiation) and impacts the flue gas outlet temperature.

#### 3.1.2 Results

The results obtained from the Aspen Plus simulation are summarized in Table 3.2, along with the percentage variation relative to the values calculated analytically (Table 2.6).

Overall, the results show strong agreement, with only minor discrepancies. These differences primarily stem from the fact that the fuel composition used in the Aspen model is not limited to pure methane (CH<sub>4</sub>), but rather reflects a more realistic mixture of hydrocarbons, as detailed in Table 3.1. This leads to a slightly higher lower heating value (LHV) compared to the reference value of pure methane assumed in the analytical method.

Specifically, the LHV in the Aspen simulation is approximately 2.7% higher than that used in the analytical model. As a result, a smaller quantity of fuel is required in the simulation to produce the same amount of steam. In addition, the thermal power required to generate 12 t/h of steam appears slightly higher in the Aspen model. This deviation is likely due to differences in the thermodynamic property calculations.

By default, Aspen Plus applies the Peng-Robinson equation of state, which is optimized for non-polar gases and hydrocarbons, but not for accurately modeling the behavior of water and steam. Although a more appropriate property method, namely Steam Tables, has been locally assigned to specific blocks, such as the pump and the heat exchanger, which involve only water and steam, minor inconsistencies in the energy balances and thermal requirements may still occur. These discrepancies

are further influenced by differences in reference states and by the estimation of the latent heat of vaporization, which Aspen Plus may slightly overestimate compared to standard steam tables.

Aspen Results			Relative Variation w.r.t.  Analytical Method
	ṁ	12000  kg/h	
Water	$\mathrm{T_{in}}$	70 °C	0%
	$T_{ m out}$	184.07 °C	
Fuel	$\dot{ m V}_{ m CH4}$	$921.4~\mathrm{Nm}^3/\mathrm{h}$	-2.16%
	λ	1.14 [-]	-0.45%
Air	$\dot{ m V}_{ m humid\ air}$	$10573.8 \text{ Nm}^3/\text{h}$	+0.93%
	$\dot{ m V}_{ m dry~air}$	$10403.0 \text{ Nm}^3/\text{h}$	+0.9370
	$\dot{V}_{\mathrm{wet\ f.g.}}$	$11533.0 \text{ Nm}^3/\text{h}$	+1.00%
Flue Gas	$\dot{V}_{dry~f.g.}$	$9496.6 \text{ Nm}^3/\text{h}$	+1.0070
	T <sub>out, f.g.</sub>	230 °C	0.00%
	LHV	$8784 \text{ kcal/Nm}^3$	+2.74%
Thermal	$ m \dot{Q}_{fuel}$	$9407.2~\mathrm{kW}$	+0.52%
Power	$\dot{Q}_{steam}$	8282.7 kW	+0.30%
rower	$\dot{Q}_{conv, \ rad}$	$95.20~\mathrm{kW}$	+1.73%
	$\dot{Q}_{\mathrm{f.g.}}$	$1029.3~\mathrm{kW}$	+2.2%

**Table 3.2:** Aspen Plus Results and Relative Variation.

#### Economizer implementation and Results

To enhance the system efficiency, the economizer (ECO) is integrated into the process and modeled in Aspen Plus. This additional heat exchanger recovers energy from the high-temperature flue gas to preheat the feed water before it enters the steam generator, thereby increasing overall thermal efficiency.

This implementation allows for a straightforward evaluation of the efficiency gain compared to the steam generator operating without the economizer. The upgraded system is evaluated under nominal conditions as shown in the figure below.

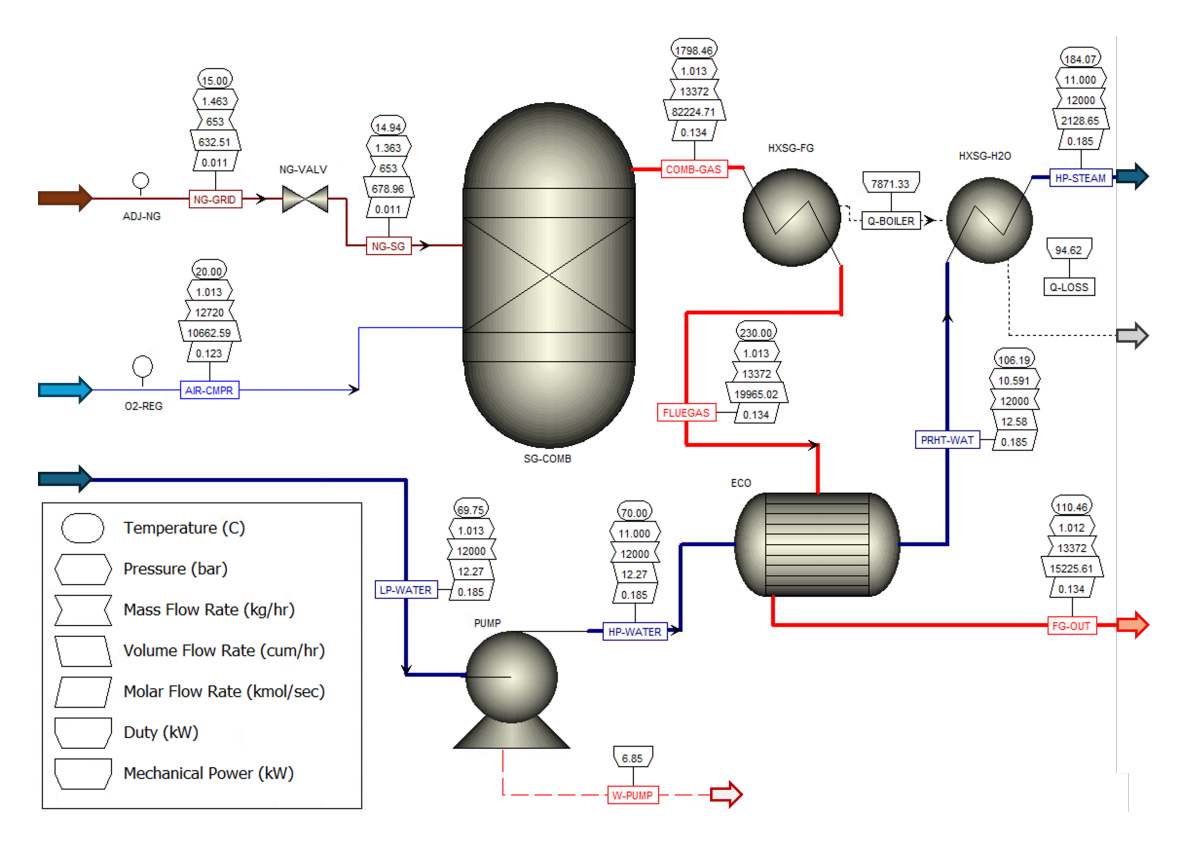


**Figure 3.2:** Aspen Plus process flow diagram of the steam generator with economizer under full-load conditions.

The simulation results (summarized in Table 3.3) show that the net thermal efficiency of the steam generator—economizer system remains effectively unchanged compared to the analytical predictions. Although the Aspen model indicates small differences, specifically, a slightly lower fuel flow rate and a marginal increase in heat recovery within the economizer, the overall performance aligns well with the analytical method.

#### 1. Heat Exchanger Parameters.

The economizer is modelled as a two-stream countercurrent heat exchanger, maintaining the same heat transfer area (as specified in the ECO datasheet in  $Appendix\ A$ ), overall heat transfer coefficient (U), LMTD correction factor, and operating under the same inlet temperature conditions.

The overall heat transfer coefficient U is assumed constant, although it is important to note that in reality it would vary, as it indirectly depends on the mass flow rate, which influences fluid velocity, Reynolds number, and consequently the Nusselt number that governs convective heat transfer.

However, since the variations in mass flow rate are minor in this case, the assumption of a constant U is considered a reasonable approximation.

#### 2. Impact of Fuel Composition on Combustion Airflow.

The simulated fuel composition reflects a realistic natural gas mixture, characterized by a higher lower heating value (LHV) (see Table 3.1). This results in a reduced fuel flow rate required to achieve the same steam production.

However, the air flow entering the steam generator is slightly higher than in the analytical model. This is due to the presence of fuel components that demand more oxygen for complete combustion, thereby increasing the stoichiometric air requirement. Since the excess air ratio is kept constant, the total air flow rises accordingly, despite the lower fuel flow, which also leads to a higher flue gas mass flow rate.

This increase in combustion air and flue gas flow may introduce slightly higher parasitic losses (e.g., increased blower power consumption).

#### 3. Higher Heat Recovery, Lower Fuel Input.

In the simulated model, the economizer recovers more heat from the flue gas than in the analytical case, since the inlet flue gas temperature matches the analytical assumption, but the flue gas flow is increased. This allows to transfers more heat in the economizer, raising the feed water temperature above that predicted by the analytical model. This means the feed water enters the steam generator at a higher temperature, reducing the required firing heat. As a result, the fuel required decreases further.

In summary, despite minor discrepancies related to increased heat recovery in the economizer and variations in fuel and air flows, the simulation exhibits only slight differences in the percentages of heat recovered in the economizer and heat released during steam generation relative to the fuel's thermal input.

As a result, the overall thermal efficiency remains essentially unchanged, confirming that the results obtained through Aspen are consistent and reliable.

Consequently, the overall thermal efficiency remains virtually unchanged, confirming the consistency and reliability of the results obtained with Aspen Plus.

Additionally, when comparing this model with the version without the economizer, both developed in Aspen Plus, we observe a similar outcome to that obtained through the analytical method: an efficiency improvement of approximately 5 percentage points. All these results are summarized in the Table 3.3.

			Aspen Results	Analytical Method
		ṁ	12000  kg/h	12000 kg/h
	Water	$T_{\rm in}$	70 °C	70 °C
		$T_{\mathrm{out}}$	106.19 °C	104.97°C
ECO		$\dot{V}_{ m wet\ f.g.}$	$10835.9~\mathrm{Nm}^3/\mathrm{h}$	+1.18 %
	Flue	$\dot{V}_{dry~f.g.}$	$8922.6~\mathrm{Nm}^3/\mathrm{h}$	w.r.t. An. Method
	Gas	T <sub>in, f.g.</sub>	230 °C	230 °C
		$T_{out, f.g.}$	110.46 °C	105.9°C
	Water	$T_{\rm in}$	106.19 °C	104.97°C
	water	$T_{ m out}$	184.07 °C	184.07 °C
G.	Fuel	$\dot{ m V}_{ m CH4}$	$865.7~\mathrm{Nm}^3/\mathrm{h}$	- 2.37 % w.r.t. An. Method
Steam	ruei	LHV	$8784~\mathrm{kcal/Nm}^3$	+2.74 % w.r.t. An. Method
Generator		λ	1.14 [-]	0.0114
	Air	$\dot{ m V}_{ m humid\ air}$	$9934.8 \text{ Nm}^3/\text{h}$	+0.71 %
		$\dot{V}_{ m dry\; air}$	$9774.2 \text{ Nm}^3/\text{h}$	w.r.t. An. Method
			Aspen Results	Analytical Method
		$\dot{Q}_{steam\_SG}$	88.0%	88.2%
Thermal	Power	$\dot{Q}_{ECO}$	5.7%	5.5%
		$\dot{Q}_{conv,\ rad}$	1.1%	1.1%
		$\dot{Q}_{ m f.g.}$	5.2%	5.2%
	$\eta_{ m GV\_ECO}$		93.71%	93.72%

**Table 3.3:** Comparison of Aspen Plus simulation results and analytical method for the SG with ECO.

### Chapter 4

# Cogeneration System Test Case

Following the initial upgrade of the thermal plant and the implementation of the flue gas heat recovery system, the textile company M. further expanded its optimization strategy by designing and commissioning a Combined Heat and Power (CHP) or cogeneration plant at the facility.

This new system was specifically engineered to achieve three key energy objectives: generate electricity, produce 10 barg process steam (thereby reducing the load on the existing thermal power station), and preheat water for the continuous washing lines.

The primary operational benefit of the CHP unit is the reduction in steam demand placed on the main boilers, which translates directly into significant natural gas savings and lower operating costs. Simultaneously, the system substantially limits the facility's reliance on the electricity grid, boosting overall energy efficiency and security.

The core of the unit is an internal combustion engine coupled to an electric generator. This generator converts the engine's rotational motion (1,500 rpm) into three-phase electricity (400 V/50 Hz). Heat recovery occurs from multiple sources:

- Engine Jacket Cooling: Supplies low-temperature heat to produce hot water for direct use in the production process (e.g., washing water).
- Exhaust Gases: Residual heat in the flue gases is exploited to produce 10 barg steam via a Gas Vapour Recovery (GVR) unit.

The successful integration of this cogeneration plant represents a strategic advancement in the company energy management, optimizing fuel use, cutting expenses, and reinforcing their commitment to sustainable industrial practices.

# 4.1 Process Scheme of the CHP Unit and HR Integration

To provide a clear overview of the system's configuration, this section illustrates the complete process scheme in Figure 4.1. The diagram highlights the main components, energy flows, and recovery stages of the CHP unit integrated with the flue gas heat recovery and hydraulic circuit, followed by a detailed explanation of their operation and interactions.

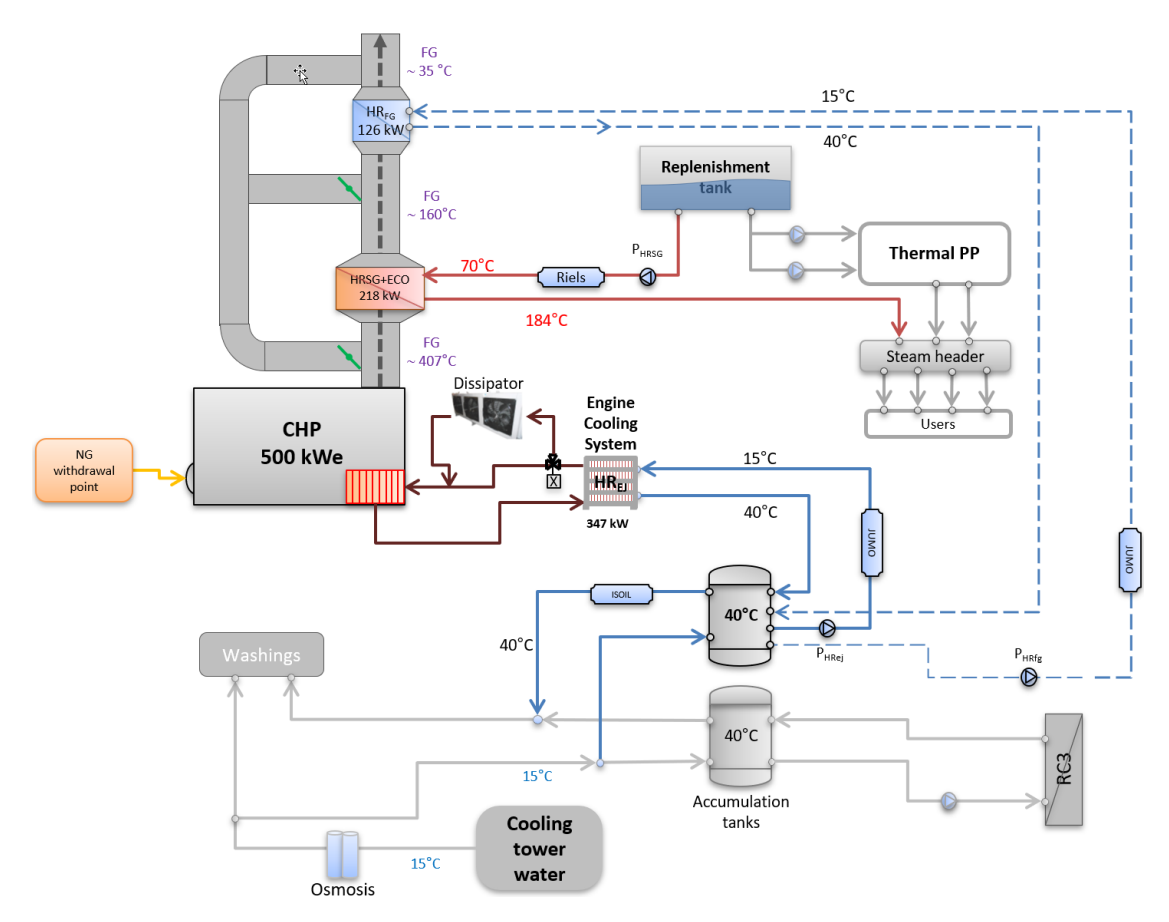


Figure 4.1: CHP Unit and Heat Recovery Scheme.

The cogeneration unit is housed within a pre-installed, sound-dampening container that features Class A1/A2 fire-resistant thermal insulation. The unit operates on natural gas, which is supplied through a dedicated gas ramp. This ramp ensures safe delivery, maintaining the precise fuel-to-air ratio required for optimal combustion within the engine's intake manifold. This controlled operation maximizes efficiency, prolongs engine life, and minimizes atmospheric pollutant emissions.

The system uses a two-stage approach for heat recovery:

I. Engine Jacket Cooling (Hot Water)

The first stage recovers heat from the engine jackets to produce hot water. This energy is used to heat the water in the stratified storage tanks to approximately 40 °C.

II. Exhaust Gas Heat Recovery (Steam and Water Preheating)

This stage fully exploits the substantial residual thermal energy contained in the engine's high-temperature exhaust gases (typically above 400 °C).

- A Fire-Tube Heat Recovery Steam Generator (HRSG), designed to generate process steam at 10 barg.
- A second heat exchanger downstream of the HRSG, used to capture the remaining low-grade heat and preheat the feed water tank, maximizing the overall thermal energy captured from the flue gases.

Heat Recovery from Engine Cooling and HT Intercooler. This heat recovery stage is implemented through a plate heat exchanger, which is fitted with a comprehensive set of accessories and control instruments to regulate water temperature and ensure proper pressure and temperature management. In the event of thermal load saturation, detected by a dedicated thermostat, the mixing thermoregulation valve begins to open, blending the water exiting the plate heat exchanger, which is no longer adequately cooled due to user saturation, with water from the dissipation circuit. The dissipation system includes a radiator composed of one or more fans, each controlled by independent thermostats that operate only when required. To enhance system compactness and lower auxiliary costs, turbocharged engines with intercooling incorporate a dual-core radiator, designed to efficiently cool separate fluid loops (e.g., the engine coolant and the intercooler fluid). This configuration enables the same fans used for engine water cooling to also cool the water serving the intercooler.

Heat Recovery from Engine Exhaust Gases for Steam Production. This stage uses a fire-tube heat exchanger capable of producing steam by exploiting the engine exhaust gases. The boiler is designed and manufactured in compliance with the current "PED" directive. It is equipped with an economizer for feed water preheating and a complete set of essential and auxiliary instruments for pressure and temperature control (pressure gauge, level indicators, safety valves, blowdown system, feed system, regulators, and pressure switches). A bypass is also provided, allowing the exclusion of heat recovery in case of load saturation. The bypass can also be manually activated via a selector on the control panel.

Heat Recovery from Exhaust Gases for Low-Temperature Hot Water Production. A finned-tube heat exchanger is installed downstream of the steam boiler. This heat recovery unit receives the flue gases exiting the HRSG at approximately 160 °C. The water from the accumulation tank is heated from 15 °C to 40 °C, as specified in Table 4.3, while the flue gases are cooled to about 35 °C before discharge.

The buffer tank illustrated in the schematic, which is connected to both the plate heat exchanger for engine jacket water cooling and the additional heat recovery unit, has been integrated as part of the cogeneration plant installation. This component was not present in the original configuration and has been introduced to increase the overall storage capacity, thereby ensuring a continuous supply of preheated water to the washing lines, even during peak demand periods.

### 4.2 Design of the Cogeneration System and Heat Recovery Integration

The design of the cogeneration system and its associated heat recovery units follows a systematic process focused on sizing, reliability, and economic feasibility.

#### 1. Data Collection and Sizing

The process began with the collection and analysis of preliminary data, including the facility's annual electricity consumption profile and corresponding natural gas usage. Based on this data, the cogeneration unit has been sized for an electricity-following configuration, ensuring optimal coverage of the site's electrical demand while maximizing valuable thermal energy output.

#### 2. Component Dimensioning

Subsequently, each component of the system has been precisely dimensioned to guarantee efficient energy recovery and seamless integration.

- Heat Recovery Units: sizing the heat exchangers for engine cooling and low-temperature recovery, the Heat Recovery Steam Generator (HRSG) for high-temperature exhaust gases, and the economizer.
- Ancillary Circuits: dimensioning the hydraulic and aeraulic circuits, including all associated pumps, fans, and control devices.

#### 3. Modelling and Economic Verification

Finally, the complete system has been modelled and simulated to verify its thermodynamic performance. This analysis serves as the foundation for a comprehensive economic evaluation, which has provided estimates of capital costs, operational savings, and the expected payback period, confirming the technical and financial viability of the proposed solution (Section 5.2).

#### 4.2.1 Preliminary Data and Input Parameters

The industrial facility is extensive, operating across multiple departments and separate buildings. Consequently, it is equipped with three medium-voltage (MV) electrical substations, from which electrical energy is drawn. This decentralized design minimizes transmission losses and voltage drops — which a single central substation with long distribution lines would incur — while also reducing cable installation costs.

Following a detailed analysis of the facility's monthly and annual energy consumption and its overall load profile, the cogeneration unit has been connected to Primary Substation A. This substation exhibits the highest electricity demand and, critically, maintains a relatively stable and continuous load profile with minimal fluctuations compared to the other substations.

The annual electricity consumption of all three substations is reported in Table 4.1.

Annual Electrical Energy				
Consumption (2019)				
Substation A	$3'678'475~\mathrm{kWh}$			
Substation B	2'698'239  kWh			
Substation C	803'967 kWh			

**Table 4.1:** Annual electrical energy consumption of Substations A, B, and C.

#### 4.2.2 Electric Load Analysis and CHP Unit Selection

To properly size and select a cogeneration unit capable of operating efficiently while following the electrical load, a detailed analysis of the electricity consumption profile for Primary Substation A is performed. This analysis focuses on the hourly electricity demand over a four-month period, spanning October  $1^{st}$  to January  $31^{st}$ .

Figure 4.2 illustrates the electrical load profile of the substation. Demand typically ranges from approximately 450 kWh to 750 kWh, with occasional peaks reaching 900 kWh during weekdays. In sharp contrast, consumption is significantly lower during weekends, usually remaining below 200 kWh. Similarly, consumption remains low for an extended duration during the Christmas holiday period due to facility shutdowns and reduced activity.

By examining this load profile, the optimal power rating at which the cogeneration unit operates most efficiently for the greatest number of hours is identified, thereby optimizing both energy production and economic performance.

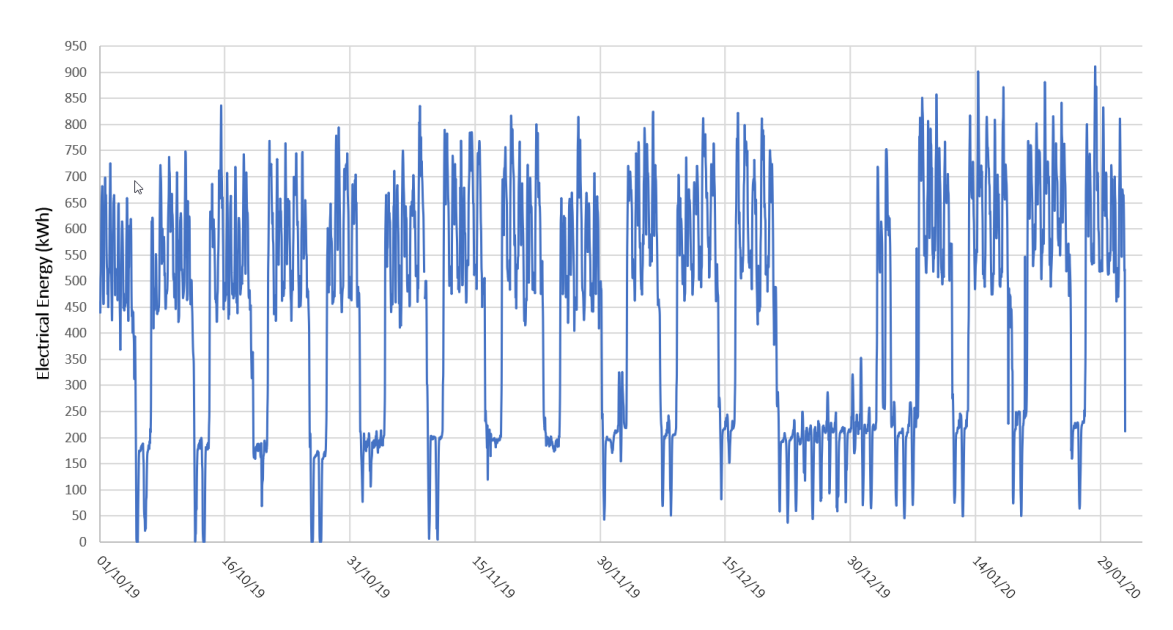


**Figure 4.2:** Hourly electricity consumption profile of Primary Substation A from October to January.

Once the electricity consumption profile has been established, three cogeneration units with nominal electrical capacities of 500 kW, 600 kW, and 800 kW have been selected and simulated under the observed load conditions. Since CHP units can only be started when operating at no less than 60% of their nominal capacity (300 kW, 360 kW, and 480 kW, respectively), the analysis evaluates the performance of each option based on the following key criteria:

- Annual operating hours, determined by the load profile and minimum load constraint.
- Average electrical output during operation, which indicates how close the unit operates to its nominal rating during active periods.
- Total annual electricity generation, providing a measure of the overall contribution to the plant's electricity demand.

This analysis makes it possible to identify the CHP size that ensures the greatest number of operating hours while maintaining efficient utilization of its installed capacity.

The calculated indicators for each configuration are summarized in Table 4.2.

P <sub>n</sub> CHP Unit	Average Output [kW]	Average Load	Annual Operating Hours	$\begin{array}{c} \textbf{Annual} \\ \textbf{Production} \\ \textbf{[kWh]} \end{array}$	Annual Demand Coverage	CF
$500~\mathrm{kW}$	488.8	97.8%	5694	2'783'398.0	75.7%	0.966
600 kW	554.3	92.4%	5586	3'096'336.6	84.2%	0.896
800 kW	621.1	77.6%	4758	2'955'398.4	80.3%	0.641

**Table 4.2:** Comparison of Simulated CHP Configurations Based on Electrical Load Profile.

The thermal load is not considered a primary selection criterion because the facility's high, continuous thermal demand ensures that virtually all heat produced by any candidate unit is fully utilized. Electrical performance and operational hours, therefore, become the primary criteria, especially since electrical efficiency decreases noticeably when the unit operates below its nominal capacity.

The comparative simulation shows that while the two larger cogenerators (600 kW and 800 kW) possess the theoretical capability to supply a greater share of annual electricity, in practice, they operate for fewer hours and, on average, at a lower load. Specifically, the 800 kW unit exhibits a significantly lower average operating load factor (77.6%), which, combined with its reduced operating hours, results in an annual electricity production even lower than that of the intermediate 600 kW unit.

The Capacity Factor (CF) of each unit is determined by considering a maximum annual operating period of 5760 h, in accordance with the facility's operational schedule. It is defined as:

$$CF = \frac{P_{\text{avg}} \cdot h_{\text{op}}}{P_{\text{n}} \cdot 5760 \ h},\tag{4.1}$$

• where  $P_{\text{avg}}$  denotes the average power output and  $h_{\text{op}}$  the annual operating hours.

The 500 kW CHP unit shows the highest CF because it runs for the greatest number of hours and maintains the highest average operating load factor (97.8%). This exceptional utilization means the unit runs at or very close to full capacity for most of the time, maximizing its electrical efficiency and overall economic performance. Based on these results, the 500 kW cogenerator is the optimal choice.

The diagrams in Fig. 4.3 illustrate the load coverage achieved by the three CHP units for the four-month period of detailed load profile data. This visualization makes evident how each unit responds to the substation's electricity demand, providing a direct comparison of utilization, average load during operation, and peak coverage for each candidate cogenerator.

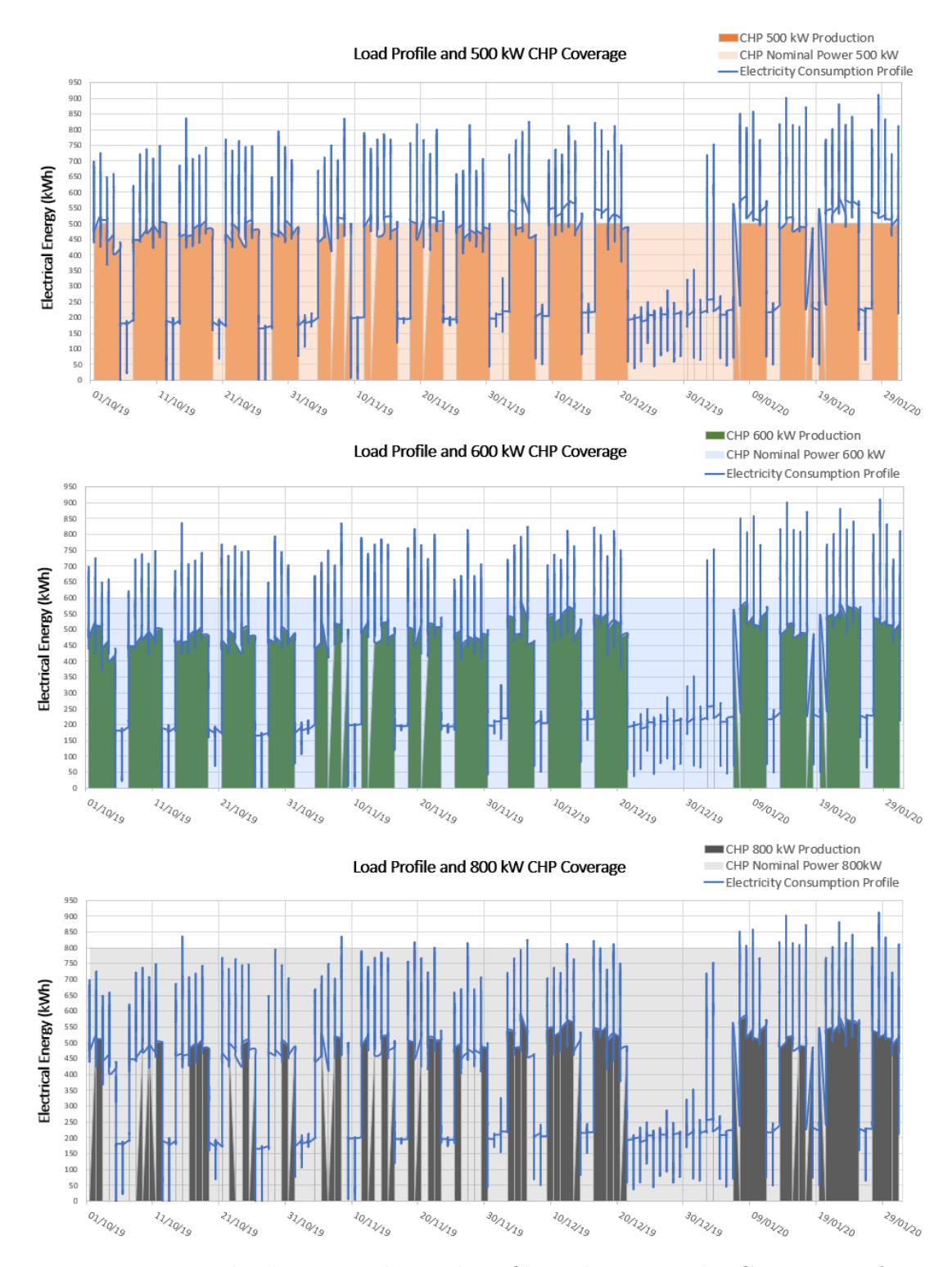


**Figure 4.3:** Hourly electricity demand profile and coverage by CHP units of 500, 600, and 800 kW, respectively, over the period October–January.

#### 4.2.3 CHP Thermal Energy Management

After selecting the 500 kW cogeneration unit, the available thermal energy for recovery and utilization within the plant has been determined using the manufacturer's technical datasheet [59].

Furthermore, since the exhaust gases leaving the HRSG (equipped with an economizer) still reach temperatures of approximately 160 °C, an additional low-grade heat exchanger has been designed to exploit this remaining thermal potential fully. This final exchanger is employed to preheat washing water, ultimately reducing the flue gas temperature to about 35 °C before discharge. Table 4.3 reports a summary of the recoverable thermal power and its distribution across the different recovery sections.

Specifications	$\mathrm{HR}_{\mathrm{EJ}}$	HRSG + ECO	$\mathrm{HR}_{\mathrm{FG}}$
Heat exchanger type	Counterflow Plate HX	Shell and Tube HX	Finned Tube HX
Thermal Power	347 kW	218 kW	126 kW
Primary Fluid	Glycol water	Flue Gases CHP	Flue Gases exiting the HRSG
$T_{\ in}$	88 °C	407 °C	≈ 160 °C
$T_{out}$	82 °C	» 160 °C	≈ 35 °C
Mass Flow	$54~\mathrm{m}^3/\mathrm{h}$	2'848 kg/h	2'848 kg/h
Secondary Fluid	Washing water	Steam	Washing Water
$T_{in}$	15 °C	70 °C	15 °C
$T_{\ out}$	40 °C	184.7 °C (11 bar)	40 °C
Mass Flow	$12~\mathrm{m}^3/\mathrm{h}$	330 kg/h	$4.3~\mathrm{m}^3/\mathrm{h}$

**Table 4.3:** Technical Specifications of Heat Recovery Units.

At this stage, it is essential to evaluate how the recovered thermal energy from the cogeneration unit integrates into the existing process. Operational data from the thermal power plant indicate that approximately 66% of the generated steam is used for both vaporization and washing. Of this, about 30% of this share is dedicated exclusively to hot washing, which means roughly 20% of the plant's total steam production is consumed for that purpose alone.

To quantify the CHP system's potential contribution, the hourly thermal load profile of the plant is analysed over the same four-month period (from October  $1^{st}$  to January  $31^{st}$ ) already considered for the electrical demand. This analysis is performed starting from the natural gas consumption of the thermal power plant, from which the portion of thermal energy required exclusively for hot washing is determined. By difference, the remaining share of steam demand is attributed to vaporization and other utilities.

Subsequently, by imposing the operational profile of the selected CHP unit (under an electric load-following strategy), the corresponding thermal energy recovery is evaluated on an hourly basis. Since the thermal output of the cogenerator is directly linked to its electrical load, the thermal energy recovery from the various heat exchangers is calculated accordingly.

Table 4.4 presents the results obtained from the thermal load profile analysis based on the CHP simulation.

The Average Utilization Factor (the ratio of actual recovered thermal energy to the nominal recovery capacity) is consistently above 97%, indicating that the heat exchangers operate nearly at full capacity throughout the year.

The Annual Coverage of Thermal Demand indicates the contribution of each recovery stage to the plant's total thermal requirements. The  $\mathrm{HX}_{EJ}$  and  $\mathrm{HX}_{FG}$  address the washing thermal load, while the HRSG's output meets a portion of the total process steam demand. This parameter allows for the direct quantification of natural gas savings and subsequent economic benefits, after accounting for the natural gas consumed by the cogeneration unit.

Finally, the ratio between the thermal energy effectively utilized by the production processes and the total thermal energy produced by the CHP system is always higher than 99.8%. This confirms that, whenever the cogenerator is operating, the recovered thermal energy is almost entirely required by the plant.

HR Unit	Average Output [kW]	Average Utilization Factor	Utilized/ Produced Heat	Annual Production [kWh]	Annual Demand Coverage	with respect to:
$HR_{\ EJ}$	338.7	97.60%	99.83%	1'930'470.3	37.2%	3371-:
$HR_{\ FG}$	123.1	97.66%	99.90%	701'428.9	13.5%	Washing
$HR_{EJ} + HR_{FG}$	461.7	-	-	2631899.2	50.7%	Thermal Load
HRSG + ECO	213.1	97.76%	99.998%	1'214'806.2	5.8%	Steam Th. Load

**Table 4.4:** Thermal performance of heat recovery systems in the CHP unit simulation.

At this stage, the corresponding natural gas savings (NG) in the thermal power plant are calculated. This calculation is based on the annual thermal energy recovered in each heat exchanger and assumes an annual operating time of approximately 5 700 hours for the cogeneration unit, along with a conservative boiler efficiency of  $\approx 93\%$  (Table 2.8).

The main technical specifications of the selected CHP unit, which are necessary to estimate its own annual NG consumption, are presented in Table 4.5. These data are sourced from the manufacturer's technical datasheet [59].

Table 4.6 presents the final simulation results. This table includes the total thermal energy recovered by each heat exchanger and the equivalent corresponding natural gas savings realized in the main thermal plant.

CHP Unit Specifications				
Model	CH4-500TI-MA			
Fuel	Natural Gas			
Electric Power at alternator terminals	$500 \; \mathrm{kWe}$			
Thermal Power (Flue Gases at 160°C)	$565~\mathrm{kWt}$			
Total Thermal Power (Flue Gases at 35°C)	691.46 kWt			
Hourly consumption at maximum power:	1282.7  kW			
$\eta_{\ thermal} \ \ (including \ HR_{\ FG})$	53.91%			
η mech	40.31%			
$\eta$ alternator	96.70%			
$\eta_{ m  electrical}$ (cos $\phi=1,~ISO~3046/1)$	38.98%			
<b>Ч</b> СНР	92.89%			

**Table 4.5:** CHP Unit Specifications at Full Load.

It should be noted that the amount of natural gas saved through the CHP's heat recovery is lower than the fuel consumption of the cogenerator itself. However, this apparent imbalance requires correct interpretation. The natural gas consumed by the CHP unit simultaneously contributes to both thermal and electrical production. This combined generation is the foundation of cogeneration, and it is precisely this dual output that justifies both the high overall efficiency and the significant economic advantage of the CHP solution.

Natural Gas Savings and Consumption of the CHP Unit					
Therma	Thermal Energy Produced				
$HR_{\ EJ}$	$1'930'470.3~\mathrm{kWh_{T}/year}$	$215'180.4 \text{ Sm}^3/\text{year}$			
HRSG+ECO	$1'214'806.2~\mathrm{kWh_{T}/year}$	$135'408.6 \text{ Sm}^3/\text{year}$			
$HR_{\ FG}$	$701'428.9~\mathrm{kWh_T/year}$	$78'184.9 \text{ Sm}^3/\text{year}$			
Total The	rmal Energy Produced	$3'846'705.4~\mathrm{kWh_T/year}$			
Total	$428'773.9 \text{ Sm}^3/\text{year}$				
Ele	ctric Production	$2'786'445.0~\mathrm{kWh_e/year}$			
Total C	$741'016.5 \text{ Sm}^3/\text{year}$				
CHP NG Cons	$393'090.4 \text{ Sm}^3/\text{year}$				
CHP NG Cons	$umption\ for\ Electrical\ Prod.$	$347'926.1 \text{ Sm}^3/\text{year}$			

**Table 4.6:** Natural gas savings from heat recovery systems and CHP unit consumption for thermal and electrical energy production.

#### 4.2.4 Sizing of Heat Recovery and Auxiliary Systems

Once the 500 kW cogeneration unit has been selected and the preliminary performance analyses completed, the detailed design of the associated heat recovery systems is undertaken.

The sizing of the heat exchangers is handled as follows:

- The exchangers associated with the engine cooling jackets and the HRSG (equipped with an economizer) are dimensioned and specified by the CHP supplier, who also provides the corresponding datasheets.
- The additional flue gas heat exchanger ( $HX_{fg}$  connected downstream of the HRSG) is designed directly. The procedure adopted for dimensioning this exchanger and its associated hoppers follows the methodology already described in *Chapter 2 (Section 2.2.2)*, ensuring consistency with the general design framework.

Following the sizing of the heat recovery units, the integration of the new systems into the existing thermal plant is analysed, with particular attention to spatial constraints, compatibility with the current layout, and required interconnections.

Based on these considerations, the hydraulic and aeraulic networks, together with the pumps and auxiliary systems, are designed according to the same methodology presented in *Chapter 2 (Section 2.3)*. The complete P&ID of the system is reported in *Appendix D*. The detailed design procedures for these networks are not reiterated here, as they have been extensively discussed in the aforementioned chapter.

A key outcome of this analysis is that the static pressure of the flue gases exiting the CHP unit is sufficient to overcome the pressure losses across the HRSG (including the economizer), the downstream heat exchanger, and the short duct sections. This eliminates the need for a forced draft fan, thereby reducing auxiliary power consumption and simplifying the overall system. This solution is confirmed only after verifying that the available exhaust pressure safely exceeds the total system pressure drop and that the resulting engine backpressure remains within the manufacturer's specified limits.

In parallel with the process design, the required civil and structural works for the proper installation of the CHP unit are developed and later included in the economic assessment. These works include a reinforced concrete foundation to support the CHP unit and ensure stability, as well as a roof equipped with an overhanging grating extending 1 m beyond the container perimeter to increase the usable surface area  $(11 \times 4.5 \text{ m}, \text{ approximately } 49.5 \text{ m}^2)$ . Safety features comprise a perimeter railing, toe boards, an inspection walkway along the flue gas path, and two vertical ladders for maintenance access.

Table 4.7 summarizes the resulting pressure drops across the hydraulic network, the main pressure specifications, and the pump characteristics. This provides a

concise technical overview and allows the discussion to proceed directly to the subsequent economic analysis.

Pump Specifications						
	$ m P_{HRej}$ $ m P_{HRfg}$ $ m P_{HRSG}$ [-]					
ρ	1	1	1	$kg/m^3$		
$\Delta P$	150'000	300'000	1'500'000	Pa		
$\Delta P + 25\%$	180'000	360'000	1'800'000	Pa		
H	18.3	36.7	183.5	m		
g	9.81	9.81	9.81	$m/s^2$		
Q	5.56	2.08	0.56	L/s		
η	80%	80%	80%	-		
$\boldsymbol{P}$	1.25	0.94	1.25	kW		
$P_{n}$	2.2	1.5	2.2	kW		

 Table 4.7: Specifications of the Pumps in the CHP System Hydraulic Network.

### Chapter 5

### **Economic Results**

Once the overall design process was completed, it became possible to consolidate the outcomes of the two proposed projects. This chapter presents the results obtained in terms of energy efficiency improvements and the associated savings, including reductions in natural gas consumption,  $CO_2$  emissions, electricity use, and overall operating costs. A comprehensive economic analysis of both projects is also provided.

The initial investment for the first intervention, involving the retrofitting of the existing thermal plant and the implementation of a heat recovery system, was undertaken by an Energy Service Company (ESCo) which provided a comprehensive, turnkey solution including diagnosis, design, execution, and performance monitoring, while assuming the financial risk of the initiative under an Engineering, Procurement, and Construction (EPC) contract.

The second intervention, regarding the implementation of a CHP system, was carried out at a later stage by the same ESCo enterprise, after it had gained the client's trust through the success of the first project. In this case, the investment was fully financed by the production facility itself, reflecting a shift in ownership and financial responsibility for the energy-efficiency improvements.

This section thus provides a consolidated overview of the technical and financial performance of both projects, highlighting their respective contributions to energy savings, environmental impact reduction, and economic viability.

# 5.1 Thermal Power Plant Retrofit and HR System Results

The upgrade of the thermal power plant to a higher-efficiency configuration, combined with an integrated heat-recovery system, significantly reduces natural gas consumption. By recovering part of the heat previously lost through flue gases,

the plant lowers the amount of steam that must be generated, thereby improving overall efficiency.

Once the annual savings in fuel consumption are quantified, the analysis proceeds with the economic analysis which quantifies annual fuel savings and assesses the resulting financial benefits, considering both CAPEX and OPEX. It includes the monetary impact of White Certificates (TEE) granted for the implemented measures and evaluates the payback period under different contractual conditions. The EPC agreement between the ESCo and the client is also examined to understand how contract duration and TEE recognition influence both the ESCo's payback time and the client's savings, providing an integrated view of the retrofit's technical and economic feasibility.

# 5.1.1 Performance Improvements: Energy Efficiency and Fuel Savings

The retrofitting of the thermal power station is conceived not simply as a replacement of ageing equipment, but as a strategy to cut primary fuel consumption by maximising the recovery of heat that was previously wasted. Before the intervention, the plant operated on a continuous schedule of 24 hours per day, 5 days per week, for 48 weeks per year. Under these conditions, the facility burned roughly  $3,500,000~\rm Sm^3/year$  of natural gas to produce an average of  $7.5~\rm t/h$  of steam. Part of this steam had to be diverted for feed water preheating, reducing the amount available for process use.

The retrofit combines three key actions:

- installation of a higher-efficiency steam generator equipped with an economiser;
- integration of a dedicated heat-recovery unit (RC2) on the flue-gas side;
- optimisation of the feedwater heating strategy.

Together, these measures allow a portion of the heat previously lost with the exhaust gases to be recovered directly into the water circuit. As a result, the steam needed from the boiler drops to about 7.0 t/h and the corresponding gas consumption decreases accordingly.

Table 5.1 lists the main operating parameters of the system prior to the retrofit and after implementation, with resulting fuel saving.

SG ANTE RETROFIT			SG POST RETROFIT	
Annual operating hours		$5'760 \ h/y$		
$CH_4\ consumption$	$3'487'938 \text{ Sm}^3/\text{y}$	$605.54~\mathrm{Sm}^3/\mathrm{h}$	$3'338'151 \text{ Sm}^3/\text{y}$	$579.54~\mathrm{Sm}^3/\mathrm{h}$
G 2 (from replenishment tank)		$T_{2}$	$G_{\it 2}$ (from RC2)	$T_{2}$
5.51 t/h		15.00 °C	5.6 t/h	64.90 °C
$G_1$ (condensate return) [t/h]		$T_{1}$	$G_1$ (condensate return)	$T_{1}$
1.49 t/h		90.00 °C	1.4 t/h	90.00 °C
$G_{s}(steamrecirculated)$				
0.46 t/h			-	
$G_{feedwater}$ (to SG)		$T_{fw}$	$G_{feedwater}$ (to $SG$ )	$T_{fw}$
7.46 t/h		70.00 °C	7 t/h	70.00 °C
$\eta_{SG}$	90.00%		93.54%	
$P_{medium\ load}$	5'133.63 kW		4'817.16 kW	
$CH_4$ Annual Saving			149'786	$\mathrm{Sm}^3/\mathrm{y}$

**Table 5.1:** Operating data and natural gas consumption before and after retrofitting

Beyond the main boiler house, the project also exploited residual heat in the flue gases to supply the continuous washing machines. In the washing area, where water is heated up to 40 °C, a third recovery unit (RC3) now preheats part of the process water, reducing the dedicated gas consumption for this service. This alone generates an additional annual fuel saving (Table 5.2).

RC3 - CONTINUOUS WASHING MACHINES			
Annual operating hours	5'760 h/y		
CH <sub>4</sub> Annual saving	$128'233~\mathrm{Sm}^3/\mathrm{y}$	$22.26~\mathrm{Sm}^3/\mathrm{h}$	
$G_{H2O,RC3}$ [t/h]	$T_{in}$ [°C]	$T_{out}$ [°C]	
7.40	15.00	39.82	
$G_{f.g.,RC3}~[\mathrm{m}^3/\mathrm{h}]$	$T_{in}$ [°C]	$T_{out}$ [°C]	
5'154.00	48.50	35.86	
$P_{\it medium load}$	213.57	kW	

**Table 5.2:** Annual reduction in fuel consumption due to RC3

Considering the reduced steam production, enhanced generator efficiency, and the recovery of flue-gas heat for ancillary processes, the plant achieves an overall fuel reduction of approximately 8%. Given that each standard cubic meter of methane saved corresponds to about 1.956 kg of avoided CO<sub>2</sub> emissions [60], this results in a substantial annual CO<sub>2</sub> reduction, as reported in Table 5.3. These combined savings constitute the foundation of the subsequent economic analysis, which assesses capital and operating costs, White-Certificate revenues, and payback scenarios, thereby offering key insights into the project's financial feasibility and contractual implications.

$CH_4$ saving (retrofitted $SG + RC2$ )	$149'786 \text{ Sm}^3/\text{y}$
$RC3$ $CH_4$ saving	$128'233 \text{ Sm}^3/\text{y}$
$Total\ CH_4\ saving$	$278'019 \text{ Sm}^3/\text{y}$
$CO_{\it 2}\ reduction$	$543'805~\mathrm{kgCO_2/y}$

Table 5.3: Annual reduction in fuel consumption

#### 5.1.2 Economic Assessment

For the economic evaluation, the annual fuel savings are converted into monetary savings by applying a unit natural gas price of  $0.40 \in /\mathrm{Sm}^3$ . This value represents a reasonable average for the 2023–2025 period, as indicated by analyses from GSE (Gestore dei Servizi Energetici), which reflect recent market trends suggesting a stabilization around this level [61]. The resulting annual fuel reduction and its corresponding economic savings are summarized in Table 5.4.

$CH_4 \;\; cost$	0.40 €/Sm <sup>3</sup>	
	$CH_4$ saving	CH <sub>4</sub> economic saving
SG + RC2	$149'786 \text{ Sm}^3/\text{y}$	59'914.49 €/y
RC3	$128'233~{ m Sm}^3/{ m y}$	51′293.02 €/y
Total	$278'019~\mathrm{Sm}^3/\mathrm{y}$	111'207.51 €/y

**Table 5.4:** Annual fuel savings and related economic benefits from the retrofit and heat-recovery intervention.

It should be emphasized, however, that the natural gas price is not fixed and may fluctuate over time depending on the supplier, influenced by factors such as geopolitical instability, fluctuations in supply and demand, seasonal trends, and changes in energy market regulations or carbon pricing policies.

Consequently, while the selected price provides a plausible reference scenario, any variation in fuel cost would directly influence the payback period and the overall economic feasibility of the investment.

In this analysis, no additional operating expenditures (OPEX) have been included, as the intervention is not expected to incur incremental costs compared with the existing configuration. The routine maintenance of the new steam generator is assumed to be equivalent to that of the previous unit, while any extra activities related to the heat-recovery exchangers are considered negligible. Moreover, because natural gas produces flue gases with very low particulate content, fouling is minimal. As a result, cleaning operations, typically carried out once per year by in-house staff during scheduled plant shutdowns, are expected to generate only marginal costs, with no material impact on the overall economic assessment. For these reasons, no additional OPEX has been accounted for in this evaluation.

#### CAPEX for the Retrofit and Heat Recovery System

The total investment cost of the retrofitting intervention, including the heat recovery system, is calculated once all the main equipment has been selected and sized. The turnkey supply encompasses a new steam generator with all associated components, including the burner, fuel supply system, air and water networks, economizer, and heat recovery exchangers. In addition, the supply covers the decommissioning and disposal of the existing boiler, transportation, unloading and positioning, installation, mechanical and electrical connections, and commissioning. Civil works required for the installation are not included in this scope.

After defining all the individual cost components, as detailed in Table 5.5, the total investment cost (supply value) can be determined. To this amount, the client (the textile company) is presented with a price increased by approximately 50% to account for additional activities and services provided by the ESCo enterprise, which include:

- site inspections and feasibility study with detailed engineering design;
- development of control and management software for the system;
- on-site supervision;
- safety-related costs, with limits and responsibilities defined between the company and the ESCo;
- insurance coverage;
- pre-assembly, preliminary workshop testing, final testing and commissioning;
- preparation of technical specifications and bill of quantities;
- compliance procedures for pressure systems according to PED and INAIL regulations, where applicable.

Breakdown of Total Capital Investment			
	Steam Generator Mingazzini PB120	110′250.00 €	
	Burner General Bruciatori	38¹960.0 €	
80	Set of auxiliary equipment and control devices	16'000.0 €	
SG	Transportation, delivery and installation	14'300.0 €	
Replacement	Economizer with hoppers	3'650.0 €	
	Aeraulic system	5'250.0 €	
	Subtotal SG	188'410.0 €	
	RC2	10′400.0 €	
	Aeraulic network with thermal insulation	19'000.0 €	
	Fan - dampers	7'200.0 €	
	Hydraulic network with thermal insulation, pump and		
	auxiliaries	7'000.0 €	
	Electrical and monitoring system with control panel,		
	software, metering devices, and remote supervision	34¹000.0 €	
	Mechanical installation including support structure,		
	control and safety systems	16′500.0 €	
HEAT	Miscellaneous and logistics 10'000.0		
	Contingencies	8'328.0 €	
RECOVERY	Subtotal RC2	112'428.0 €	
	RC3	6′500.0 €	
	Aeraulic network with thermal insulation	2'400.0 €	
	Hydraulic network with thermal insulation, pump and		
	auxiliaries	34 600.0 €	
	Electrical and monitoring system with control panel,		
	software, metering devices, and remote supervision	7¹500.0 €	
	Mechanical installation including support structure,		
	control and safety systems	3'400.0 €	
	Subtotal RC3	54'400.0 €	
Data acquisition and remote monitoring system (for TEE compliance)		20'000.0 €	
	Overall Investment Cost	375′238.0 €	
Final	Investment Cost with Enterprise Markup	562'857.0 €	

**Table 5.5:** Detailed investment cost breakdown with total and enterprise markup included

#### White Certificates (TEE) and Incentives for Energy Savings

The reduction in natural gas consumption achieved with the new plant configuration yields direct economic benefits by lowering fuel expenditure and generating additional revenue through White Certificates (*TEE - Titoli di Efficienza Energetica*). These certificates, issued in Italy by the *Gestore dei Servizi Energetici* (GSE) [62], officially certify the energy savings obtained through efficiency measures. TEE are expressed in tonnes of oil equivalent (toe or *tep - tonnellate di olio equivalente*); one tep corresponds to approximately 1,220.9 Sm<sup>3</sup> of natural gas [63], equivalent to 41.86 GJ.

The monetary value of these certificates has been estimated using the average market price recorded between January and June 2025. Figure 5.1 shows this price stabilization trend over the past two years and the historical evolution of the average TEE price from 2021 to 2025 [64]. TEE can be traded between companies implementing energy-efficiency projects and those required to meet specific savings targets.



Figure 5.1: TEP Price Fluctuations over the Period 2021–2025

Reducing methane (CH<sub>4</sub>) consumption, for instance through cogeneration systems or heat-recovery solutions, is one of the most effective ways to obtain TEE. Such reductions not only produce measurable, certifiable energy savings but also bring significant environmental benefits by lowering CO<sub>2</sub> emissions. On a broader

scale, cutting methane use simultaneously supports national and corporate energy-efficiency targets and contributes to greenhouse gas mitigation, reinforcing the goals of the ecological transition. Table 5.6 provides a comprehensive overview of the estimated savings and corresponding incentives resulting from the intervention.

Energy Savings and White Certificates (TEE) Incentives		
$1 \text{ tep} = 1220.867 \text{ Sm}^3 \text{ of natural gas (CH}_4)$		
Average market price of 1 tep (Jan - Jun 2025)	249.11 €/tep	
$CH_{\ 4} \ saving$	$278'019~\mathrm{Sm}^3/\mathrm{y}$	
Energy Savings in tep	227.72  tep/y	
Total TEE Incentives	56'727.93 €/year	

Table 5.6: CH<sub>4</sub> savings and white certificates incentives

### Contractual Framework and Cash-Flow Sensitivity Analysis under EPC Models

The production facility benefiting from the energy-efficiency measures (hereafter referred to as "the company") has entered into an Energy Performance Contract (EPC) with an Energy Service Company (ESCo) (also referred to as "the enterprise"). Under this agreement, the ESCo is responsible for designing and implementing the energy-efficiency project, financing it with its own or third-party capital, and recovering its investment through the verified energy savings achieved at the Company's facilities.

In practice, the ESCo may fund the project directly or arrange *Third-Party Financing (TPF)*, an internationally established mechanism for energy-efficiency investments [65]. Under TPF, a third party supplies the capital for the intervention and is repaid through a portion of the resulting energy savings. The third party may be the ESCo itself or an external financier. Two main TPF models exist, differing primarily in which entity (the ESCo or the client) assumes the debt. In the case analysed here, the ESCo secures the financial resources required for the investment (Figure 5.2).

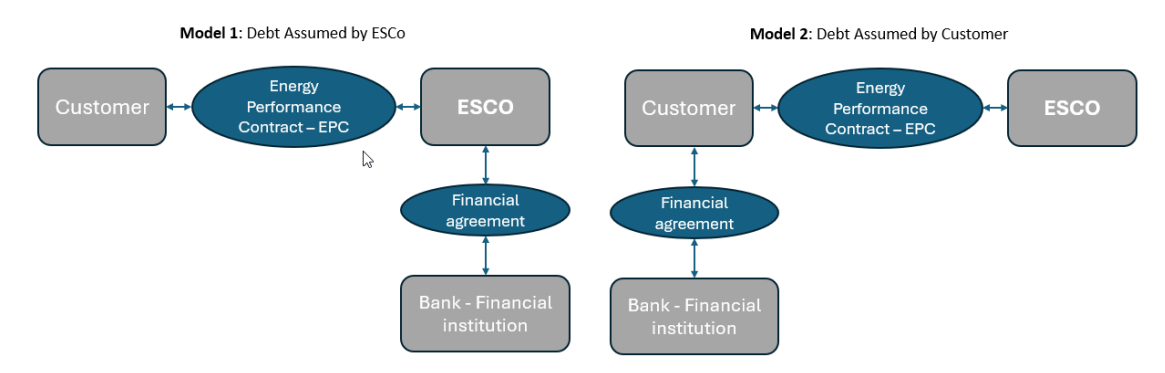


Figure 5.2: Main Third-Party Financing (TPF) models showing debt allocation and repayment flows [65].

This analysis compares two possible contractual frameworks and performs a cash-flow sensitivity assessment to evaluate the effects of different contract durations and a scenario without White Certificate (TEE) recognition.

To ensure a realistic assessment of profitability, all cash flows are discounted using the project's Weighted Average Cost of Capital (WACC) (detailed in Table 5.7). The WACC, representing the combined cost of equity and debt, serves as the discount rate to account for the time value of money and the risk associated with future savings. This approach effectively captures both the financial cost of the investment and the uncertainties inherent in long-term cash flows.

Using this WACC-based discounting, the analysis determines key economic indicators for both the ESCo and the host company, including the:

- Net Present Value (NPV);
- Discounted Payback Time (DPBT);
- Discounted Cumulative Cash Flow.

As discounting reduces the value of future cash flows, the calculated discounted payback period is, as expected, longer than the simple payback period. Together, these indicators provide a robust and realistic measure of the project's economic feasibility.

It must be noted that the final results are based on estimated values and remain subject to inherent market uncertainty. In particular:

- The market price of White Certificates (TEE), while stable over the last two years, cannot be predicted with certainty and has historically decreased by approximately 15% over the past five years;
- Natural gas and electricity prices are inherently volatile, influenced by market dynamics, geopolitical factors, regulatory changes, and fuel supply conditions.

#### Weighted Average Cost of Capital (WACC)

WACC represents the average return required by all providers of capital, and is computed as the weighted average of the cost of equity and the after-tax cost of debt [66]. It reflects the proportionate contributions of equity and debt to the overall capital structure, and has been calculated separately for both the ESCo and the textile company. The formula is:

$$WACC = \left(\frac{E}{V} \cdot r_e\right) + \left(\frac{D}{V} \cdot r_d \cdot (1 - T)\right) \tag{5.1}$$

where:

- E = market value of equity;
- D = market value of debt;
- V = total market value of capital (E + D);
- $r_e = \cos t$  of equity;
- $r_d = \cos t \text{ of debt};$
- T = corporate tax rate.

The ratios **E/V** and **D/V** denote, respectively, the proportions of equity and debt employed to finance the investment. In this analysis, the shares for both the ESCo and the company have been derived from the statistical averages published by Damodaran [67], reflecting the typical capital structures of firms in their respective industries: the Green and Renewable Energy sector for the ESCo and the Apparel sector for the textile company. This approach ensures that the assumed equity—debt mix mirrors the prevailing financial profiles of comparable businesses.

Firms generally aim for a mix of equity and debt that balances funding requirements with financial risk, while also exploiting the tax advantages associated with debt financing. When the return generated by a project exceeds the cost of debt, leveraging can enhance the overall return on equity.

The **cost of equity**  $(r_e)$  is commonly estimated using the Capital Asset Pricing Model (CAPM):

$$r_e = r_f + \beta \cdot (r_m - r_f) \tag{5.2}$$

where:

•  $r_f = risk$ -free rate, chosen as the current 10-year Italian government bond (BTP) yield, which represents a long-term, low-risk debt instrument issued by the Italian government [68];

•  $\beta$  = the beta coefficient measures a project's systematic risk, i.e. its sensitivity to fluctuations in the overall market. A higher  $\beta$  indicates greater exposure to market volatility, whereas a lower  $\beta$  signals more stable, market-independent performance. Under an EPC, the ESCo finances, designs and implements the intervention, bearing both the technological and financial risks of the project. By contrast, the client is largely shielded from market risks linked to technology prices or economic conditions; its main exposure lies in the ESCo's ability to fulfil its contractual obligations. Consequently, the client's risk depends on the ESCo's reliability, the regulatory framework, the penalties and guarantees defined in the contract, and the ESCo's financial soundness rather than on market volatility.

**Estimation of beta** The project's beta was derived from sector data on publicly traded companies comparable to the ESCo. Specifically, as already mentioned, the average beta of Green and Renewable Energy firms reported by Damodaran [67] was used for the ESCo. The unlevered beta (which removes the effect of debt) was first taken from the sector data and then re-levered to match the capital structure of the project.

$$\beta_{levered} = \beta_{unlevered} \cdot \left(1 + (1 - T) \cdot \frac{D}{E}\right)$$
 (5.3)

In principle, the client's different risk profile would warrant a distinct beta. A full qualitative risk analysis, considering ESCo reliability, regulation, financial stability, penalties and execution risk, would be required to estimate a bespoke value. However, to keep the analysis conservative and manageable, and to avoid assigning an unrealistically low beta, the same unlevered beta used for the ESCo is applied to the client and subsequently re-levered according to the equity/debt structure of comparable businesses in the apparel industry, as previously described. Since the ESCo operates in a relatively low-risk segment, this assumption remains prudent.

•  $r_m - r_f = equity \ risk \ premium$ , i.e. the additional return that investors require for holding a risky equity investment instead of a risk-free asset. In this expression,  $r_m$  refers to the expected market return. This parameter is derived from the 2024 analysis by Damodaran, which presents country-specific equity risk premiums. These values are based on default spreads and are adjusted by a global scalar to reflect equity market volatility relative to government bonds [69].

The Cost of Debt  $(r_d)$  represents the effective interest rate applied to the outstanding or newly contracted debt. It reflects the rate at which the entity can borrow capital and is adjusted for taxes, since interest expenses are tax-deductible.

In this analysis, the cost of debt for both the ESCo and the textile company was estimated using the May 2025 monthly report published by ABI, which reports an average interest rate of 3.64% on new corporate loans [68]. The after-tax cost of debt is calculated as:

$$After-tax \ r_d = r_d \cdot (1 - T) \tag{5.4}$$

Table 5.7 summarizes all the parameters described above and presents the resulting cost of equity and WACC for both the ESCo and the textile company.

Composable Industry Cotegory		ESCo: Green and	Company: Apparel
Comparable Industry Categor	Comparable Industry Category:		Industry
Proportion of Equity	E/V	58%	88%
Proportion of Debt	D/V	42%	12%
Corporate Tax Rate	Т	24%	24%
β coefficients	$\beta_{\mathrm{unlevered}}$	0.535	0.535
p coemcients	$\beta_{\mathrm{unlevered}}$ $\beta_{\mathrm{levered}}$	0.834	0.592
Risk Free Rate	$r_{\rm f}$	3.49%	3.49%
Equity Risk Premium	r <sub>m</sub> - r <sub>f</sub>	7.81%	7.81%
Cost of Debt	$ m r_d$	3.64%	3.64%
Cost of Equity	$ m r_e$	10.00%	8.11%
Weighted Average Cost of Capital	WACC	6.93%	7.45%

**Table 5.7:** Summary of parameters used to calculate the WACC for both the ESCo and the client company.

#### Cumulative Cash Flow, PBT, and NPV

Once the WACC parameters are determined (Table 5.7), they are applied as the discount rate to all future cash flows generated by the project for both the ESCo and the client company. Discounting the cash flows allows the calculation of the Net Present Value (NPV) and the discounted payback time (DPBT) for each entity. The discounted cumulative cash flow and the NPV are computed using Equations 5.5 and 5.6, respectively.

$$DCF = \sum_{t=1}^{n} \frac{CF_t}{(1 + WACC)^t}$$

$$(5.5)$$

$$NPV = \sum_{t=1}^{n} \frac{CF_t}{(1 + WACC)^t} - I_0$$
 (5.6)

This detailed approach strengthens the robustness of the financial assessment by explicitly accounting for the opportunity cost of capital and the volatility of energy prices. In doing so, it clarifies the project's inherent risks and delivers critical insights into its economic viability, thereby supporting more informed and reliable investment decisions.

Three-Year Contract Model Under this contractual model, the ESCo finances the entire upfront cost of the retrofit. In return, the company reimburses the ESCo through the transfer of the value of energy savings, plus an additional margin, totalling €150 000 per year over the first three years. This mechanism provides partial repayment of the initial investment.

During this initial period, the ESCo retains 100% of the White Certificates (TEE), which significantly contributes to recovering its outlay. Starting from the fourth year, the company ceases direct payments and begins receiving 80% of the TEE generated by the project, while the remaining 20% continues to be retained by the ESCo for an additional four years. According to current GSE regulations, TEEs for this type of intervention are valid for seven years, as established by the Ministerial Decree of January 11, 2017 and subsequent GSE clarifications [70]. Table 5.8 summarizes the key financial indicators — Net Present Value (NPV) and Payback Time (PBT) — for both the textile company and the investment enterprise under the three-year contract model.

	Company PBT	Company NPV	ESCo PBT	$Enterprise\ NPV$	
	[years]	(7 years)	[years]	(10 years)	
3-year contract model	3.86	497'290.2 €	5.38	11′803.1 €	

**Table 5.8:** NPV and PBT for the company and the investment enterprise under the three-year contract model.

Four-Year Contract Model In this alternative framework, the four-year contract model, the ESCo again finances the entire investment. The company reimburses approximately 70% of the initial cost, drawing partly on the savings achieved and partly on its own funds. Payments start at about €130,000 in the first year and gradually decrease over the following three years, reaching €70,000 in the fourth

year. Under this arrangement, the ESCo retains 100% of the White Certificates (TEE) for the entire seven-year incentive period.

	Company PBT	Company NPV	ESCo PBT	$Enterprise\ NPV$	
	[years]	(7 years)	[years]	(10 years)	
4-year contract model	2.96	423'741.8 €	4.26	88'491.9 €	

**Table 5.9:** NPV and PBT for the company and the investment enterprise under the four-year contract model.

Contingency Clause – Absence of TEE Approval If the GSE does not approve the allocation of White Certificates, a contingency clause stipulates that the company reimburses the ESCo directly over a four-year period. This repayment is partially offset by the energy savings generated by the retrofit, which continue to reduce the company's net outlay during the payback period.

Key outcomes: Even in the absence of TEE incentives, the analysis shows that both parties maintain positive economic outcomes: the ESCo achieves a positive NPV by the end of the contractual period, while the company reaches a positive NPV at the ten-year horizon (Table 5.10).

	Company PBT	Company NPV	ESCo PBT	$Enterprise\ NPV$
	[years]	(4 years)	[years]	(10 years)
4-year contract model assuming no TEE approval	6.49	206'576.5 €	3.98	2'102.6 €

**Table 5.10:** NPV and PBT for the company and the investment enterprise under the contingency scenario without TEE (White Certificate) approval.

The financial outcomes of the three contract options are illustrated in Figures 5.3 and 5.4, showing the cumulative cash flows over time for the investment enterprise and the company, respectively.

Figure 5.3 depicts the enterprise's cumulative cash flow, reflecting its recovery of the initial investment through retained TEE incentives (when available) and a share of the energy savings during the early contract years.



**Figure 5.3:** Cumulative Cash Flow for the Investment Enterprise under the Three EPC Contract Scenarios

The four-year contract with TEE approval yields the highest enterprise profit, while the absence of TEE incentives reduces the return but still allows the enterprise to reach payback within four years.

Figure 5.4 highlights the evolution of the company's cash flow resulting from energy savings, partially shared with the enterprise during the contract period. Among the three scenarios, the three-year contract produces the highest total savings by the end of the ten-year horizon. In all cases, the company achieves payback within ten years and maintains a positive NPV, even without White Certificate (TEE) approval. Although the initial years show negative cash flow, this model proves most advantageous long-term, as the company retains all subsequent savings after the repayment period.

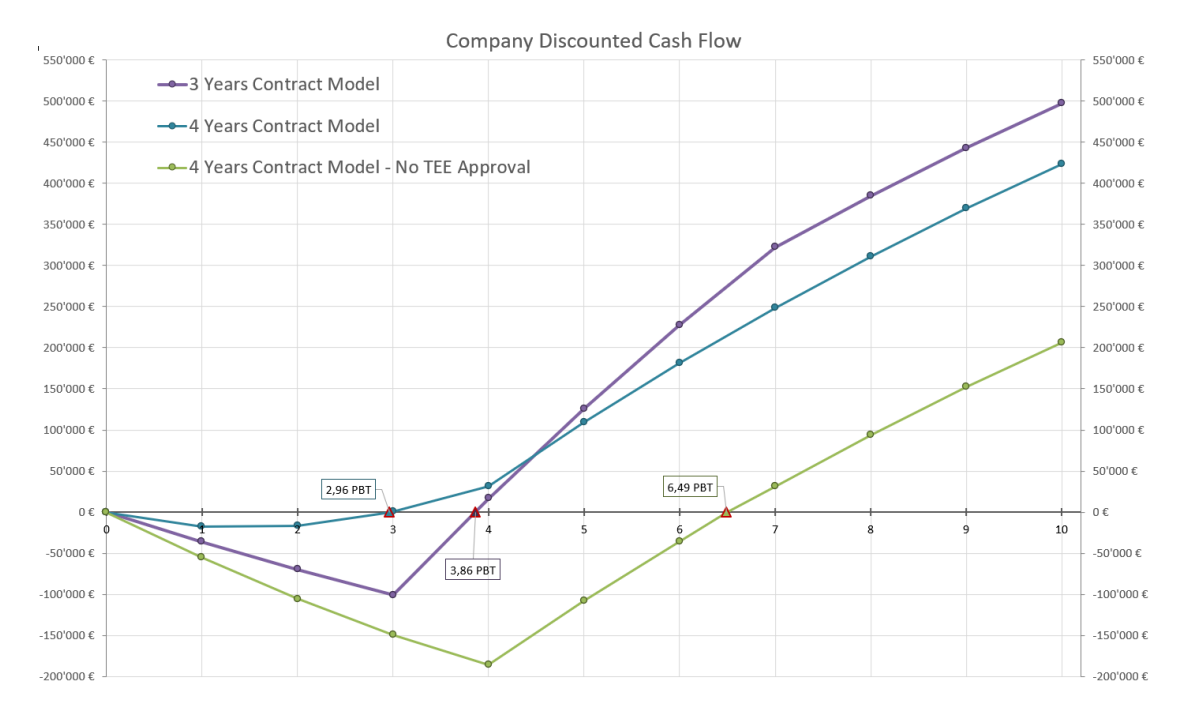


**Figure 5.4:** Cumulative Cash Flow for the Company under the Three EPC Contract Scenarios

## 5.2 CHP System Performance and Economic Assessment

Once the design and sizing of the CHP plant and its main components have been completed, this section summarizes the resulting performance, focusing on fuel savings for thermal energy through the combined heat and power (CHP) unit and the heat-recovery system, as well as the associated electricity savings.

Although the CHP system entails a higher natural gas consumption than the current configuration, since it simultaneously produces both electricity and thermal energy, it achieves a higher overall efficiency compared with separate production, leading to significant economic savings.

The subsequent analysis presents the main outcomes in terms of electricity and heat generation, operating costs, and associated savings, providing a comprehensive overview of the investment required, including civil and structural works. This framework makes it possible to assess the overall financial viability and benefits of the CHP unit. In this scenario, the company bears the entire investment cost without entering into an EPC contract with the ESCo enterprise, thus allowing the direct calculation of the project's payback time.

## 5.2.1 CHP System Fuel Consumption and Energy Outputs

The main results of the fuel consumption analysis and the associated energy outputs of the cogeneration system are summarized in Table 5.11. Specifically, it presents:

- the annual natural gas consumption required by the CHP unit;
- the natural gas savings at the steam generator due to partial replacement of steam production with the recovered heat from the CHP unit;
- the net additional natural gas consumption attributable to the CHP, considering that it also generates electricity.

	Annual Quantity
NG Consumption (CHP Unit)	$741'016.49 [{ m Sm}^3/{ m year}]$
NG Saved in Steam Generator	$428'773.95 [\mathrm{Sm}^3/\mathrm{year}]$
Additional NG Consumption	$+312'242.55 [{ m Sm}^3/{ m year}]$
CHP System Thermal Output	$3'846'706.31 \text{ [kWh}_t/\text{year]}$
CHP Unit Electrical Output	$2'786'445.00 [kWh_e/year]$

**Table 5.11:** Annual Natural Gas Consumption, Savings, and outputs of the CHP Unit

Despite the additional natural gas consumption of the CHP system compared to the amount saved at the steam generator for producing the same thermal output, this extra fuel also contributes to on-site electricity generation, thereby increasing overall efficiency relative to separate production and yielding a net economic benefit for the facility.

#### Primary Energy Savings (PES) Evaluation

It is essential to evaluate the Primary Energy Savings (PES) achievable with the CHP unit compared to separate production of electricity and heat. The PES indicator quantifies the reduction in primary energy consumption obtained through cogeneration and is one of the key parameters used at European level to classify high-efficiency CHP systems. Calculating the PES provides an objective measure of the energy performance of the installation and, together with the financial analysis, allows a comprehensive assessment of the overall benefits associated with

the investment. It is typically defined as:

$$PES = \left[1 - \frac{1}{\frac{\eta_{\text{CHP,H}}}{\eta_{\text{Ref,H}}} + \frac{\eta_{\text{CHP,E}}}{\eta_{\text{Ref,E}}}}\right] \cdot 100\%$$
 (5.7)

where:

- $\eta_{\text{CHP,H}}$ : thermal efficiency of heat production by cogeneration;
- $\eta_{\text{CHP,E}}$ : electrical efficiency of electricity production by cogeneration;
- $\eta_{\text{Ref},H}^{-1}$ : reference efficiency for separate heat production;
- $\eta_{\text{Ref.E}}^{-1}$ : reference efficiency for separate electricity production.

To determine  $\eta_{\text{Ref,H}}$  and  $\eta_{\text{Ref,E}}$ , it is necessary to follow the procedure described in Commission Delegated Regulation (EU) 2015/2402 [15]. In particular, the correction factors for avoided grid losses must first be taken into account for the application of the harmonised efficiency reference values for separate electricity production.

The alternator, according to its datasheet, has a rated power of 800 kVA at 400 V. Based on the values provided in Annex IV of [15], Table 5.12 lists the corresponding correction factors. In this table, *off-site* denotes the correction factor to be applied when electricity is injected into the grid or used elsewhere, whereas *on-site* denotes the factor applicable in the present case, referring to electricity consumed within the same facility where it is produced.

<sup>&</sup>lt;sup>1</sup>The reference efficiencies mentioned above ( $\eta_{\rm Ref,H}$  and  $\eta_{\rm Ref,E}$ ) are specified in Commission Delegated Regulation (EU) 2015/2402 — Annex I for separate electricity production and Annex II for separate heat production. Where applicable, the values from Annex I must be adjusted to the relevant climatic conditions using Annex III, and corrected for avoided grid losses according to Annex IV [15].

Connection voltage level	Correction factor	Correction factor
Connection voltage level	(Off-site)	(On-site)
≥ 345 kV	1.000	0.976
$\geq 200 - < 345 \text{ kV}$	0.972	0.963
≥ 100 - < 200 kV	0.963	0.951
≥ 50 - < 100 kV	0.952	0.936
≥ 12 - < 50 kV	0.935	0.914
$\geq 0.45 - < 12 \text{kV}$	0.918	0.891
$< 0.45 \; \mathrm{kV}$	0.888	0.851

**Table 5.12:** Correction Factors for Avoided Grid Losses in Separate Electricity Production

Table 5.13 reports the harmonised efficiency reference values for separate electricity production. These values are based on the net calorific value of natural gas under standard ISO atmospheric conditions (15  $^{\circ}$ C ambient temperature, 1.013 bar, 60 % relative humidity). The highest reference value is considered, as the CHP unit is a state-of-the-art installation commissioned after 2016.

Catamany	TT 1	Year of construction		
Category	Type of fuel	Before 2012	2012-2015	From 2016
	Natural gas,			
Gaseous	LPG, LNG and	52.50	52.50	53.00
	biomethane			

**Table 5.13:** Harmonised Efficiency Reference Values for Separate Electricity Production

Given that the average annual ambient temperature at the plant location (Lombardia) is 11.32 °C, correction factors related to the average climatic conditions and the method for establishing climate zones must be applied for the use of the harmonised efficiency reference values for separate electricity production, as specified in ALLEGATO VI of the Official Gazette of the Italian Republic [71].

The applicable correction is defined as follows:

- a 0.1%-point decrease in efficiency for each degree above 15°C;
- a 0.1 %-point increase in efficiency for each degree below 15 °C.

Accordingly, the corrected efficiency reference value for separate electricity production amounts to  $53.369\,\%$ .

The value of  $\eta_{\text{Ref,E}}$  is then determined as follows:

$$\eta_{\text{Ref,E}} = 53.369\% \times (0.851 \times 100\% + 0.888 \times 0\%) = 45.42\%$$
(5.8)

Once all efficiency coefficients have been determined, the PES can be calculated as shown in Table 5.14.

It should be noted that, in Table 5.11, the CHP system's thermal output also includes the heat recovered in the heat exchanger downstream of the HRSG. Similarly, when calculating the PES, the thermal efficiency  $\eta_{\text{CHP,H}}$  accounts for the heat recovered in the  $HR_{FG}$ , even though this recovery is an additional system that utilizes the flue gases from the CHP unit. Meanwhile, the reference thermal efficiency  $\eta_{\text{Ref,H}}$  corresponds to the value reported in Table 5.1, representing the efficiency of the steam generator equipped with the economizer.

$\eta_{\mathrm{CHP,H}}$	53.91%	$\eta_{\mathrm{Ref;H}}$	93.54%
$\eta_{\mathrm{CHP,E}}$	38.98%	${f \eta}_{ m Ref,E}$	45.42%
P	ES	30.29%	

**Table 5.14:** Summary of CHP Unit Efficiencies and Primary Energy Savings Including Heat Recovery from Flue Gases  $(HR_{FG})$ 

In Table 5.15, the PES is calculated without considering the  $HR_{FG}$  in the CHP Unit thermal efficiency. In this case, the thermal efficiency of the CHP unit is taken directly from the datasheet, since the heat exchanger downstream of the HRSG was not included by the CHP supplier but added later to exploit the thermal energy from the flue gases and improve the overall system efficiency.

$\eta_{\mathrm{CHP,H}}$	44.04%	$\eta_{\mathrm{Ref,H}}$	93.54%
$\eta_{\mathrm{CHP,E}}$	38.98%	$\eta_{\mathrm{Ref,E}}$	45.42%
P	ES	24.76%	

**Table 5.15:** Summary of CHP Unit Efficiencies and Primary Energy Savings Excluding Heat Recovery from Flue Gases  $(HR_{FG})$ 

In both cases, a positive PES greater than 10% is obtained, which confirms that the CHP unit qualifies as high-efficiency, satisfying the criteria for assessing the high-efficiency status of a cogeneration unit over the given reference period.

### 5.2.2 Economic Assessment

The following analysis provides a comprehensive overview of the CAPEX and OPEX of the cogeneration project.

The economic assessment of fuel consumption and energy outputs for the CHP unit is based on the reference energy prices listed in Table 5.16. The natural gas price is set at  $0.40 \in /\text{Sm}^3$ , consistent with the value used in Table 5.1, although it may vary over time depending on the supplier. For electricity, several tariff components are regulated by ARERA, and the average selling price adopted here reflects the levels indicated in the ARERA database [72].

Unit Cost		
Electricity Price	$0.18~[\mathrm{\epsilon/kWh_e}]$	
Natural Gas Price	0.0415 [€/kWh]	
Natural Gas Price	0.40 [€/Sm³]	

**Table 5.16:** Prices of Electricity and Natural Gas Considered in the Study

#### Operational Expenditures Analysis (CAPEX)

First, Table 5.17 summarizes the operational costs sustained by the plant before the implementation of the CHP system, reporting electricity and natural gas consumptions for thermal energy generation together with their corresponding costs.

Parameter	Value	Annual cost [€/y]
Operating hours (year)	5760 h/y	
Electricity consumption (total)	$3'678'475 \text{ kWh}_{e}/\text{y}$	651'090.08
Natural gas consumption (thermal plant)	$2'847'104 \text{ Sm}^3/\text{y}$	1'138'841.60
TOTAL ANNUAL ENERGY COST (no CHP)	1'789'931.68	€/y

**Table 5.17:** Operational costs sustained by the plant before the implementation of the CHP system.

#### Investment Cost Analysis (CAPEX)

Subsequently, Table 5.18 presents the estimated operational costs of the plant after integrating the CHP and heat recovery systems, highlighting the additional costs introduced by the new installation, the savings achieved, and the resulting total expenditure for the whole facility.

This framework provides the basis for comparing pre- and post-implementation scenarios and for assessing the overall economic performance of the cogeneration project.

Parameter	Unit	Value / Formula	Annual cost [€/y]
CHP nominal power	kW	500.00	_
CHP operating hours	h/y	5'700.00	
Average Load	%	0.98	
Power consumption at rated power	kW	1'282.70	
Hourly fuel consumption (CHP) at avg. $\label{eq:charge} \mbox{load}$	$\mathrm{Sm^3/h}$	130.00	
Annual fuel consumption (CHP)	$\mathrm{Sm^3/y}$	741'016.49	-296'406.60
Annual thermal energy produced (useful)	kWh <sub>th</sub> /y	3'846'706.31	
NG saved in SG $(Sm^3/y)$	$\mathrm{Sm^3/y}$	428'773.95	+171'509.58
Annual electrical production (CHP)	$kWh_{el}/y$	2'786'445.00	+493'200.77
Dissipated electricity (export or dumped)	$\mathrm{kWh_{el}/y}$	22'800.00	-4'035.60
Excise duties on NG	€/y	$0.45  €  \cdot  \text{NG}_{\text{EE}} / 1000  +$ $0.0125  €  \cdot  \text{NG}_{\text{TH}}$	-5'069.41
Hourly maintenance & consumables (oil, urea, etc.)	€/h	7.00	-39'900.00
Other operating costs (insurances, service contracts, permits)	<b>€</b> /y	(insurances, service contracts, permits)	-5'000.00
TOTAL ANNUAL COST (CHP)	€	(includes NG cost, maintenance, excise, other)	-350'411.61
TOTAL ANNUAL SAVINGS	€	NET benefit	+664'710.34
NET ANNUAL BALANCE	€	Saving-Cost	314'298.74
NEW ENERGY EXPENDITUR	E	1'475'632.94	€/y

**Table 5.18:** Estimated operational costs of the plant after integrating the CHP and heat recovery systems.

Several key parameters used in this cost analysis require clarification:

- Dissipated electricity refers to the self-consumption of electricity within the plant's internal distribution network, typically amounting to about 1–3% of the electricity absorbed.
- Excise duties on natural gas are special indirect taxes imposed by the State on the consumption of certain goods. In the case of natural gas used in cogeneration, special incentives apply: the excise duty is almost negligible

for the fraction used to generate electricity (about  $\leq 0.45$  per 1000 Sm<sup>3</sup>) and equals  $\leq 0.012498$  per Sm<sup>3</sup> for other industrial uses [73].

• Hourly maintenance and consumables include all operational costs related to inspection, maintenance, cleaning, lubricants, and other consumables for the CHP unit. Based on supplier information, these costs are fixed at approximately €7,00 per operating hour.

After assessing the operational expenditures, the next step is to evaluate the investment costs required for the implementation of the cogeneration system. Table 5.19 summarises the initial investment associated with the installation of the CHP unit and the auxiliary systems.

The breakdown includes the main equipment (engine with integrated heat recovery systems), civil works (foundation), hydraulic and electrical connections, authorisation procedures, safety measures, and other ancillary costs. This comprehensive overview provides a clear picture of the capital expenditure required to commission the project.

CAPEX	Cost
Engine (including HRSG with ECO, $HR_{EJ}$ and dissipator)	715′000.00 €
Authorisation procedures and CAR certification	27'000.00 €
Electrical connection (including design)	45′000.00 €
Hydraulic system including $\mathrm{HR}_{\mathrm{FG}}$	126'360.00 €
Concrete foundation (60 m <sup>2</sup> )	21′600.00 €
Safety measures	12'600.00 €
Miscellaneous	14'400.00 €
Total Investment	961'960.00 €

Table 5.19: Initial Investment (CAPEX) for the CHP Unit and Auxiliary Systems

#### TEE Incentives for High-Efficiency CHP

Cogeneration units classified as High-Efficiency Cogeneration (CAR - Cogenerazione ad alto rendimento) under the Ministerial Decree (DM) of 5 September 2011 are eligible for incentives through Type II White Certificates (TEE) [16].

The incentives apply for a period of 10 years, starting from January 1 of the year following the unit's commissioning, including cases where the unit has been refurbished. The number of White Certificates issued is proportional to the primary energy savings achieved by the unit. The quantity of certificates is calculated as:

$$TEE = RISP \cdot 0.086 \cdot K \tag{5.9}$$

where:

• **RISP** is the primary energy savings (MWh) realized by the cogeneration unit, recognized by the GSE for the purposes of White Certificates. For any cogeneration unit and for each calendar year, the primary energy savings are computed using:

$$RISP = \frac{E_{CHP}}{\eta_{Ref,E}} + \frac{H_{CHP}}{\eta_{Ref,H}} - F_{CHP}$$
 (5.10)

with:

- $-E_{\rm CHP}$ : electricity produced in cogeneration (MWh).
- $-H_{\rm CHP}$ : useful thermal energy produced in cogeneration (MWh).
- $-\eta_{Ref,E}$ : conventional average efficiency of the Italian electricity production mix, adjusted as per DM 5 September 2011 [16].
- $-\eta_{Ref,H}$ : conventional average efficiency of the Italian thermal production mix; assumed as 0.82 for direct use of exhaust gases and 0.9 for hot water or steam production [16].
- $-F_{\rm CHP}$ : fuel energy consumed by the cogeneration unit during the year.
- **K** is an adjustment factor depending on the unit's power. It is determined as a weighted average over power classes, based on the measured cogeneration power during the reporting period, following the Guidelines for the Application of DM 5 September 2011 [16]. The values are defined as follows:
  - -K = 1.4 for power shares up to 1 MWe;
  - -K = 1.3 for power shares above 1 MWe and up to 10 MWe;
  - -K = 1.2 for power shares above 10 MWe and up to 80 MWe;
  - -K = 1.1 for power shares above 80 MWe and up to 100 MWe;
  - -K = 1.0 for power shares above 100 MWe.

All the key parameters required for calculating the savings eligible for White Certificates (TEE) have now been defined. The resulting values, including the recognized energy savings (RISP) and the corresponding number of TEE, are reported in Table 5.20. The associated monetary value has already been presented in Table 5.6, where it was estimated based on the average market price observed between January and June 2025.

Parameter	Unit	Value
PES	%	30.29
RISP	MWh	0.591
TEE awarded by GSE	tep/y	405.28
TEE in 10 years	tep	4052.84
TEE Revenue	<b>€</b> /y	100960.3
Tep average value	€/tep	249.11

**Table 5.20:** Results of the PES, RISP, and White Certificates (TEE) associated with the CHP unit.

#### Weighted Average Cost of Capital (WACC)

Unlike the previous plant, where the company adopted an Energy Performance Contract model and the entire investment was financed upfront by the ESCo enterprise, in this case the ESCo only designed and supplied the cogeneration unit, acting as an intermediary. The factory itself financed the project directly, combining its own funds (equity) with bank loans (debt).

As with the previous heat-recovery system, the profitability of this project was assessed by discounting the cash flows using the Weighted Average Cost of Capital (WACC), which represents the average cost of capital and accounts for the time value of money. This approach evaluates the investment in present-value terms, acknowledging that future cash flows are worth less than immediate ones.

The WACC was determined using the same methodology adopted for the heatrecovery system described previously (see Section 5.1.2). The only differences concern the estimation of the beta coefficient and the capital structure. Since the investment is borne directly by the company (rather than by an ESCo), the entire risk is assumed by the firm itself. Accordingly, the unlevered beta of a business comparable to the production facility, namely within the Apparel industrial sector, was taken from Damodaran's sector studies [67] and then relevered to reflect the company's capital structure.

Similarly, the equity and debt shares were derived from statistics of firms operating in comparable industries. All other parameters follow the same approach already applied to the previous case study.

The WACC and CAPM formulas (Eqns. 5.1 and 5.2) have already been presented and discussed; they are therefore not repeated here.

Table 5.7 summarizes all the parameters assumed for the WACC calculation in this analysis.

Comparable Industry Catego	Company: Apparel Industry	
	ı	maustry
Proportion of Equity	E/V	88%
Proportion of Debt	$\mathrm{D/V}$	12%
Corporate Tax Rate	Т	24%
Q coefficients	$\beta_{\rm unlevered}$	0.908
$\beta$ coefficients	$\beta_{\rm levered}$	1.005
Risk Free Rate	$ m r_f$	3.49%
Equity Risk Premium	$ m r_m$ - $ m r_f$	7.81%
Cost of Debt	$ m r_d$	3.64%
Cost of Equity	$ m r_e$	11.34%
Weighted Average Cost of Capital	WACC	10.28%

**Table 5.21:** Summary of the key parameters used to calculate the WACC.

### Cumulative Cash Flow, PBT, and NPV

Based on the adopted methodology, the discounted cumulative cash flow, payback time (PBT), and Net Present Value (NPV) were calculated, taking into account the revenues from White Certificates (TEE). Together, these indicators provide a comprehensive measure of the project's economic feasibility.

A degree of uncertainty remains, as the analysis relies on estimated values. In particular, the future market value of TEE is uncertain, while natural gas and electricity prices are subject to volatility driven by market dynamics, geopolitical factors, regulatory changes, and supply conditions.

The WACC, once determined, was applied as the discount rate to the projected cash flows of the cogeneration project. Through this procedure, the discounted cumulative cash flow, NPV, and PBT were obtained according to Equations 5.5 and 5.6, introduced in *Section 5.1.2*. Applying the WACC as discount rate ensures that the evaluation reflects the time value of money, the opportunity cost of capital, and the uncertainties associated with future energy markets, thereby offering a robust assessment of the financial viability of the cogeneration investment.

PBT	2.79 years
NPV (15 years)	2'004'279.87 €

**Table 5.22:** Net Present Value (NPV) and payback time (PBT) for the cogeneration project.

Table 5.22 reports the calculated NPV and PBT for the cogeneration project, while Figure 5.5 illustrates the discounted cumulative cash flow over the expected 15-year lifetime of the unit. The analysis highlights how discounting affects the timing and magnitude of cash inflows, offering a detailed perspective on the economic sustainability of the CHP system.

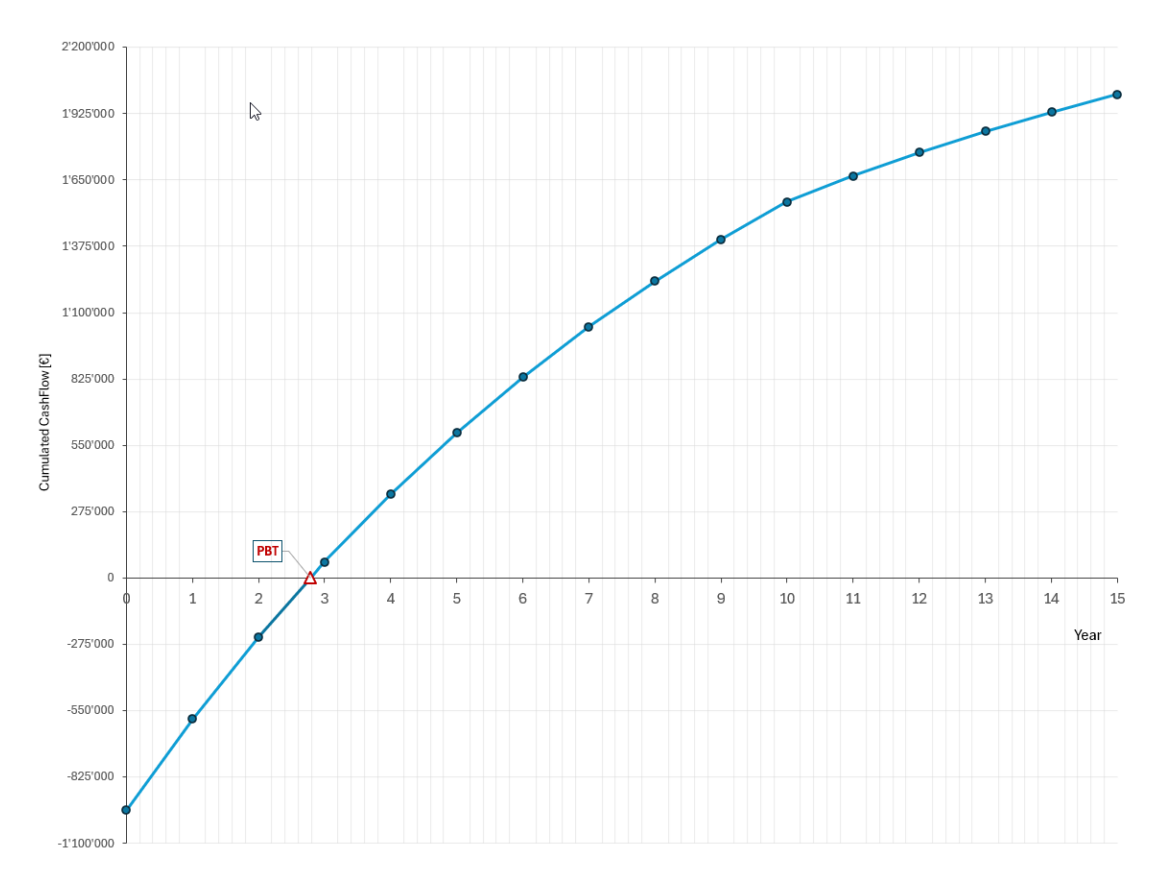


**Figure 5.5:** Discounted cumulative cash flows of the cogeneration unit over its expected lifetime, with respective payback times (PBT).

## Chapter 6

## Conclusions

This thesis was developed in response to the urgent global need to reduce green-house gas emissions associated with energy use. In a context of steadily rising energy demand, the industrial sector — responsible for nearly 40% of total energy consumption — faces increasing pressure to adopt sustainable solutions. Two main strategies are generally available to industry: the integration of renewable energy systems and the reduction of energy consumption through efficiency improvements. Within this framework, the present work has investigated the potential of heat recovery (HR) and cogeneration (CHP), focusing on the design, simulation, and economic assessment of a combined heat and power system integrated with heat recovery for an industrial application.

The study began with an overview of heat recovery fundamentals, analysing the technical feasibility of different recovery technologies applied to industrial streams at varying temperature levels. This preliminary assessment confirmed that significant amounts of thermal energy could be recuperated from exhaust gases and other process flows, creating opportunities to reduce primary energy demand. Subsequently, an overview of cogeneration technologies was presented, highlighting their ability to simultaneously generate electricity and useful heat, thus improving overall system efficiency and reducing primary energy consumption.

Building on these foundations, two case studies were developed and analysed for the same textile company. The first case study focused on the retrofit of the existing thermal power plant, specifically the steam generator (SG), with the integration of a heat recovery system. To support the design, a dedicated Aspen Plus model of the SG was created. The simulations validated the hand calculations and provided a more detailed characterization of the system's performance, confirming the energy savings potential.

The second case study investigated the integration of a gas engine—based CHP unit combined with a dual-stage heat recovery system. In the first stage, engine exhaust gases were exploited for high-pressure steam production, while the second

stage recovered residual heat for water preheating. Additional recovery from the engine jacket cooling system contributed non-negligibly to the overall thermal balance. The technical assessment showed that this solution could ensure substantial energy savings while remaining compatible with the site's operational requirements.

The economic evaluation encompassed both case studies. Results demonstrated that both the SG retrofit with HR and the CHP with HR are financially attractive, with positive Net Present Values (NPV) and payback times (PBT) compatible with typical industrial investment horizons. The analysis also highlighted the role of incentive schemes, such as White Certificates (TEE), in further improving project profitability.

Nonetheless, some practical limitations must be acknowledged. The deployment of CHP and HR systems is not always straightforward: beyond technical or spatial constraints, managerial decisions play a critical role. In some cases, plant managers may hesitate to implement new systems due to concerns about potential risks for manufacturing processes, even when projects are designed to guarantee seamless integration and safeguard production quality.

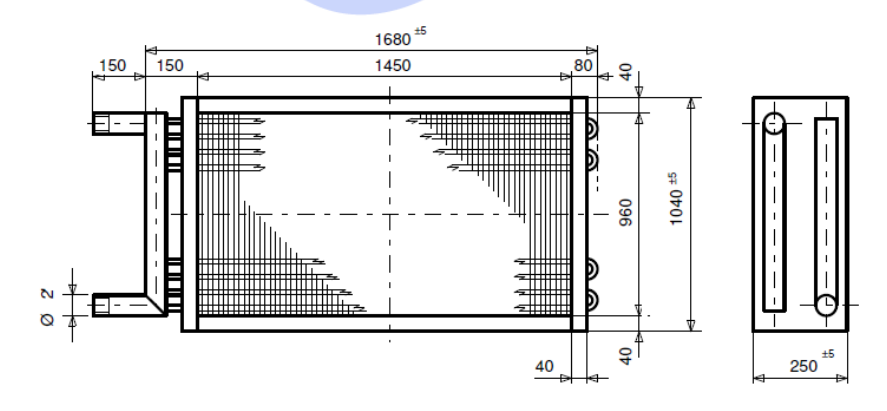
In conclusion, this thesis demonstrates that the implementation of CHP systems and heat recovery retrofits represents a technically feasible and economically advantageous strategy for improving industrial energy efficiency. The combination of primary energy savings, reduced operating costs, and favourable financial indicators positions these technologies as strategic tools for reducing both costs and environmental impact. More broadly, the methodology developed throughout this work provides a replicable framework for assessing similar interventions in other industrial contexts. By promoting the deployment of these solutions, industry can contribute meaningfully to the dual challenge of competitiveness and sustainability, supporting the transition toward a low-carbon economy.

## Appendix A

## **ECO** Datasheet

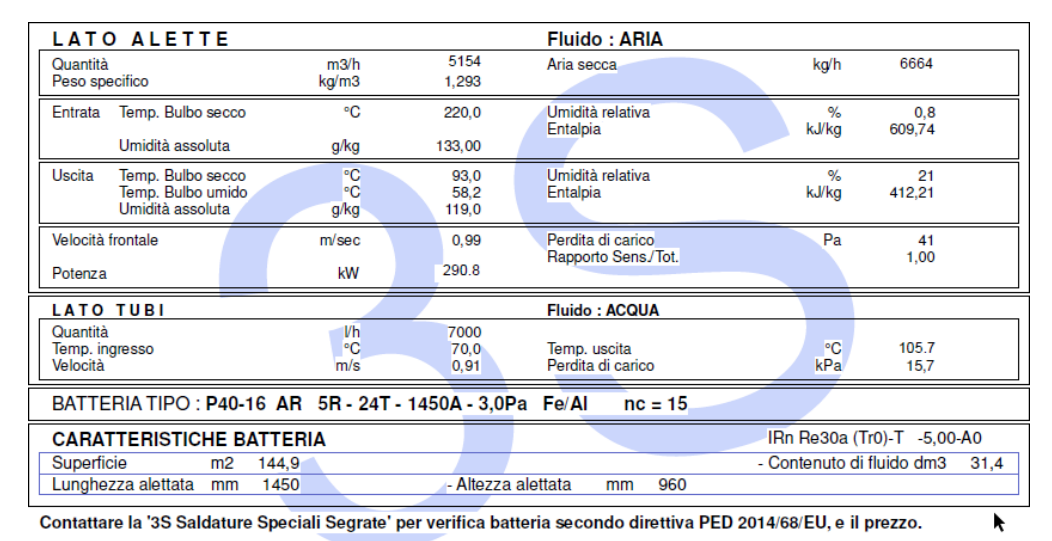
LATO ALETTE			Fluido : ARIA				
Quantità Peso specifico	m3/h kg/m3	8818 1,293	Aria secca	kg/h	11402		
Entrata Temp. Bulbo secco	°C	230,0	Umidità relativa Entalpia	% kJ/kg	0,6 618,85		
Umidità assoluta	g/kg	133,00					
Uscita Temp. Bulbo secco Temp. Bulbo umido Umidità assoluta	°C °C g/kg	105,9 59,6 124,2	Umidità relativa Entalpia	% kJ/kg	13,5 440,14		
Velocità frontale	m/sec	1,70	Perdita di carico Rapporto Sens/Tot.	Pa	100 1.00		
Potenza	kW	487,97			.,		
LATO TUBI			Fluido: ACQUA				
Quantità Temp. ingresso Velocità	l/h °C m/s	12000 70,0 1,55	Temp. uscita Perdita di carico	°C kPa	104,97 40,9		
BATTERIA TIPO : P40-16 AR 5R - 24T - 1450A - 3,0Pa Fe/Al nc = 15							
CARATTERISTICHE BAT	TERIA			IRn Re30a	(Tr0)-T -5,00-A0		
Superficie m2 1	44,9			- Contenuto d	di fluido dm3 31,4		
Lunghezza alettata mm 1	450	- Altezza	alettata mm 960				

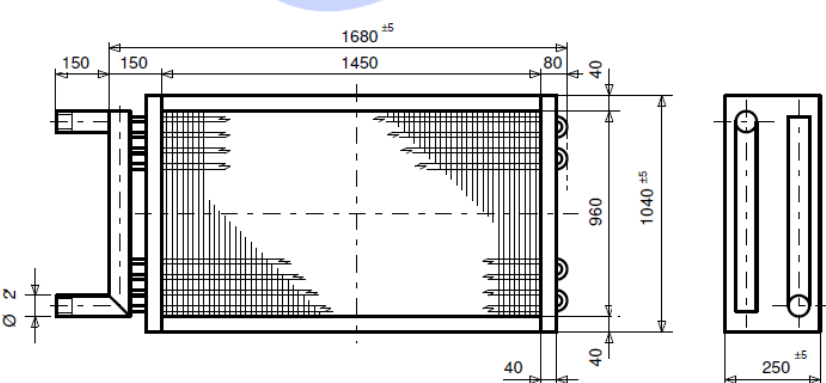
Contattare la '3S Saldature Speciali Segrate' per verifica batteria secondo direttiva PED 2014/68/EU, e il prezzo.



MATERIA	<b>ALI</b>									
Tubi scan	nbio	Acciaio al	carbonio	- Diame	tro	mm 16,50	- Spesso	ore	mm	1,50
Alette		Alluminio		- Spesso	ore	mm 0,23				
Collettori		Acciaio al	carbonio	- Telaio		Lamiera zincata	- Attacchi	File	ettati EN 10	226-2
1-DX	2-5X	Incl. Dx	Incl. Sx	5	•	† † † 7	† † † 8	Fo	oglio n. 1	/ 1

Figure A.1: Economizer Datasheet provided by the manufacturer, Full Load.





MATERIALI						
Tubi scambio	Acciaio al carbonio	<ul> <li>Diametro</li> </ul>	mm 16,50	<ul> <li>Spessore</li> </ul>	mm	1,50
Alette	Alluminio	- Spessore	mm 0,23			
Collettori	Acciaio al carbonio	- Telaio	Lamiera zincata	- Attacchi	Filettati EN 1022	6-2

Figure A.2: Economizer Datasheet provided by the manufacturer, Medium Load.

## Appendix B

## RC2 and RC3 Manufacturer Datasheet

LATO A	LETTE				Fluido : ARIA		
Quantità			m3/h	14870	Aria secca	kg/h	19226
Peso specific	0		kg/m3	1,293			
Entrata Ten	np. Bulbo sec	co	°C	132,0	Umidità relativa Entalpia	% kJ/kg	6,2 498,80
Um	idità assoluta		g/kg	133,00	Entarpia	Korky	430,00
	np. Bulbo sec		°C	51,0	Umidità relativa	%	98
	np. Bulbo umi idità assoluta	do	°C g/kg	50,7 89.4	Entalpia	kJ/kg	283,57
Velocità fronta			m/sec	2,00	Perdita di carico	Pa	304
Acqua conde			kg/s	0,2226	Rapporto Sens./Tot.	Fd	0,45
Potenza			kW	1090,00			
LATO TU	ВІ				Fluido: ACQUA		
Quantità Temp, ingress			l/h °C	20000 15,0	Temp. uscita	°C	61.9
Velocità	50		m/s	2,10	Perdita di carico	kPa	
BATTERIA	TIPO · DAI	16 AB	12D 33	Γ - 1500A - 3,0I	Pa Aisi304L/AI	nc 16	
				1 - 1300A - 3,01	AISISU4L/AI		(T-0) T0 44 07 40
Superficie	RISTICHE m2		IA	- Deco au	vuoto, circa kg 550		ן (Tr0)-T0 -11,97-A0 di fluido dm3 - 115,4
Lunghezza				- Altezza		- Contenut	rai nalao amb 115,4
	150	2		16,0 bar / 204,0°C		progetto (lato aria) 250	
		175		1500	90		
24					9	1 1	
0 2 112'					50 1320		
oratura ad as Manicotti ½" s	ole della cor ugli attacchi ccolta conde	nice ester dell'cqua nsa in ino	na per acco per scarico x con scaric	ppiamento con c e sfiato o Ø 1" dallo stess	rivettati (no guarnizion anali fumi so lato degli attacchi del	•	
MATERIALI							
Tubi scambi	io		ox Aisi 304l			- Spessore	e mm 1,0
Alette		Alluminio		- Spess		i=: 2041 AH= :	Flore:-*
Collettori Flange			ox Aisi 304l N 1092-1 To	Telaio /pe 01 - PN16 (e:		Aisi 304L - Attacchi	Flangiati
1-0x	2-5X	Incl. Dx	Incl. Sx	- 5	• • • 7	* * * * * * * * * * * * * * * * * * * *	Foglio n. 2 / 4

 $\textbf{Figure B.1:} \ \, \textbf{RC2} \ \, \textbf{Datasheet provided by the manufacturer, Full Load}.$ 

LATO ALETTE			Fluido : ARIA		
Quantità Peso specifico	m3/h kg/m3	5154 1,293	Aria secca	kg/h	6664
Entrata Temp. Bulbo secco	°C	93,0	Umidità relativa Entalpia	% kJ/kg	22,8 449,63
Umidità assoluta	g/kg	133,00			
Uscita Temp. Bulbo secco Temp. Bulbo umido Umidità assoluta	°C °C g/kg	48,5 48,5 79,2	Umidità relativa Entalpia	% kJ/kg	100 254,08
Velocità frontale Acqua condensata Potenza	m/sec kg/s kW	0,70 0,0963 324,80	Perdita di carico Rapporto Sens./Tot.	Pa	56 0,29
LATO TUBI			Fluido : ACQUA		
Quantità Temp. ingresso Velocità	l/h °C m/s	5600 15,0 0,59	Temp. uscita Perdita di carico	°C kPa	64,9 20,1
BATTERIA TIPO : P40-16	AR 12R - 33	Γ - 1500A - 3,0	Pa Aisi304L/AI nc 1	16	
CARATTERISTICHE BAT	TERIA			I3S Re30q (	Tr0)-T0 -12,00-A0
Superficie m2 49	94,8	- Peso a	vuoto, circa kg 550		
Lunghezza alettata mm 1	500	Altezza	alettata mm 1320		

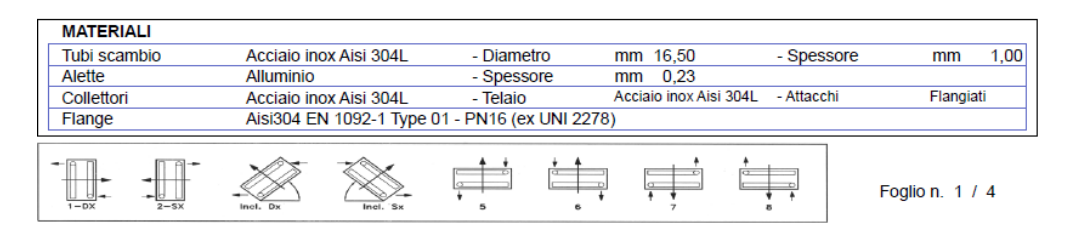
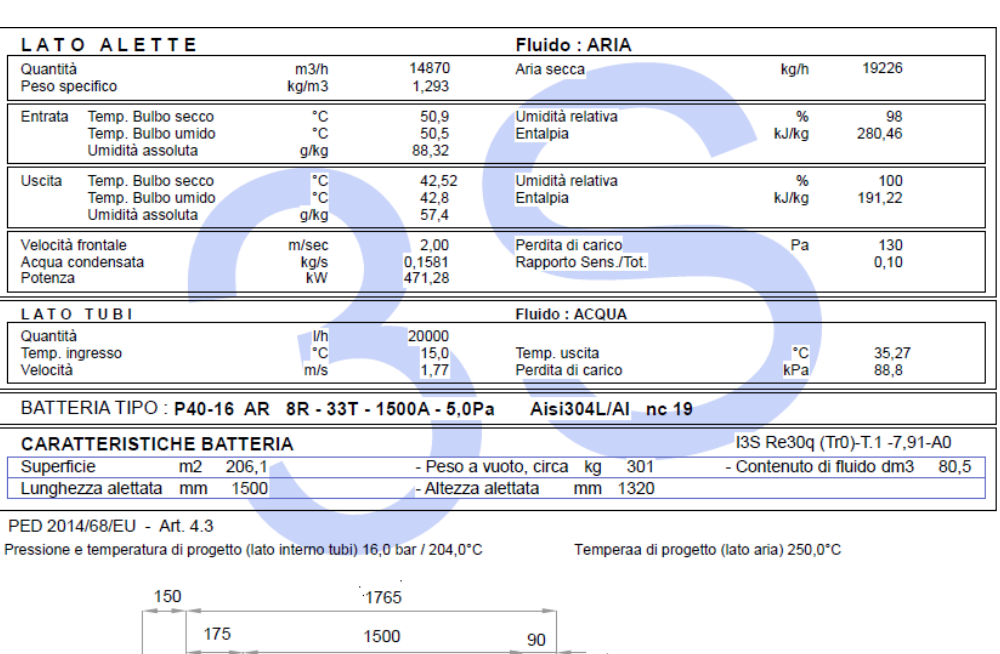
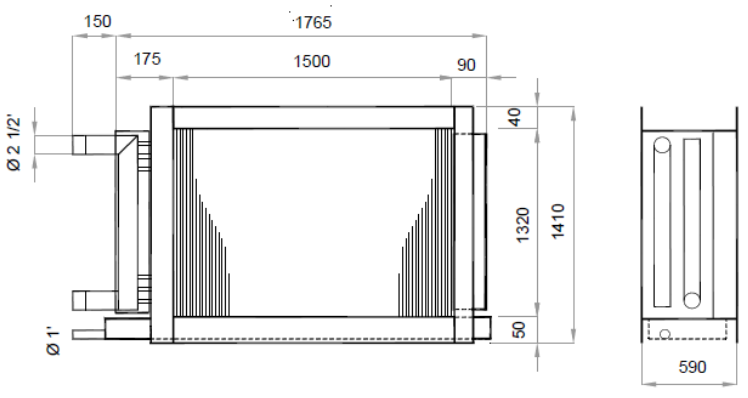


Figure B.2: RC2 Datasheet provided by the manufacturer, Medium Load.





Carter lato collettori e curvette saldati (no estraibile) con portelli rivettati (no guarnizione tubo-carter)
Foratura ad asole della cornice esterna per accoppiamento con canali fumi
Manicotti ½" sugli attacchi dell'cqua per scarico e sfiato
Bacinella di raccolta condensa in inox con scarico Ø 1" dallo stesso lato degli attacchi dell'cqua
"piedi" per ancoraggio a terra e scarico del peso tipo Martini

MATERIALI						
Tubi scambio	Acciaio inox Aisi 304L	- Diametro	mm 16,50	- Spessore	mm	1,00
Alette	Alluminio	<ul> <li>Spessore</li> </ul>	mm 0,23			
Collettori	Acciaio inox Aisi 304L	- Telaio	Acciaio inox Aisi 304L	- Attacchi	Flangia	ti
Flange	Aisi304 EN 1092-1 Type 0	1 - PN16 (ex UNI 2	278)			



Foglio n. 4 / 4

Figure B.3: RC3 Datasheet provided by the manufacturer, Full Load.

LATO ALETTE			Fluido : ARIA		
Quantità Peso specifico	m3/h kg/m3	5154 1,293	Aria secca	kg/h	6664
Entrata Temp. Bulbo secco Temp. Bulbo umido Umidità assoluta	°C °C g/kg	48,5 48,5 79,15	Umidità relativa Entalpia	% kJ/kg	100 253,92
Uscita Temp. Bulbo secco Temp. Bulbo umido Umidità assoluta	°C °C g/kg	35,86 35,4 37,4	Umidità relativa Entalpia	% kJ/kg	100 131,59
Velocità frontale Acqua condensata Potenza	m/sec kg/s kW	0,70 0,0747 213,53	Perdita di carico Rapporto Sens./Tot.	Pa	20 0,12
LATO TUBI			Fluido: ACQUA		k
Quantità Temp. ingresso Velocità	l/h °C m/s	7400 15,0 0,66	Temp. uscita Perdita di carico	°C kPa	39,82 15,7
BATTERIA TIPO : P40-16	AR 8R-33T	- 1500A - 5,0P	a Aisi304L/Al nc 19		
CARATTERISTICHE BAT	TERIA			I3S Re30q (7	Tr0)-T.1 -7,90-A0
	06,1 1500	- Peso a	vuoto, circa kg 291 alettata mm 1320	- Contenuto di	fluido dm3 73,7

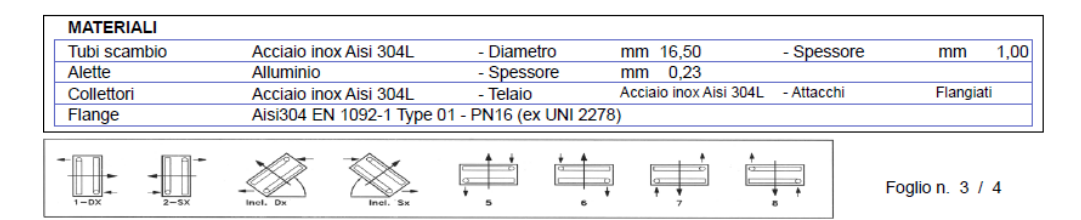


Figure B.4: RC3 Datasheet provided by the manufacturer, Medium Load.

# Appendix C **P&ID of the Heat Recovery System**

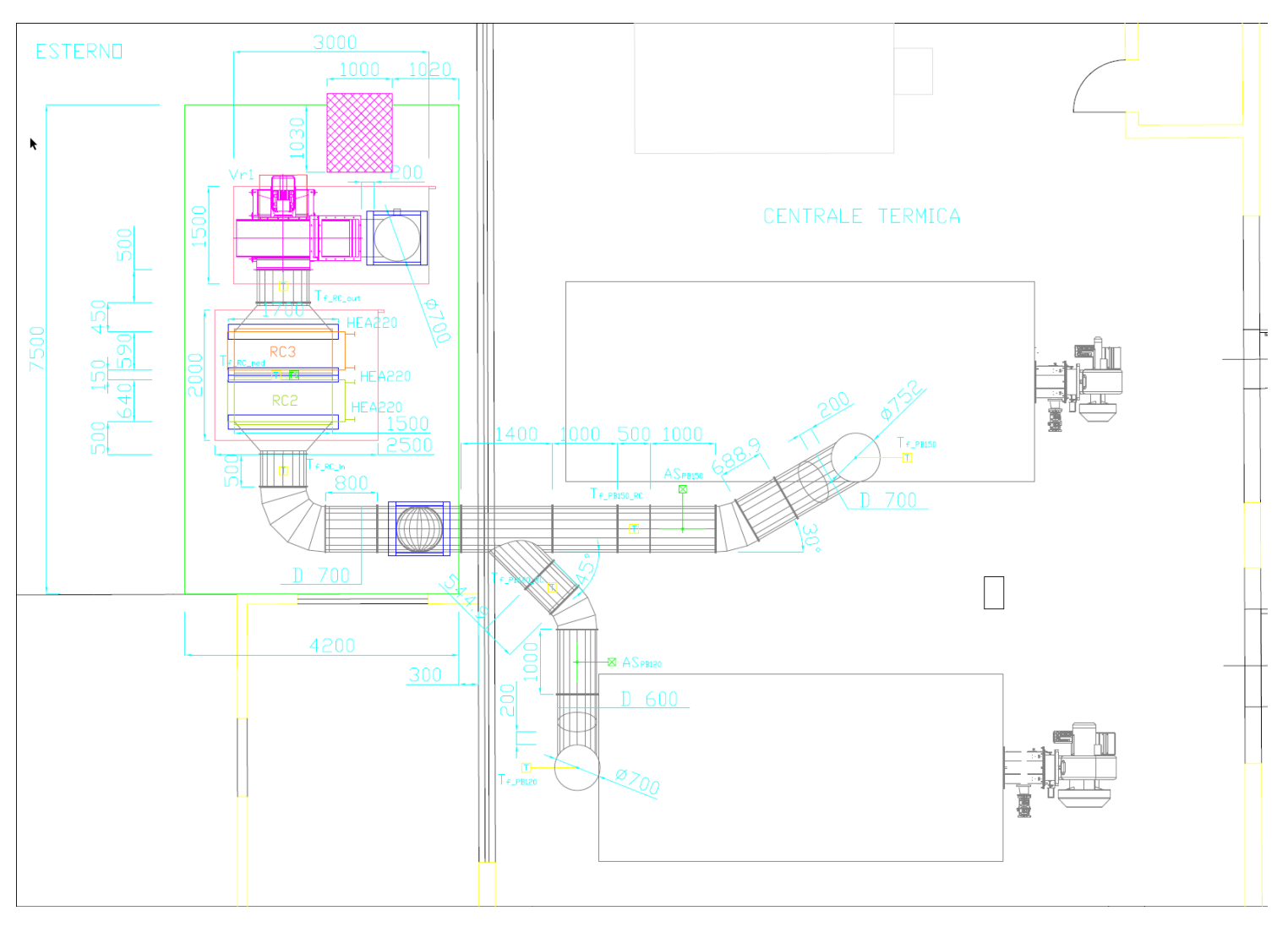


Figure C.1: Top view of the aeraulic system, P&ID.

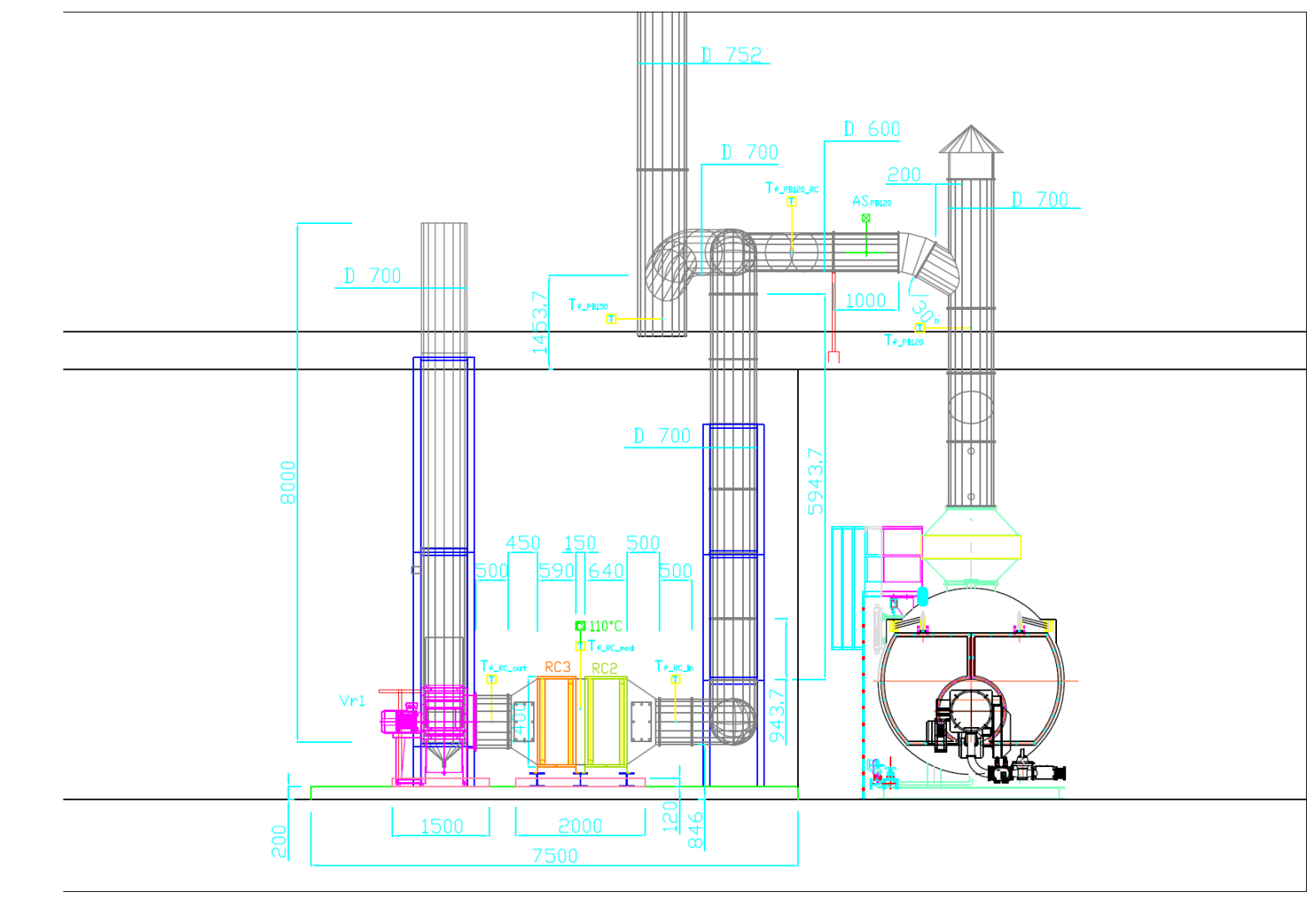


Figure C.2: Front view of the aeraulic system, P&ID.

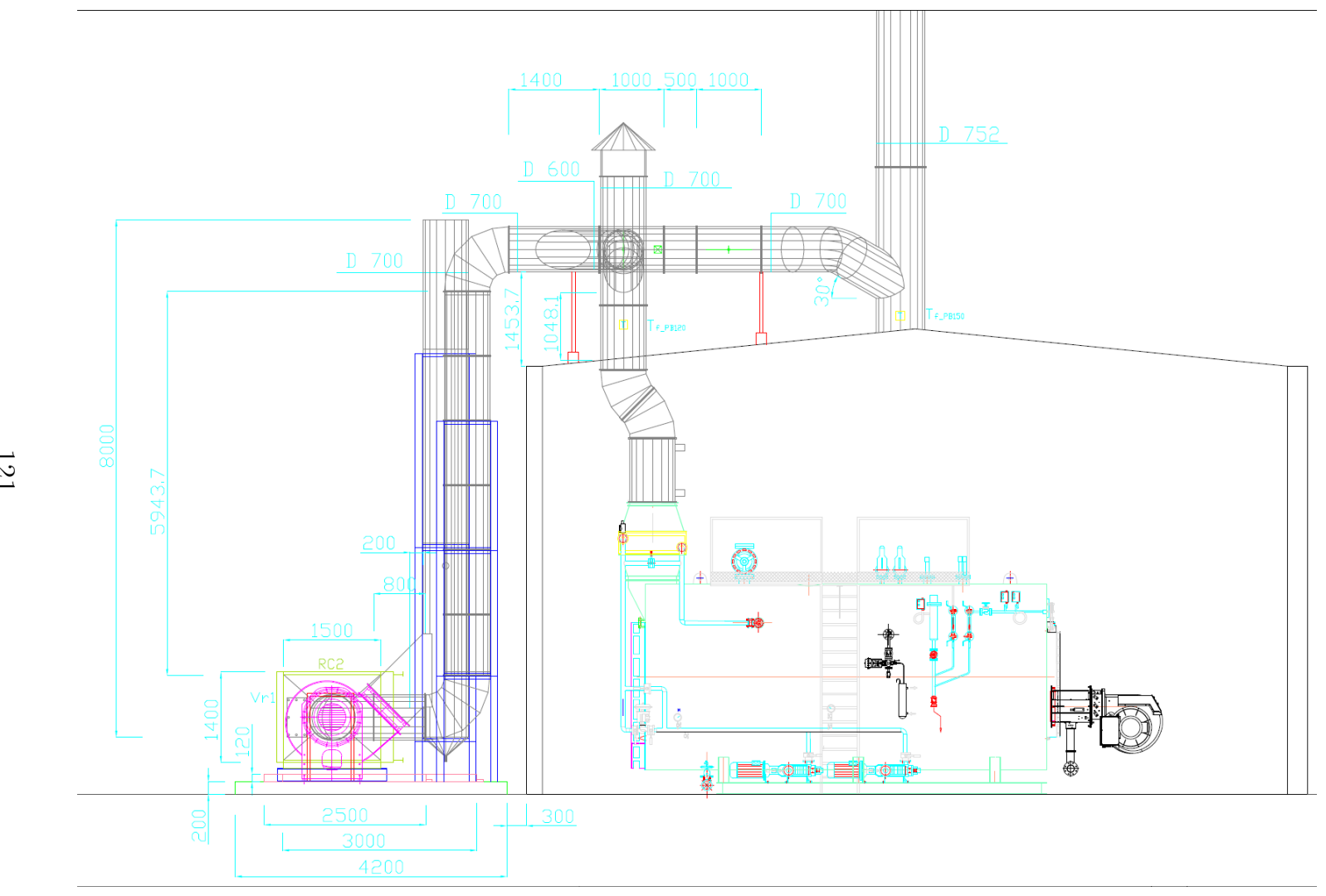


Figure C.3: Side view of the aeraulic system, P&ID.

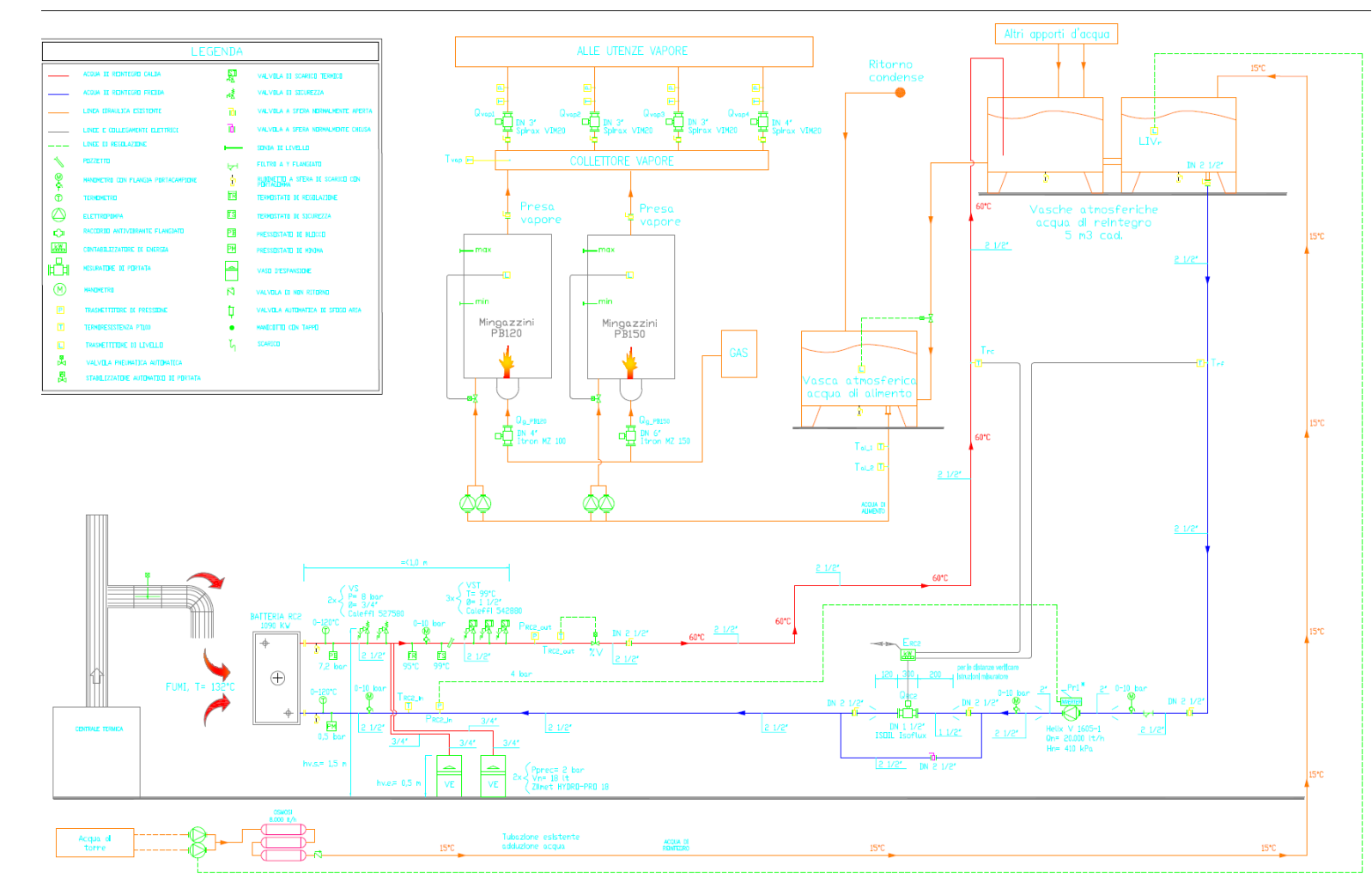


Figure C.4: P&ID of the hydraulic system serving the RC2 heat recovery exchanger.

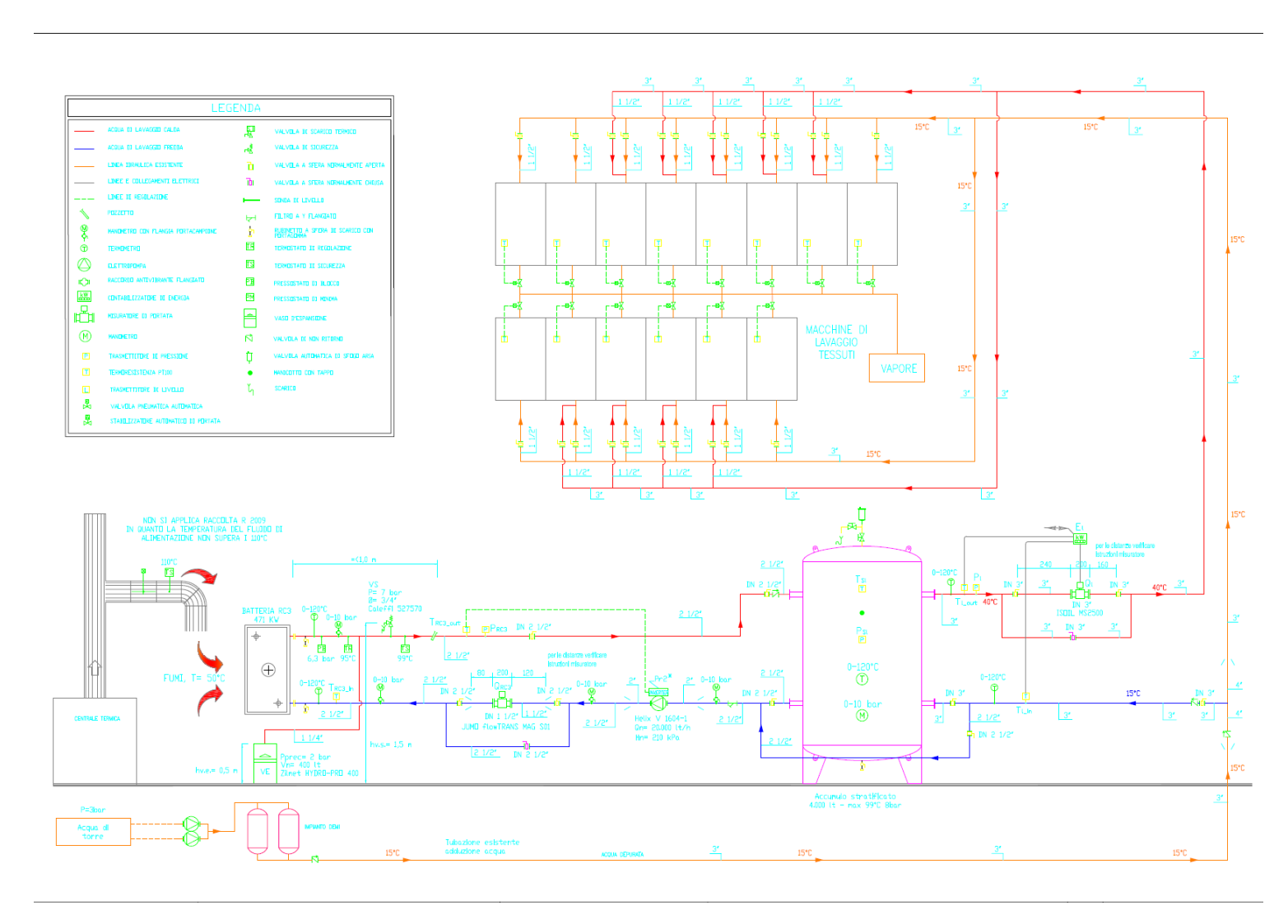


Figure C.5: P&ID of the hydraulic system serving the RC3 heat recovery exchanger.

## Appendix D P&ID of the CHP system

Ritorno condense

ALLE UTENZE VAPORE

Figure D.1: Hydraulic P&ID of the GVR unit

LEGENDA

VALVOLA A SEERA NORMALMENTE APERTA

LINEE E COLLEGAMENTI ELETTRICI

Figure D.2: Hydraulic P&ID of the  $\mathrm{HX}_{EJ}$  and  $\mathrm{HX}_{FG}$  heat exchangers.

## **Bibliography**

- [1] International Energy Agency. Energy Efficiency 2024. https://iea.blob.core.windows.net/assets/f304f2ba-e9a2-4e6d-b529-fb67cd13f646/EnergyEfficiency2024.pdf. 2024 (cit. on p. 1).
- [2] International Energy Agency. Energy Efficiency 2023. https://iea.blob.core.windows.net/assets/dfd9134f-12eb-4045-9789-9d6ab8d9fbf4/EnergyEfficiency2023.pdf. 2023. URL: https://iea.blob.core.windows.net/assets/dfd9134f-12eb-4045-9789-9d6ab8d9fbf4/EnergyEfficiency2023.pdf (cit. on p. 1).
- [3] International Energy Agency. World Energy Outlook 2024. IEA, 2024. URL: https://iea.blob.core.windows.net/assets/c036b390-ba9c-4132-870b-ffb455148b63/WorldEnergyOutlook2024.pdf (cit. on p. 1).
- [4] European Commission: Directorate-General for Energy. EU Energy in Figures Statistical Pocketbook 2024. Publications Office of the European Union, 2024. URL: https://data.europa.eu/doi/10.2833/802460 (cit. on p. 2).
- [5] European Parliament. Greenhouse gas emissions by country and sector. https://www.europarl.europa.eu/pdfs/news/expert/2018/3/story/20180301 ST098928/20180301ST098928\_en.pdf. 2018. URL: https://www.europarl.europa.eu/pdfs/news/expert/2018/3/story/20180301ST098928/20180301ST098928\_en.pdf (cit. on p. 2).
- [6] UNFCCC. The Paris Agreement. https://unfccc.int/process-and-meetings/the-paris-agreement (cit. on p. 3).
- [7] European Union. Regulation (EU) 2021/1119 of the European Parliament and of the Council of 30 June 2021 establishing the framework for achieving climate neutrality (European Climate Law). https://eur-lex.europa.eu/legal-content/EN/TXT/?uri=CELEX:32021R1119. 2021 (cit. on p. 4).
- [8] Climate Clock. https://climateclock.world/. Accessed: 2025-09-25 (cit. on p. 4).
- [9] Research and Markets / GlobeNewswire. Industrial Decarbonization Global Market Outlook 2025-2035, with Profiles of 1000 Companies including Boston Metal, Carbon Clean, H2 Green Steel, Antora Energy, Electrified Thermal Solutions. https://www.globenewswire.com/news-release/2025/02/27/3033590/0/en/Industrial-Decarbonization-Global-Market-Outlook-2025-2035-with-Profiles-of-1-000-Companies-including-Boston-Metal-Carbon-Clean-H2-Green-Steel-Antora-Energy-Electrified-Thermal-Sol.html. 2025 (cit. on p. 4).

- [10] European Parliament and Council. Directive 2012/27/EU of the European Parliament and of the Council of 25 October 2012 on energy efficiency, amending Directives 2009/125/EC and 2010/30/EU and repealing Directives 2004/8/EC and 2006/32/EC. Official Journal of the European Union, L 315, 14.11.2012, p. 1–56. 2012. URL: https://eur-lex.europa.eu/eli/dir/2012/27/oj/eng (cit. on pp. 6, 9).
- [11] Gestore dei Servizi Energetici (GSE). Guida CAR: Aggiornamento Cogenerazione ad Alto Rendimento. PDF document, GSE. Accessed: 20 September 2025. 2025. URL: https://www.gse.it/documenti\_site/Documenti%20 GSE/Servizi%20per%20te/COGENERAZIONE%20AD%20ALTO%20RENDIMENTO/Guide/GUIDA\_CAR\_AGGIORNAMENTO.pdf (cit. on p. 6).
- [12] Ibrahim Dincer and Marc A. Rosen. Exergy: Energy, Environment and Sustainable Development. 3rd. Efficiency reference at page 357. Amsterdam: Elsevier, 2021 (cit. on p. 7).
- [13] MWM. Cogeneration & Trigeneration Plants. MWM Gas Expertise. 2025. URL: https://www.mwm.net/en/gas-expertise/cogeneration-trigener ation-plants/ (cit. on p. 7).
- [14] Paul Otis. CHP Industrial Bottoming and Topping Cycle with Energy Information Administration Survey Data. Discussion Paper EIA Working Paper. Washington, DC: U.S. Energy Information Administration, Aug. 2015. URL: https://www.eia.gov/workingpapers/pdf/chp-industrial\_81415.pdf (cit. on p. 7).
- [15] European Union. Commission Delegated Regulation (EU) 2015/2402 of 12 October 2015 reviewing harmonised efficiency reference values for separate production of electricity and heat in application of Directive 2012/27/EU of the European Parliament and of the Council and repealing Commission Implementing Decision 2011/877/EU. 2015. URL: https://eur-lex.europa.eu/legal-content/EN/TXT/PDF/?uri=CELEX%3A32015R2402 (cit. on pp. 9, 99).
- [16] ReteAmbiente. Linee guida per l'applicazione del Decreto del Ministero dello Sviluppo Economico 5 settembre 2011 Cogenerazione ad Alto Rendimento (CAR). Mar. 2012. URL: https://www.reteambiente.it/repository/normativa/16133\_lineeguidacar.pdf (cit. on pp. 9, 104, 105).
- [17] COGEN World Coalition. 3rd Global Cogeneration Market Report. Dec. 2024. URL: https://cogenworld.org/wp-content/uploads/2024/12/CWC\_3rd\_Global\_Market\_Overview\_Dec-2024.pdf (cit. on pp. 9-11).

- [18] Eurostat. nrg\_chp\_cpfe: Combined heat and power and related data (Eurostat). https://ec.europa.eu/eurostat/databrowser/view/nrg\_chp\_cpfe/bookmark/table?lang=en&bookmarkId=d6cf9d6d-fe0a-407b-b2f9-9d7613850d09&c=1741876148521. 2025 (cit. on p. 12).
- [19] International Energy Agency. Renewables 2024: Analysis and forecast to 2030. Tech. rep. IEA, Oct. 2024. URL: https://iea.blob.core.windows.net/assets/17033b62-07a5-4144-8dd0-651cdb6caa24/Renewables2024.pdf (cit. on p. 12).
- [20] U.S. Department of Energy. Waste Heat Recovery: Technology and Opportunities in U.S. Industry. Technical Report ITP. Office of Energy Efficiency & Renewable Energy, 2008. URL: https://www1.eere.energy.gov/manufacturing/intensiveprocesses/pdfs/waste\_heat\_recovery.pdf (cit. on p. 13).
- [21] European Commission. Recycling industrial waste heat for a greener Europe thanks to Interreg. https://ec.europa.eu/regional\_policy/en/projects/Italy/recycling-industrial-waste-heat-for-a-greener-europe-thanks-to-interreg. European Regional Development Fund project. 2020 (cit. on p. 13).
- [22] Christopher Forman, Isaac K. Muritala, Ronald Pardemann, and Björn Meyer. «Estimating the global waste heat potential». In: Renewable and Sustainable Energy Reviews 57 (2016), pp. 1568–1579. DOI: 10.1016/j.rser.2015. 12.098. URL: https://www.sciencedirect.com/science/article/pii/S1364032115015750 (cit. on pp. 14–18).
- [23] Giuseppe Bianchi, Gregoris P. Panayiotou, Lazaros Aresti, Soteris A. Kalogirou, Georgios A. Florides, Kostantinos Tsamos, Savvas A. Tassou, and Paul Christodoulides. «Estimating the Waste Heat Recovery in the European Union Industry». In: *Energy, Ecology and Environment* 4.5 (2019), pp. 211–221. DOI: 10.1007/s40974-019-00132-7. URL: https://doi.org/10.1007/s40974-019-00132-7 (cit. on pp. 14–16, 18, 19).
- [24] Sarah Brückner, Laia Miró, Luisa F. Cabeza, Martin Pehnt, and Eberhard Lävemann. «Methods to estimate the industrial waste heat potential of regions: A categorization and literature review». In: Renewable and Sustainable Energy Reviews 38 (2014), pp. 164–171. DOI: 10.1016/j.rser.2014.04.078. URL: https://doi.org/10.1016/j.rser.2014.04.078 (cit. on pp. 16, 19).
- [25] B. Metz, O. R. Davidson, P. R. Bosch, R. Dave, and L. A. Meyer, eds. Climate Change 2007: Mitigation of Climate Change. Contribution of Working Group III to the Fourth Assessment Report of the Intergovernmental Panel on Climate Change. from reference Methods to estimate WHP. Cambridge,

- United Kingdom and New York, NY, USA: Cambridge University Press, 2007 (cit. on p. 17).
- [26] H. Roth, K. Lucas, W. Solfrian, and F. Rebstock. Die Nutzung industrieller Abwärme zur Fernwärmeversorgung Analyse der Hemmnisse für die Nutzung industrieller Abwärme zur Fernwärmeversorgung. from reference Methods to estimate WHP. Berlin: Umweltbundesamt, 1996 (cit. on p. 17).
- [27] Mohammad Ja'fari, Muhammad Imran Khan, Sami G. Al-Ghamdi, Artur J. Jaworski, and Faisal Asfand. «Waste heat recovery in iron and steel industry using organic Rankine cycles». In: *Chemical Engineering Journal* 477 (2023). DOI: 10.1016/j.cej.2023.146925. URL: https://doi.org/10.1016/j.cej.2023.146925 (cit. on p. 20).
- [28] Mingazzini. *Homepage*. Website. n.d. URL: https://www.mingazzini.it (cit. on pp. 25, 26, 61, 62).
- [29] ASHRAE. 2021 ASHRAE Handbook: Fundamentals. SI. See p. 1.9 for absolute humidity equation; p. 28.12 for excess air advantages and drawbacks. Atlanta, GA: American Society of Heating, Refrigerating and Air-Conditioning Engineers, Inc., 2021. ISBN: 978-1-947192-90-4 (cit. on p. 27).
- [30] V. Ganapathy. *Industrial Boilers and Heat Recovery Steam Generators: Design, Applications, and Calculations.* See p. for Excess air ranging from 10 to 20 percent. New York, NY: Marcel Dekker, Inc., 2003. ISBN: 978-0-8247-0814-8 (cit. on p. 27).
- [31] Nationwide Boiler Inc. O Trim for Increased Boiler Efficiency & Emissions Compliance. 2015. URL: https://nationwideboiler.com/boiler-blog/o2-trim-for-increased-boiler-efficiency-emissions-compliance.html (cit. on pp. 28, 63).
- [32] EUROPEAN COMMITTEE FOR STANDARDIZATION. BS EN 676:2003+A2:2008
   Automatic forced draught burners for gaseous fuels. Standard specification for automatic gas burners with or without a fan. 2008 (cit. on p. 29).
- [33] Cristian David Mojica-Cabeza, Carlos Eduardo García-Sánchez, Ramón Silva-Rodríguez, and Luis García-Sánchez. «A review of the different boiler efficiency calculation and modeling methodologies». In: *Informador Técnico* 86.1 (2022), pp. 53-77. DOI: 10.23850/22565035.3697. URL: https://www.researchgate.net/publication/356349709\_A\_review\_of\_the\_different\_boiler\_efficiency\_calculation\_and\_modeling\_methodologies (cit. on p. 30).
- [34] Elif Gül Göçer, Elif Melek Öztürk, Gülşen Şahin Andaş, and Yahya Aktaş. «Efficiency Factors in Natural Gas Fired Steam Boilers». In: *Digital Refining* (2020). Online; accessed 2025-05-17, pp. 31-35. URL: https://www.digitalrefining.com/article/1002461/efficiency-factors-in-natural-gas-fired-steam-boilers (cit. on p. 31).

- [35] Brundaban Patro. «Efficiency Studies of Combination Tube Boilers». In: Alexandria Engineering Journal 55.1 (2015). DOI: 10.1016/j.aej.2015. 12.007. URL: https://www.researchgate.net/publication/289998355\_ Efficiency\_studies\_of\_combination\_tube\_boilers (cit. on p. 31).
- [36] William G. Acker. Energy Survey for Boiler and Plant Operations. AckerAssociates. 2001. URL: https://ackerandassociates.com/article/boiler\_analysis/energy\_survey\_for\_boiler\_and\_plant\_operations.pdf (cit. on pp. 32, 40).
- [37] A. Bhatia. Improving Energy Efficiency of Boiler Systems. CED Engineering Course No. M06-022. 2011. URL: https://www.cedengineering.com/userfiles/M06-022%20-%20Improving%20Energy%20Efficiency%20of%20Boiler%20Systems%20-%20US.pdf (cit. on p. 32).
- [38] Kuppan Thulukkanam. Heat Exchanger Design Handbook. 2nd. See Chapter 5, Section 5.16.6 (page 297) for recommended fluid velocity criteria in shell-and-tube heat exchanger design. CRC Press, 2013. ISBN: 978-1-4398-4212-6. URL: https://www.taylorfrancis.com/books/mono/10.1201/b14877/heat-exchanger-design-handbook-kuppan-thulukkanam (cit. on pp. 32, 37).
- [39] T. Agami Reddy, Jan F. Kreider, Peter S. Curtiss, and Ari Rabl. *Heating and Cooling of Buildings: Principles and Practice of Energy Design*. Boca Raton, FL: CRC Press Taylor Francis Group, 2017, pp. 445–446 (cit. on pp. 33, 40).
- [40] Michael Short, Tracey Crosbie, Muneeb Dawood, and Nashwan Dawood. «Load Forecasting and Dispatch Optimisation for Decentralised Co-generation Plant with Dual Energy Storage». In: *Applied Energy* (2016). DOI: 10.1016/j.apenergy.2016.04.052 (cit. on pp. 33, 40).
- [41] M.C. Barma, R. Saidur, S.M.A. Rahman, A. Allouhi, B.A. Akash, and Sadiq M. Sait. «A review on boilers energy use, energy savings, and emissions reductions». In: *Renewable and Sustainable Energy Reviews* 79 (2017), pp. 970–983. DOI: https://doi.org/10.1016/j.rser.2017.05.187. URL: https://www.sciencedirect.com/science/article/abs/pii/S1364032117308249?via%3Dihub (cit. on p. 33).
- [42] Xuejun Qian, Seong W. Lee, and Yulai Yang. «Heat Transfer Coefficient Estimation and Performance Evaluation of Shell and Tube Heat Exchanger Using Flue Gas». In: *Processes* 9.939 (2021). Flue Gas cp from Figure 5 considering T=220°C, EA=1.15. DOI: 10.3390/pr9060939. URL: https://www.mdpi.com/2227-9717/9/6/939 (cit. on p. 34).

- [43] Ahmad Mahmoudi Lahijani and Eris E Supeni. «Evaluating the Effect of Economizer on Efficiency of the Fire Tube Steam Boiler». In: *Innovative Energy & Research* 7.1 (2018). ISSN: 2576-1463. DOI: 10.4172/2576-1463. 1000193. URL: https://www.researchgate.net/publication/324196534\_Evaluating\_the\_Effect\_of\_Economizer\_on\_Efficiency\_of\_the\_Fire\_Tube\_Steam\_Boiler (cit. on pp. 35, 41).
- [44] 3s Coils. 3S Coils Home Page. https://www.3scoils.it/(cit. on p. 35).
- [45] Ian C. Kemp. Pinch Analysis and Process Integration: A User Guide on Process Integration for the Efficient Use of Energy. 2nd. See Chapter 3.3.2, 'Threshold problems', p. 54. Butterworth-Heinemann, 2007. ISBN: 978-0-7506-8260-2 (cit. on p. 36).
- [46] Yee Qing Lai, Sharifah Rafidah Wan Alwi, and Zainuddin Abdul Manan. «Heat Exchanger Network Synthesis Considering Different Minimum Approach Temperatures». In: Chemical Engineering Transactions 72 (2019), pp. 283–288. ISSN: 2283-9216. DOI: 10.3303/CET1972048. URL: https://www.aidic.it/cet/19/72/048.pdf (cit. on p. 36).
- [47] Sergio Alencar de Souza and Wendell de Queiroz Lamas. «Thermoeconomic and ecological analysis applied to heating industrial process in chemical reactors». In: Renewable and Sustainable Energy Reviews 29 (2014), pp. 96–107. DOI: https://doi.org/10.1016/j.rser.2013.08.095. URL: https://www.sciencedirect.com/science/article/pii/S1364032113006357 (cit. on p. 41).
- [48] Gruppo di Studio per la Progettazione Termotecnica. Esercitazioni CS PRES-SIONE UNI 3384-1. 2019. URL: https://www.gbd.it/filegbd/Software/ Esercitazioni CS PRESSIONE UNI 3384-1.pdf (cit. on p. 47).
- [49] Robert L. Mott. Applied Fluid Mechanics. 5th. Upper Saddle River, NJ: Pearson Prentice Hall, 2006 (cit. on p. 50).
- [50] Frank M. White. Fluid Mechanics. 7th. New York, NY: McGraw-Hill, 2011 (cit. on p. 50).
- [51] ASHRAE. 2001 ASHRAE Handbook: Fundamentals. SI. Chapter 34: Duct Design. Atlanta, GA: American Society of Heating, Refrigerating and Air-Conditioning Engineers, 2001 (cit. on p. 50).
- [52] Marco Doninelli and Mario Doninelli. *Tabelle e diagrammi perdite di carico aria*. n.d. URL: https://www.caleffi.com/sites/default/files/media/external-file/Tabelle%20e%20diagrammi%20perdite%20di%20carico%20aria\_IT.pdf (cit. on p. 50).

- [53] Lafert Group. Global Minimum Energy Performance Standards (MEPS). 2021. URL: https://www.lafert.com/storage/files/853203GLOBALMEPS.pdf (cit. on p. 53).
- [54] Marco Doninelli and Mario Doninelli. Tabelle e diagrammi perdite di carico acqua. n.d. URL: https://www.caleffi.com/sites/default/files/media/external-file/acqua.pdf (cit. on p. 55).
- [55] Inc. Aspen Technology. Aspen Plus / Leading Process Simulation Software. 2025. URL: https://www.aspentech.com/en/products/engineering/aspen-plus (cit. on p. 59).
- [56] American Society of Mechanical Engineers. Steam Tables ASME. Accessed on May 16, 2025. 2009. URL: https://www.academia.edu/36447071/Steam\_Tables\_Asme (cit. on p. 61).
- [57] Commissione Europea. Regolamento (UE) 2019/1781 della Commissione dell'1 ottobre 2019 che stabilisce specifiche per la progettazione ecocompatibile dei motori elettrici e dei variatori di velocità in applicazione della direttiva 2009/125/CE del Parlamento europeo e del Consiglio, recante modifica del regolamento (CE) n. 641/2009 della Commissione per quanto riguarda le specifiche per la progettazione ecocompatibile dei circolatori senza premistoppa indipendenti e dei circolatori senza premistoppa integrati in prodotti e abroga il regolamento (CE) n. 640/2009 della Commissione. Gazzetta ufficiale dell'Unione europea, L 272, 25.10.2019, pp. 74–94. Testo rilevante ai fini del SEE. Accesso il 16 maggio 2025. 2019. URL: https://eur-lex.europa.eu/legal-content/IT/TXT/PDF/?uri=CELEX:32019R1781 (cit. on p. 62).
- [58] Salvatore Robuschi & C. S.r.l. Catalogo Tecnico TS: Pompe centrifughe multistadio a girante chiusa. see page 21, characteristic curve TS40 stage. 2021. URL: https://www.salvatorerobuschi.com/public/PDF/tab173/Catalogo%20Tecnico%20TS;%20Technical%20Catalogue.pdf (cit. on p. 62).
- [59] MTM Energia Impianti di cogenerazione, motori a combustione interna, gruppi elettrogeni. https://www.mtmenergia.com/it/(cit. on pp. 77, 78).
- [60] Ministero dell'Ambiente e della Sicurezza Energetica. Tabella parametri standard nazionali. https://www.mase.gov.it/portale/sites/default/files/archivio/allegati/emission\_trading/tabella\_coefficienti\_standard\_nazionali\_2011\_2013\_v1.pdf. 2013 (cit. on p. 85).
- [61] Gestore dei Mercati Energetici S.p.A. Dati Storici MGP-GAS. 2025. URL: https://www.mercatoelettrico.org/it-it/Home/Esiti/Gas/MGP-GAS/Statistiche/DatiStorici (cit. on p. 85).
- [62] Gestore dei Servizi Energetici S.p.A. Gestore dei Servizi Energetici. 2025. URL: https://www.gse.it/ (cit. on p. 88).

- [63] Regione Lombardia. Fattori di conversione e fattori di emissione 2023. 2023. URL: https://www.energialombardia.eu/documents/401875/1143005/Fattori+di+conversione+e+fattori+di+emissione+2023/f7e49d0d-608d-472b-9de2-fd56f362fe7d (cit. on p. 88).
- [64] Gestore dei Mercati Energetici (GME). Statistiche storiche Titoli di Efficienza Energetica (TEE). 2025. URL: https://www.mercatoelettrico.org/it-it/Home/Esiti/Ambiente/TEE/Statistiche/DatiStorici#IntestazioneGrafico (cit. on p. 88).
- [65] M. Pilar Pérez, Carmen Castells, Valeria Stacchini, Carlo Maria Venturi, Pier Federico Fileni, Athena Mantidi, and Panagiotis Konstantinopoulos. Il finanziamento tramite terzi per investire nell'efficienza e nel risparmio energetico. Tech. rep. Progetto ECOMARK, Programma Europeo MED. Provincia di Bologna / Città Metropolitana di Bologna, 2011. URL: https://www.cittametropolitana.bo.it/progetti\_europei/Engine/RAServeFile.php/f/APEA/FTT\_ITA.pdf (cit. on pp. 89, 90).
- [66] Richard A. Brealey, Stewart C. Myers, and Franklin Allen. *Principles of Corporate Finance*. 13th. New York: McGraw-Hill Education, 2020. ISBN: 9781260013900 (cit. on p. 91).
- [67] Aswath Damodaran. Betas. 2025. URL: https://pages.stern.nyu.edu/~adamodar/New\_Home\_Page/datafile/Betas.html (cit. on pp. 91, 92, 106).
- [68] Associazione Bancaria Italiana. RAPPORTO MENSILE ABI1 Giugno 2025. June 2025. URL: https://www.abi.it/wp-content/uploads/2025/06/Comunicato-stampa-giugno-2025.pdf (cit. on pp. 91, 93).
- [69] Aswath Damodaran. Equity Risk Premiums (ERP): Determinants, Estimation, and Implications The 2024 Edition. Tech. rep. Available at SSRN: https://ssrn.com/abstract=4751941 or DOI: http://dx.doi.org/10.2139/ssrn.4751941. SSRN, Mar. 2024. DOI: 10.2139/ssrn.4751941. URL: https://ssrn.com/abstract=4751941 (cit. on p. 92).
- [70] GSE S.p.A. Certificati Bianchi Allegato 4 alla Guida Operativa: Chiarimenti relativi agli interventi della Tabella 1. https://www.certifico.com/component/attachments/download/33771. 2021 (cit. on p. 94).
- [71] Ministero dell'Ambiente e della Tutela del Territorio e del Mare Ministero dello Sviluppo Economico. Integrazioni al decreto legislativo 8 febbraio 2007, n. 20, di attuazione della direttiva 2004/8/CE sulla promozione della cogenerazione basata su una domanda di calore utile sul mercato interno dell'energia, e modificativa della direttiva 92/42/CE. 2011. URL: https://www.gazzettaufficiale.it/eli/id/2011/09/19/11A12046/sg (cit. on p. 100).
- [72] ARERA. Prezzi e tariffe. 2025. URL: https://www.arera.it/area-operat ori/prezzi-e-tariffe (cit. on p. 102).

[73] Agenzia delle Dogane e dei Monopoli (ADM). Aliquote nazionali per il gas naturale – aggiornamento al 1 gennaio 2025. 2025. URL: https://www.adm.gov.it/portale/documents/20182/43975520/Aliquote%2Bnazionali%2Baggiornamento%2Bal%2B1%2Bgennaio%2B2025.pdf (cit. on p. 104).